# STRAIN-HARDENING BEHAVIOR OF FIBER REINFORCED CONCRETE

By

Liying Jiang

Department of Civil Engineering and Applied Mechanics
McGill University
Montreal, Canada

A thesis submitted to the Faculty of Graduate Studies and Research in partially fulfillment of the requirement for the degree of Master of Civil Engineering

September 2003

# Table of Contents

# List of Figures

# List of Tables

# Abstract

Fiber reinforced concrete with postpeak strain hardening type of response contributes significantly to the load carrying capacity, the impact and fatigue resistance and the reduced crack opening width, and is developed for special applications when large energy absorption capacity is required. While the strain hardening fiber reinforced cement paste and mortar are extensively studied, the strain hardening fiber reinforced concrete (SHFRC) with large quantity of coarse aggregates is not readily achievable. In this research, two approaches were investigated to fabricate strain hardening fiber reinforced concrete with polyvinyl alcohol (PVA) fiber and steel fiber: One used polymer addition and the other employed hybrid fiber reinforcement. The results showed that both PVA fibers and steel fibers with hooked flat ends could be used to produce fiber reinforced concrete with strain hardening behavior. With polymer modification and hybrid fiber system, the hardening response was enhanced. Fiber reinforced concretes were tested under severe environmental condition: freeze-thaw cycling and drying shrinkage. The results indicated that PVA fibers were vulnerable to cold temperature change and the strain hardening behavior deteriorated under freeze-thaw cycling. Polymer modification could protect the polymer fibers from frost damage. The strain hardening fiber reinforced concrete did not show its ability to delay crack initiation under severe drying condition. Finally, a toughness method (Ductility factor) was proposed to quantify the strain-hardening behavior.

# Résumé

Le béton renforcé de fibres avec le type de réponse avec écrouissage 'postpeak' contribue de manière significative à la capacité de charge, à la résistance à l'impact et à la fatigue et à la réduction de la largeur des fissures, il est développé pour des applications spéciales quand un grand potentiel de dissipation d'énergie. Alors que la pâte et le mortier de ciment renforcés de fibres d'écrouissage sont largement étudiés, le béton renforcé de fibres d'écrouissage (SHFRC) avec une grande quantité d'agrégats bruts n'est pas aisément réalisable. Dans cette recherche, deux approches ont été étudiées pour fabriquer du béton renforcé de fibres d'écrouissage avec la fibre de l'alcool polyvinylique (PVA) et la fibre d'acier: L'une a employé l'addition de polymère et l'autre un renfort de fibres hybrides. Les résultats ont montré que les fibres PVA ainsi que les fibres d'acier avec des embouts plats pouvaient être utilisés pour produire le béton renforcé de fibres avec le comportement d'écrouissage. La modification de polymère et le système de fibre d'hybride ont permis d'améliorer la réponse d'écrouissage. Des bétons renforcés de fibres ont été examinés dans des conditions environnementales extrêmes: le cycle gel-dégel et le retrait de séchage. Les résultats ont indiqué que les fibres de PVA étaient vulnérables au changement de température au froid et le comportement d'écrouissage se détériorait sous le cycle gel-dégel. Des modifications de polymère ont pu protéger les fibres polymères des dommages dus au gel. Le béton renforcé de fibres d'écrouissage n'a pas montré ses capacités à retarder l'initiation de la fissuration dans des conditions extrêmes de séchage. En conclusion, on a proposé une méthode d'évaluation de la ténacité (facteur de ductilité) pour mesurer le comportement en contrainte-durcissement.

# Acknowledgement

I would like to express my gratitude to my advisor, Professor Yixin Shao for his support, knowledgeable guidance, time and effort throughout my research work and in the classroom. Many thanks to Mr. Ye gang for the great help with the tests.

I would like to acknowledge my family especially Zhu Liu for their encouragement and praise while I pursued my master's degree and everything else in my life.

# Chapter 1 Introduction

Concrete is a brittle material, effective in resisting compressive forces but weak in tension, and its tensile strength is typically only about one tenth of its compressive strength resulting in cracking at low stress levels. Regular concrete is therefore normally reinforced with steel reinforcing bars and prestressing tendons, which is relatively limited in standalone application. For many applications, it is becoming increasingly popular to reinforce the concrete with small, randomly distributed fibers. Their main purpose is to increase the energy absorption capacity and toughness of the material. But also the increase in tensile and flexural strength is often the primary objective. While steel fibers are probably the most widely used and effective fibers for many applications, other types of fiber might be considered to be appropriate for special applications as well.

## 1.1 Materials Characteristics of Fiber Reinforced Concrete

Depending on the level of property improvement, fiber reinforced concretes are subdivided into two groups: Conventional fiber reinforced concretes and high performance fiber reinforced concrete.

## 1.2 Conventional Fiber Reinforced Concrete (FRC)

Conventional FRC is made by premixing discontinuous fiber with concrete. Maximum fiber length, volume fraction, and geometry are limited by workability requirement. The typical fiber content used in steel FRCs is 30 kg/m$^3$, which equals to volume fraction of 0.4%. With such low fiber volume fraction, fibers mainly contribute to crack-arresting capacity and post-crack ductility. However, stress at the first cracking,

maximum stress and corresponding strain are not significantly improved over plain concrete (matrix), as is shown in Figure 1.1 [Naaman et al. 1995].

*Cracking mechanism* — Cracking mechanism of conventional FRCs is that, once first crack generates, the presence of fiber will prevent sudden failure (happened in plain concrete) and allow the load transfer across the crack. In this process, the first crack localized once it initiates, and crack width is controlled and reduced by fiber resisting. Depending on the fiber volume fraction and fiber characteristics, further load increase leads to fiber pull-out or fiber rupture. Therefore, conventional FRCs show a strain-softening behavior with single cracking due to first crack localization, and reduce the maximum crack size by fiber transferring load.

Conventional FRC which shows a strain softening response is a well established material. With relatively low quantity of discontinuous fiber, the conventional FRC is easy to make. A wide variety of different types of fiber have been proposed for use in concrete, such as steel fiber, polypropylene, glass Fiber etc. For each application it needs to be determined which type of fiber is optimal in satisfying the product specifications. It is found that all these FRCs show a strain-softening behavior [Soroushian et al. 1991, Bayasi et al. 1993, Shah et al. 1988].

## 1.3 High Performance Fiber Reinforced Concrete

Recent advancements in materials science have led to the development of a new type of fiber reinforced concrete called High-Performance Fiber Reinforced Concrete. It is defined as a material that exhibits a quasi strain hardening type of (or pseudo strain hardening) behavior, which is generally accompanied by multiple cracking and large

energy absorption capacity after first crack, as is shown in Figure 1.1 [Naaman et al. 1995], represented by curve of HPFRCC. Therefore, it is also called strain-hardening fiber reinforced concrete (SHFRC). The strain-hardening behavior is expressed as a post-cracking strength larger than the first cracking strength, or elastic-plastic response.

Sequential and distributed multiple cracking contributes significantly to the strain hardening behavior in concrete. Figure 1.1 [Naaman et al. 1995] also shows the multiple cracking mechanisms. Point A represents the load at which the matrix or plain concrete begins to crack, referred to as the first crack strength. Usually, it is at about the same stress at which the first crack occurs in matrix, conventional fiber reinforced concrete and postpeak ductile fiber reinforced concrete. After this point, the curves of the matrix and conventional FRC begin to softening down due to first crack localization. However, in the case of postpeak ductile fiber reinforced concrete, the first crack stress is sustained, and load is transferred through fibers to the other part of the matrix. Therefore, the first crack does not localize with the further load increases. Instead, another crack will form somewhere else in the concrete which is also the weak part of the matrix. Thus, increase in load beyond the first crack strength will lead to formation of a series of very fine, disconnected cracks invisible to the naked eye, and thus more fracture energy absorption. Finally, the crack localization will occur in the weakest section of the multiple matrix cracks, followed by fiber breakage or fiber pullout, leading to a softening type of behavior in load-deflection curve.

Why strain hardening fiber reinforced concrete has attracted more attention recently? An example is shown in Figure 1.2. The roofing was made of two different kinds of tiles, as the left part was made of asbestos-cement composite, the right part made of strain hardening fiber reinforced composite with continuous polypropylene fiber. This photo

describes the condition of roofing tiles after a big hale storm. It was realized that the asbestos-cement composite roofing was damaged significantly although it had high tensile stress but was more brittle. The continuous polypropylene glass cement composite which had less tensile stress but more ductility, was still in good condition since multiple matrix cracking dissipated energy in a large area and prevented crack opening localization. Therefore, the application of this strain hardening fiber reinforced concrete is more related to the large energy absorption capacity and crack width control of the materials.

Because of the unique properties, SHFRC can find special applications which require large energy absorption, controlled crack width and high impact and fatigue resistance. Stand-alone applications include the cement boards and roofing tile. Some structure applications include the beam-columns connections in earthquake resistance frames [Krstulovic-opara et al. 2000], selected plastic hinge, and the disturbed regions near the anchorages at the end of prestressed concrete girders, etc [Dogan et al. 2000]. SHFRC have been used in repair application, retrofit and strengthening such as in tunnel lining by shotcreeting, expansion joint and cover repair [Naaman 2000]. In particular, these unique properties of SHFRC make it ideally suitable for bridge deck overlays [Krstulovic-opara et al. 1995], pavement overlay [Zia et al. 1994] and industry floor. And it is so called ultra-thin white topping on the deck or pavement base [Scott 1998], which is cost-efficient and relatively easy to construct. By using this ultra-thin white topping, the cracking of overlay caused by shrinkage–induced stress, thermally-induced stress, and fatigue-induced stress is controlled and minimized. The thickness of overlays could be reduced when sufficient

fatigue life is provided. Moreover, as fiber has the potential to reduce the cracking opening in SHFRC, the long-term permeability of the material has been tremendously reduced.

## 1.4 Parameters Affecting Strain Hardening Response in Fiber Reinforced Concrete

Various parameters could affect the postpeak ductility of the discontinuous fiber concrete in a matter of combination. Those parameters relating to the reinforcement include the type of fiber, fiber volume ratio, fiber aspect ratio (the length of a fiber divided by its diameter), fiber orientation, state of fiber dispersion and the degree of adhesion to the matrix. The selection or presence of these primary variables is in turn influenced by the matrix type, the presence of additives, and the processing conditions. The latter acts through controlling the state of dispersion, establishing a fiber orientation pattern and enhancing the adhesive bond between fiber and matrix [Shao et al. 2000].

As there were many different discussions about the parameters affecting the strain hardening response, it is generally agreed that the fiber-matrix interfacial bond plays major role in achieving hardening behavior [Li 1991]. Microstructure between steel fiber and cement interface was examined by scanning electric microscope with the observation that several different weak regions may exist in the zone around the interface [Bentur et al. 1985]. Moreover, the interfacial characteristic of FRC could not be discussed only in terms of simple parameter such as interfacial bond, since the interfacial zone is quite complex and can not be adequately accounted by the simple pull out model [Tjiptobroto et al. 1993].

Fiber type is another important factor to achieve strain-hardening behavior. It was studied that the properties of fibers had significantly influence on multiple cracking

mechanism [Chen et al. 1996]. As for the requirement of sustaining first crack stress, fibers should have sufficient tensile strength. As for the requirement of transferring loading in the matrix, the fiber should have the ability to be stretched and good bond property to the matrix. Therefore, the fiber type used in postpeak ductile fiber reinforced concrete should meet requirement: high tensile strength, low modulus and good bond to concrete matrix.

## 1.5 The State-of-The-Art of SHFRC

Study of SHFRC has not been well documented. The material is still considered as an exotic family because of the lack of sound understanding. Currently, most previous studies were focused on fiber reinforced cement paste and mortar, which are called strain hardening fiber reinforced cement composites. With certain quantity of fibers, the reinforced cement paste and mortar are relatively easy to produce as well as strain hardening behavior. Strain hardening cement paste and mortar have achieved significant improvement in properties of cement products.

How to achieve fiber reinforced concrete with strain-hardening behavior is not readily available. It is a challenge to achieve SHFRC while also allowing more coarse aggregate to be mixed with less cement content. It is likely that since the paste content is reduced when more coarse aggregates are used, the binder which allows the fiber transferring the load is decreased. There is no single dominant parameter which controls the postpeak ductile response in SHFRC. Therefore, it is not easy to make the strain hardening FRC and more difficult to quantify and evaluate this strain hardening FRC which allows the use of coarse aggregates.

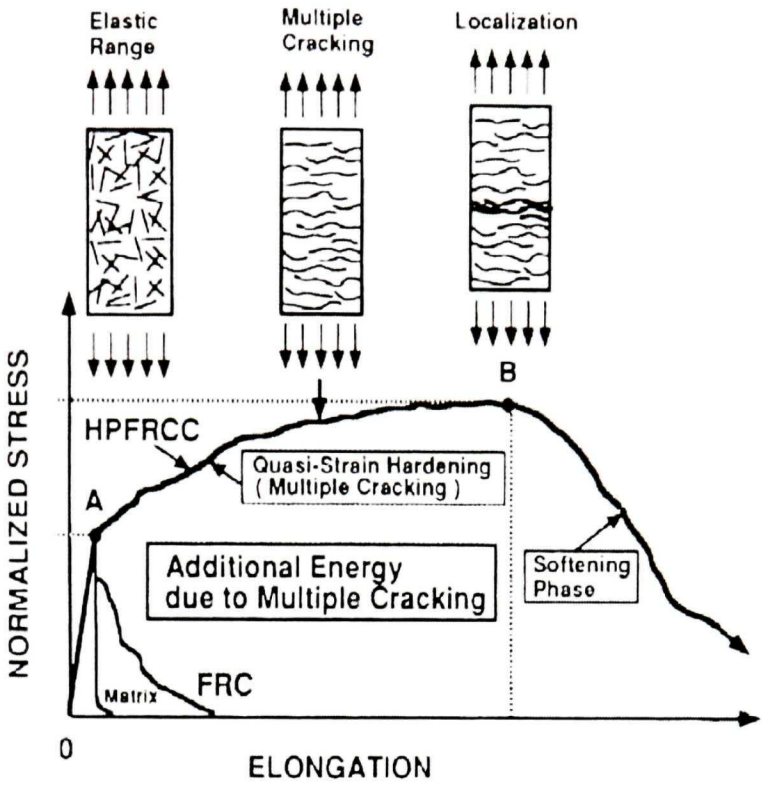


**Figure 1.1 Explanation of "Multiple Cracking Mechanism" and Effect of Fibers on Energy Dissipation Capacity [Naaman et al. 1995]**

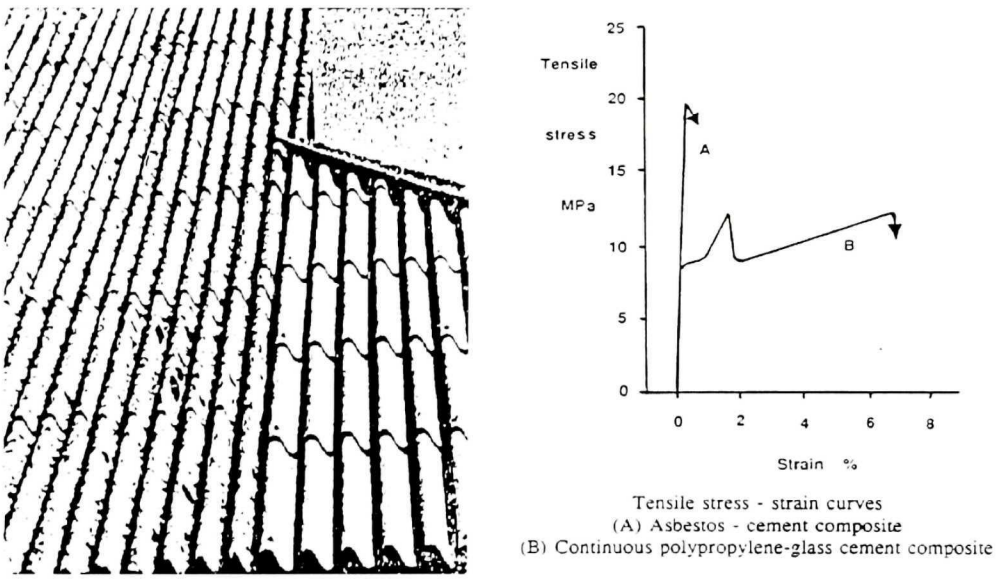


**Figure 1.2 The comparison of roofing tile made by different materials after big hale storm.**

# Chapter 2 Literature Review

Studies on the fiber reinforced concrete with postpeak strain hardening are limited. Most studies were focused on fiber reinforced cement paste and mortar composites. Steel fibers, polyethylene fibers, PVA fibers and carbon fibers were employed to fabricate strain hardening fiber reinforced cement composites.

## 2.1 Steel Fiber Reinforced Concrete

Steel fiber is mostly common used fiber type in FRC for structural application, since it is not only economical but also has good properties, such as high tensile strength, good thermal compatibility with concrete. Steel fiber reinforced concretes have been in use since early 1960s, including structural and non-structural application, such as hydraulic structures, industrial floor [Robinson et al. 1991], thin shell structures, etc.

Addition of steel fibers improve concrete with higher flexural strength, fatigue strength, toughness and the ability to resist cracking and spalling. The extent of improvement in the concrete properties varies based on the type and quantity of fiber used and the quality of the concrete matrix [Li et al. 1996]. Steel FRC usually exhibits the strain-softening response, and the improvement of toughness is from fiber pull out process when high volume fraction and long length fibers are applied [Krstulovic-Opara et al. 1995].

A special strain hardening steel FRC was developed by B.P. Hughes [1977]. A basic concrete matrix having the proportions 1.5: 2.5: 1.0: 0.49 and aggregates having maximum size of 10mm were used. There were two size specimens tested by flexural test. The concrete for the 102 × 102 × 508mm beams was reinforced with1.5% by volume

of different fibers, which included round straight and Duoform steel, crimped steel(GkN) and hooked steel (Bekart). The concrete for the 102 × 152 × 2135mm beams were reinforced with 2% by volume of 0.64 × 59 mm ordinary and double-indented Duoform steel fibers. After finish curing either at fog room (17-20°C and 90% R.H) or curing tank (18 ± 1°C), the beams were tested with Avery 1000KN machine. The so-made FRCs achieved quasi strain-hardening behavior reflected by load-deflection curves without any special admixture, as is shown in Figure 2.1. The results showed that the addition of 0.64 × 59 mm ordinary Duoform steel fibers approximately doubled the ultimate flexural strength. Similar improvements were achieved with hooked fiber. The fracture toughness (as indicated by the area under the load-deflection curves) produced by beams reinforced with these two fibers were considerably greater than that of other forms of fibers, such as round and small-diameter fiber, indicating the importance of an efficient form of mechanical anchorage by longer fibers. Therefore, it was conclusive that as to steel fiber, the strong mechanical bond with matrix could be achieved by the long and hooked end fiber. There was no information about the cracking pattern. With steel fiber addition, it was the ONLY example of strain hardening steel FRCs with course aggregates through literature review.

## 2.2 Fiber Reinforced Cement Paste with Plasma-Treated Polyethylene Fiber

Victor C. Li et al. did extensive research on fiber reinforced cement paste and mortar with strain-hardening response. To make these special materials, he found that the polymer fibers had certain advantages over other fibers. However, they also had limitations. In the case of polypropylene fiber, poor adhesion and wettability to a

cementitious material was one of them. To enhance the interfacial bond of polypropylene fiber reinforced cementitious composites, the surface modification of fiber by the cold gas plasma was applied. The presence of polar functional chemical groups on the fiber surface enhanced reactivity. Therefore, although polyethylene fiber had the unique characteristics of poor interfacial bond strength with cementitious matrices, the plasma treatment process improved the interfacial bond strength by 100% over untreated fiber as well as achieved strain-hardening behaviors [Li et al. 1994] (Figure 2.2). And the matrix designed was cement paste matrix with w/c ratio of 0.4.

A polyethylene fiber reinforced mortar was produced to study ductile fracture in fiber reinforced cementitious materials [Maalej et al. 1995]. It explained the cracking mechanism of strain-hardening FRCs in microstructure level. When fracture of brittle materials was characterized by a very small microcrack zone at the crack tip typically of submillimeter scale with low energy absorption, the fracture of ductile strain hardening cementitious composites could be expressed as an expanded zone matrix cracking surrounding the crack tip prior to crack propagation. This expanded zone was created by the stress transfer capability of the reinforcing bar, in a manner similar to multiple cracking process. The stress-displacement curve of strain hardening polyethylene fiber reinforced mortar is shown in Figure 2.3. The fiber used had a length of 12mm and a diameter of 38μm, and the fiber volume ratio was 2%. And finally, it was demonstrated that cementitious materials could be made to fail in a ductile fracture mode if the material was properly reinforced with fibers so that strain-hardening occurred after its first crack.

It was concluded that high strain capacity and fracture resistance observed in the polyethylene fiber cement paste could be obtained with other types of fibers, if conditions

for strain hardening behavior were satisfied in term of micromechanics [Li et al. 1992]. A critical fiber content was then defined by the fracture mechanics.

## 2.3 Polyvinyl Alcohol (PVA) Fiber Reinforced Concrete

Among polymeric fibers, PVA fiber is a relatively new fiber and durable in the alkaline environment present in concrete [Garcia et al. 1997]. Then, with respect to the mechanical properties, PVA fibers are characterized by a higher tensile strength around 0.9 GPa, more significantly, low modulus of 29 GPa, and hydrophilic surface which creates a strong chemical bond with cementitious material. When cracks are generated in the matrix, the high tensile strength of the fiber sustains the first crack stress and resists the pulling out force due to good bond with the matrix. Low modulus of fiber helps elongating and transferring the load to other place, distributing load over the whole loading surface. In addition, the cost of PVA fiber is about 1/8 that of high-modulus polyethylene fiber, and even lower than that of steel fiber on an equal volume basis [Li et al. 2001]. Therefore, PVA fiber is considered as a promising alternative reinforcement to achieve strain-hardening cementitious materials.

Previous research works included a PVA fiber reinforced cement matrix composites fabricated by extrusion process [Shao et al. 1997], PVA fiber reinforced cement composites with addition of soluble PVA powder and temperature treatment [Garcia et al. 1997], and cementitious composites containing 2% of PVA fiber with surface oil coating [Li et al. 2001].

Extrusion process fabricated PVA fiber reinforced cement composites were produced by Shao et al. [1997]. Extrusion process is a continuous mass production method, which is

capable of applying additional compressive and shear forces to compact fibers with matrix and aligning fibers in the load-bearing direction. By this process, not only the bond between matrix and fiber is strengthened, but also fibers have more effect to take and transfer the load, thus develop the strain hardening response with multiple cracking. Fiber volume between 2.2 to 4.2% with a length of 4mm to 6mm in a cement paste matrix were investigated. Mechanical properties including tensile and flexural response were tested. In addition, the microstructure of interfacial bond between PVA fiber and cement matrix was studied by scanning electron microscope and Laser Moire Interferometry test. The results showed that PVA fiber reinforced cement paste exhibited high tensile strength and exceptional postpeak toughness, while all the batches designed with a high fiber volume higher than 2% achieved strain hardening response in tension and flexure. Behavior in tension is shown in Figure 2.4. By Laser Moire Interferometry test, it was observed that the preferred orientation of fibers and the spatial distribution of fibers contributed to the multiple matrix cracking formation, and then developed the strain-hardening type of behavior.

Garcia et al. [1997] investigated on the possible use of PVA short fibers as reinforcement in cement based matrices. Two different long PVA fibers (4mm and 12mm) and two matrix mix composition were tested by three point bending test, along with different test variable: addition of a soluble PVA powder to mix; temperature treatment (including curing at 130°C for 20 minutes or 230°C for 10 minutes); mechanical abrasion of fibers' surface. Fiber volume fraction of 2% was used. The results indicated that the use of 2% by volume of PVA fibers in cementitious matrices generally led to multiple cracking and pseudo-strain hardening behavior. The longer the fiber, the

greater strain capacity. Both of addition of PVA powder and the heat treatment of 130°C could improve the bond properties and ultimate deflection (shown in Figure 2.5), respectively.

Victor C. Li et al. [2001] also studied strain hardening fiber reinforced mortar containing 2% of PVA fiber with surface oil coating. He noticed that the strong chemical bond between matrix and fiber led to the rupture of a bridging fiber rather than pullout during the opening of a matrix crack. Therefore, a fiber surface oiling was applied to weaken bond. The mortars having sand to cement ratio of 0.5 to 1.2 with fiber content of 2% to 2.5% treated by oil coating of 0.3% to 0.8% were tested to search for an optimal and practical mixture proportioning of strain hardening cement mortar. All the specimens showed clear pseudo strain hardening behavior. Moreover, the stress-strain curves indicated that PVA fiber reinforced mortar with 0.5% and 0.8% oiled fibers had better overall performances with 0.3% oiled fibers in term of strain capacity and ductility.

## 2.4 Slurry Infiltrated Fiber Concrete (SIFCON) and Slurry-infiltrated mat concrete (SIMCON)

SIFCON is made by infiltrating of mortar slurry into a fiber network made of high fiber volume fraction of discontinuous fiber (more than 10%), while SIMCON is made by infiltrating slurry into continuous fiber mats with fly ash and fiber volume fraction of more than 5% [Krstulovic-Opara et al. 1995], as is shown in Figure 2.6. The fiber mostly used is steel fibers. These special fiber reinforced concretes exhibit unparalleled improvement in strength, toughness, fatigue resistance, crack control, compared with

conventional steel fiber reinforced concrete [Krstulovic-Opara et al. 1995, 2000], as is indicated in Figure 2.7.

The SIFCON and SIMCON have found applications. They were used in bridge deck overlay with reduced thickness due to the increased impermeability, durability, and service life of the overlay. The improvements were indicated by the previous successful use of SIFCON in a number of repair applications, including: 1) 1 in thick overlay of a deteriorated concrete parking lot. Core samples taken 9 years after the construction showed that the overlay was still tightly bonded to the old concrete, and there was no sign of fiber corrosion or penetration of chloride salts [Lankard 1983]. 2) Precast SIFCON panels were placed over a fleshly poured concrete sub-base at an airport gate parking lot. Panels were 8 ft by 10 ft by 2in and were designed to support the main wheel carriage of a Boeing 727. Slab indicated no cracking after 1 year of service [Lankard 1985].

The mechanical properties of SIMCON including tensile stress-strain behavior and flexural load-deflection relation were reviewed by Zeng et al. [2000]. SIMCON with a fiber volume fraction of 3.3% had improved strength and ductility, which made it a potential overlay material. The permeability test indicated that the relative permeability of SIMCON overlay before cracking was about 25% that of plain concrete.

The other applications of these two strain hardening fiber reinforced cementitious composites included the retrofit of existing structural members by wrapping around or laying over the member, manufacture of thin element such as jacket and stay-in-place formwork, cast-in-place connection and beam-column subassemblages in seismic application [Krstulovic-Opara et al. 2000].

It is conclusive that fiber reinforced cement composites with strain hardening behavior are readily available for applications. However, most of the successful examples were developed based on the matrix of cement paste or mortar with special techniques. For fiber reinforced concrete with coarse aggregates, to achieve the strain hardening type of response is still a challenge.

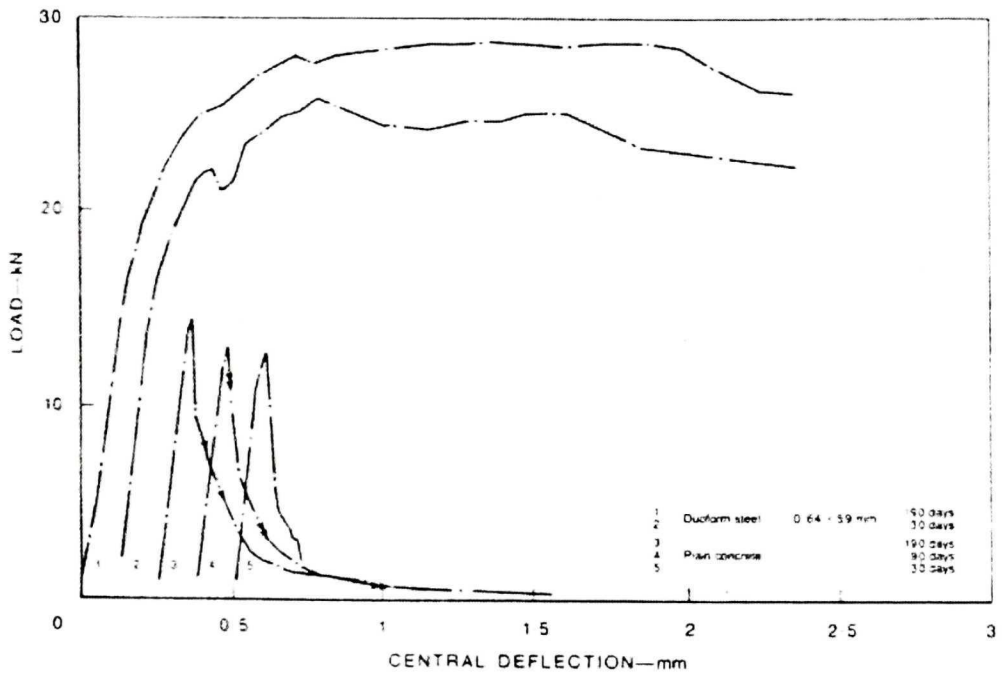


**Figure 2.1 Load-Deflection curves for plain concrete beams and beams reinforced with Duoform Steel fibers [Hughes 1977]**

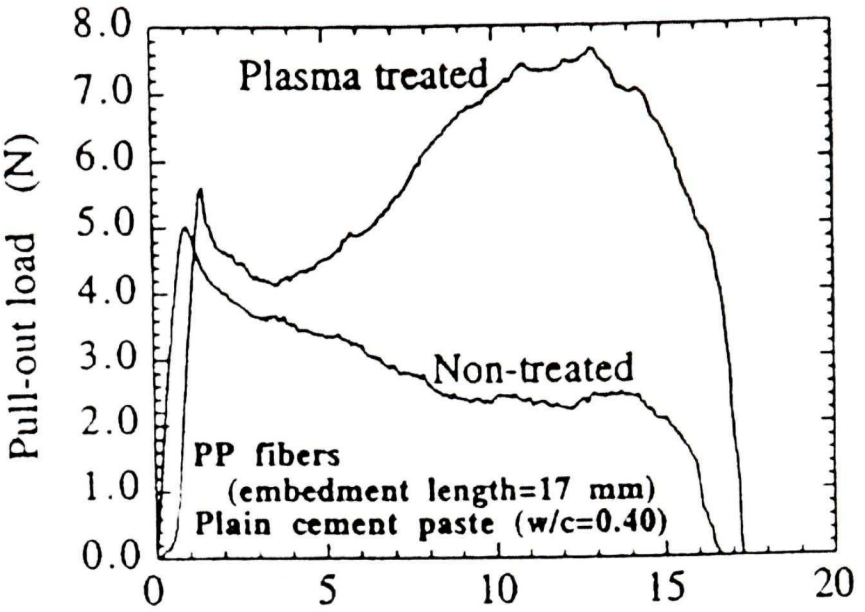


**Figure 2.2 Comparison of pull-out curves of treated and untreated pp fiber [Li et al. 1994]**

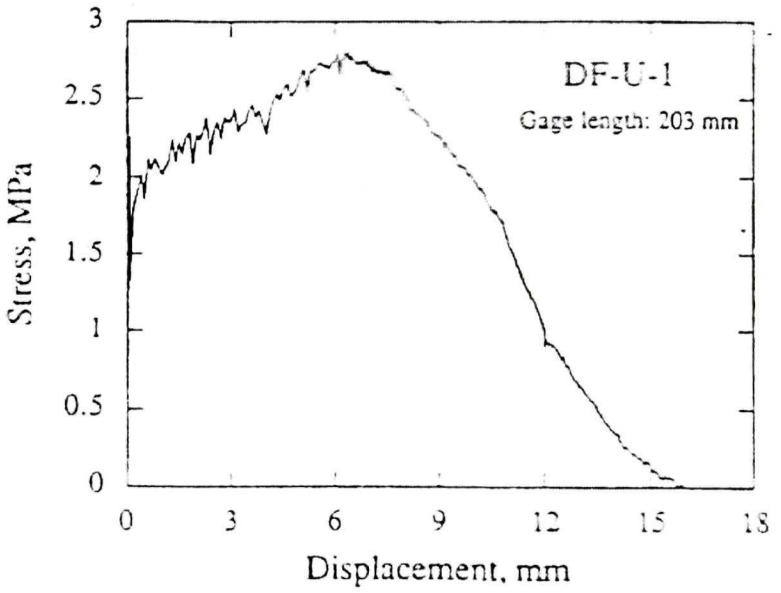


**Figure 2.3 Stress-deflection relation of polyethylene fiber reinforced mortar ($V_f$ = 2%) [Maalej et al. 1995]**

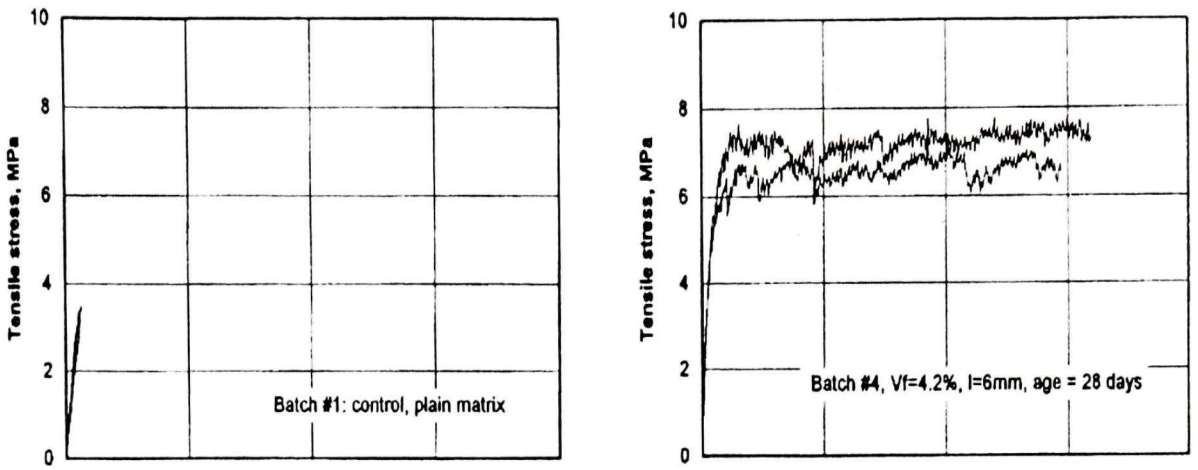


**Figure 2.4: Comparison of tensile stress and strain curves of extruded cement matrix (left figure) and extruded cement composite (right figure) [Shao et al. 1997]**

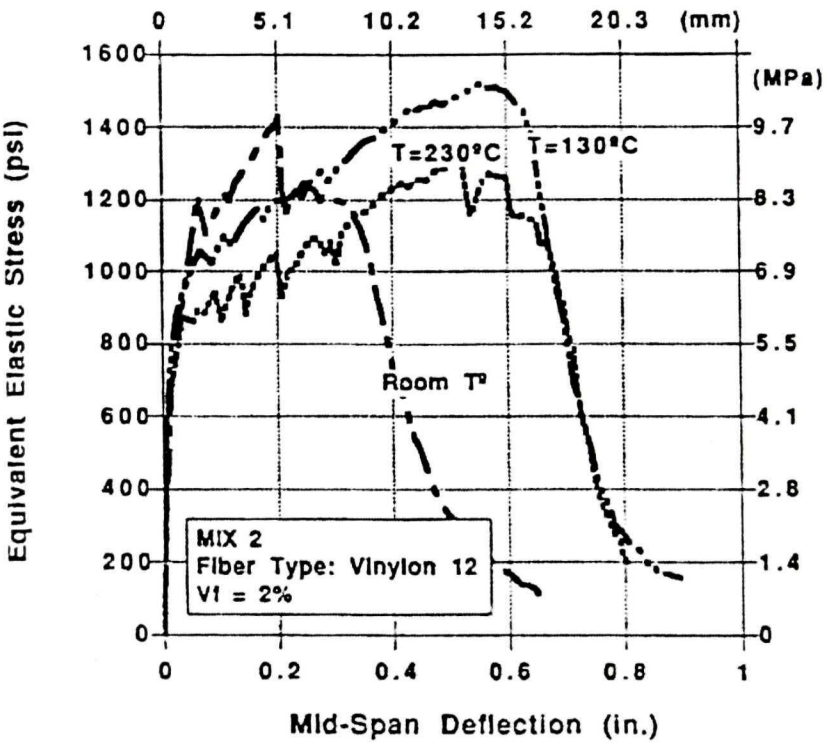


**Figure 2.5 Influence of temperature treatment of the specimen after curing on the bending response of Mix 2 with PVA fiber (12mm length) [Garcia et al. 1997]**

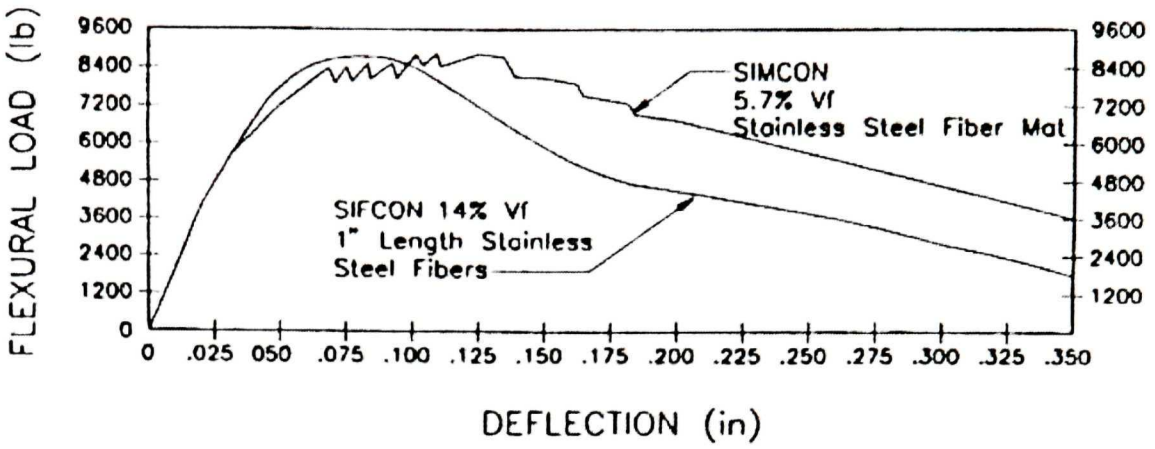


**Figure 2.6 Load-deflection behavior of SIFCON and SIMCON beam specimen in three-point loading [Krstulovic-Opara et al. 2000]**

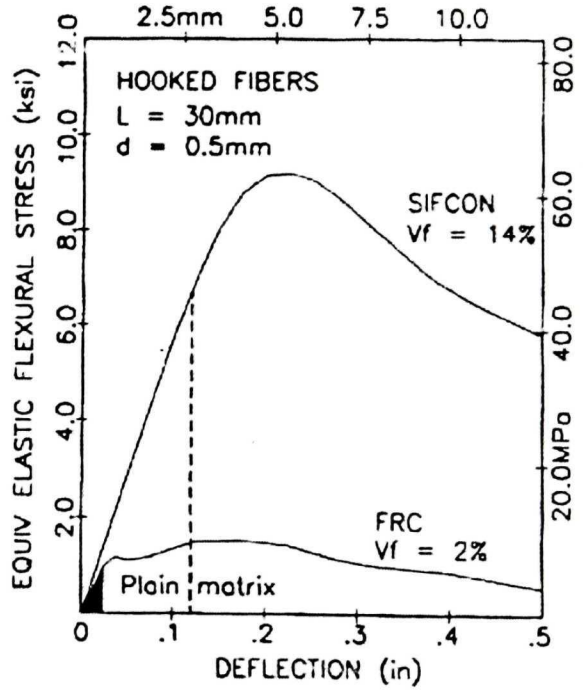


**Figure 2.7 Comparison of load-deflection curves for SIFCON, conventional FRC, and plain matrix [Krstulovic-Opara et al. 1995]**

# Chapter 3 Objectives

The main objective of this study is to explore the possibility of making fiber reinforced concrete with strain hardening response. The specific objectives are described below:

**1. To investigate the mixture proportion to achieve strain hardening behavior.**

To achieve strain hardening fiber reinforced concrete (SHFRC) with coarse aggregate is not straightforward. The coarse aggregates added are to replace partially the cement binder, leading to less binder in the mix and weaker interfacial bond between fiber and matrix. Therefore, in the first part of this research work, a rich cement matrix mix, which allows certain quantity of coarse aggregates, was designed with the volume ratio of cement paste equal to the volume ratio of aggregates including the fine aggregates and coarse aggregates.

To achieve SHFRCs, two methods were investigated in this research, polymer modification and hybrid fiber FRC system. To enhance the bond characteristic between fiber and matrix, matrix modification was developed. Methylcellulose (MC) was added to help disperse fibers dispersion, and enhance the bond between fiber and matrix.

In the hybrid system, two types of fibers were used, PVA fiber and steel fiber. The former which was polymer fiber, with hydrophilic surface, low modulus, and high strength, was claimed to have good chemical bond with matrix. The latter was metallic fiber, mostly used fiber type in FRC for structural applications. It had high tensile strength to increase first peak strength, hooked ends to improve the mechanical interlock.

Furthermore, the weathering effect on durability of SHFRCs in severe exposed environment was also examined. Two experiments were conducted, freeze-thaw cycling and shrinkage test.

2. **To examine the possibility of obtaining fiber reinforced concrete with strain hardening response using low cement content.**

In this phase, normal strength concrete designed for applications in overlays was studied with less cement content. The purpose was to see if it was possible to obtain strain hardening behavior with a normal strength mix. Long PVA fiber and deformed steel FRCs were applied to establish a hybrid system. Flexural behavior of this hybrid FRCs was studied.

3. **To quantify and evaluate the toughness index for SHFRC.**

Toughness, defined as a measure of the energy absorption capacity under flexion was used in this project. The current methods of measuring toughness index of fiber reinforced concrete might not be suitable to quantitatively reflect strain-hardening behavior under flexion. A modified toughness method was examined to evaluate the SHFRCs. And the design consideration of toughness concept was also discussed.

4. **Methodology.**

Comparing the properties of different fibers, the most suitable fiber for use to achieve strain-hardening behavior in FRC is PVA fiber. PVA fiber has high tensile strength close to steel fiber, low modulus which is only 1/10 that of steel fiber leading to the ability of transferring the load and distributing load, and hydrophilic surface which provide good chemical bond to cementitious material and sustain the load. The other fibers, such as polypropylene fiber, which has low tensile strength, and glass fiber, which could be

subjected to a physical attack by calcium hydroxide crystals leading to a decrease of ductility, were not suitable in the new system. Two different length PVA fibers were used in the project, the short fiber in rich cement mix, and long fiber in low cement matrix.

To enhance the bond characterise between fiber and matrix, matrix modification was developed. According to previous studies, there are many admixtures such as polymer products and latex which could lead to significant improvement in the flexural strength and toughness characteristic. And it is discovered that when the fiber bundles are mixed with polymer-modified matrix, the fiber filaments are surrounded by the polymer particles and thus protect against the migration of products. However, since the suggested dosage of polymer and latex used in concrete was about 15 percent weight of cement [Chen et al. 1996], considering the application and cost, they are not recommended in this project. Methylcellulose (MC), a type of water-soluble polymer, has been used commonly as an antiwashout admixture, was chosen as a product for matrix modification. Methylcellulose modifies the rheological properties of fresh concrete by reducing external bleeding and significantly enhancing resistance of concrete to water dilution and segregation. In engineering practice, it provides water retention for proper curing, improved workability and pumpability for cement paste [Khayat 1995]. The suggested dosage is 0.4 to 0.8 percent by weight of cement [Fu et al. 1998]. Although the mechanism how the MC change the properties of matrix is not well documented, it has been proved that MC added to cementitious matrix could help the fiber dispersion, and enhance the bond between fiber and matrix.

An alternate way was developed to keep the strain hardening behavior and high-energy absorption without admixture addition, which is hybrid fiber system. Steel fiber, the economical product with high strength was considered to use in this study. Steel fiber

reinforced concrete was well studied in the previous work, and it has been proved that steel fiber reinforced concrete showed high flexural strength and strain-softening behavior under four-point loading. Relative high energy absorption was found due to high first crack strength and pull out process of fiber after crack localization. Therefore, using a hybrid system with use of both steel fiber and PVA fiber, it is possibly that the new system could achieve strain hardening behavior with high total energy absorption. Different length and different end shaped steel fibers were chosen in hybrid system for study and comparison of fiber contribution to strain hardening behavior.

# Chapter 4 Experimental Program

## 4.1 Materials

ASTM type 10 Portland cement was used in all batches. The fine aggregates used were river sand having a finess modulus of 2.3, and the coarse aggregates were crushed limestone with maximum aggregate size of 9.5mm. All aggregates were washed and air dried. The effective moisture absorption was 0.9% for the coarse aggregates and 1.0% for fine aggregates.

Chemical admixtures were used in some batches. There were air entraining agent (Microair, Master Builder); Superplastizer, (CONCHEM SPN, Master Builder); Antifoamer, (Surfynol DF110D, Air Product); Methylcellulose, (F4M, Dow Chemical), was used in an attempt to enhance the bond as described in methodology. As a side effect, methylcellulose modification entrains a large number of air content into concrete, which may cause negative effect to the properties of concrete. Antifoamer is therefore employed to reduce the air volume.

Five different fibers were used in this project: Two polyvinyl alcohol (PVA) fiber (Kuraray Co., Japan): short fiber (length = 12mm, diameter = 0.2mm), long fiber (length = 30mm, diameter =0.66mm); Three different steel fibers (Sunny steel Wool Co, China): Flat end steel fiber (Length = 26mm, diameter = 0.7mm), hooked flat end steel fiber (length = 32.9 mm, diameter = 0.5mm), Microsteel fiber (length = 16mm, diameter = 0.25mm). The hooked flat end fibers are recently developed new fibers. The fiber combines two different shape, hooked angle close to the end with pressed flat end. It is hoped the combined end will provide better mechanical bonding with the concrete. The geometries

and properties of fibers are shown in table 4.1. Figure 4.1 to Figure 4.5 show these five types of fibers.

## 4.2 Sample preparation

Fine and coarse aggregates were firstly dry mixed for two minutes. Cement was then added to mix for another two minutes. Water was then added for at least four minutes. The air entraining agent or antifoamer was added if necessary. If methylcellulose was used, it was added to the cement and dispersed in dry. The concrete was then mixed again for another three minutes after the fibers were added. This procedure was followed for the control and all fibrous batches.

The mix was cast into mould to make cylinder specimens with dimension of 50mm(diameter) × 100mm(height), beam specimens with dimension of 25mm × 75mm × 350mm, dimension of 50mm × 75mm × 350mm, dimension of 100mm × 100mm × 400mm, ring specimens with dimension of 50mm (thickness) × 152mm. The samples were demoulded one day after casting, and kept in a moisture room with temperature of 25°C and relative humidity of 100%. The specimens for drying shrinkage tests were placed in an environmental chamber where the temperature ranged in between 28°C to 31°C and the relative humidity ranged in between 20 % to 25 %.

Three different mixture proportions were investigated. They were cement rich mix with polymer addition; cement rich mix with hybrid fibers and normal cement content mix.

### 4.2.1 Cement rich mix with 12 mm Long PVA fiber and polymer addition

Mix proportion was designed based on the volume method. The total volume of the paste (cement + water) represented the binder that had ability to bond with aggregates and fibers. It was selected that volume of cement paste equal to the volume of aggregates, including the fine aggregates and coarse aggregates, leading to a cement rich mix.

In this mix proportion, water to cement ratio by weight was kept at 0.4 for all the batches, and the designed compressive strength was 50MPa. PVA fibers of 12mm long and flatend steel fiber of 26 mm long were used. Six batches were designed in this series. The mixture proportions by volume and by weight are shown in Tables 4.2 and 4.3, respectively. Fiber volume content of 2% was kept constant for all fiber concretes. The control concrete (#1) was plain concrete. Batch #2 was PVA FRC as reference for other fiber batches. Batch #3 was steel FRC for comparison. Batch #4 (MCPVA2) was PVA fiber reinforced concrete with methylcellulose addition without antifoamer, and batch #5 was the same as batch #4 but with antifoamer to reduce entrained air content. Batches #1 to #5 used coarse aggregates with maximum aggregate size of 9.5mm and a volume ratio of 25%. PVA fiber reinforced mortar in batch #6 had no coarse aggregates. The volume ratio of paste to fine aggregates was 2:1. It was intended to investigate the effect of coarse aggregate content on the hardening behavior.

### 4.2.2 Cement rich mix of hybrid PVA-steel fibers

The hybrid technique using PVA fibers with steel fibers was also considered to improve the strain hardening behavior without special admixture addition. Steel fiber reinforced concrete was well studied in the previous work, and in most cases, it had

shown strain softening behavior under flexion. However, relative high energy absorption was found due to improved first crack strength and pull out process of fiber after first crack localization, it is probably because the strong mechanical bond between fiber and matrix. Therefore, a concept of hybrid system using both steel fibers and PVA fibers was introduced.

Another six batches were designed and shown in Tables 4.4 and 4.5. The matrix design of batch #7 to #12 were the same as batch #1 to #6, that is, volume of cement paste equal to the volume of aggregates including the fine aggregates and coarse aggregates. Two volume fractions of PVA fibers of 12mm long were chosen, 2% and 1%. Hooked flat end steel fiber and microsteel fiber were used, and the volume ratio of steel fiber was chosen as 0.4%, equivalent to $30Kg/m^3$.

In Table 4.4 and 4.5, Batch #2, PVA FRC was listed as a reference. Batch #7 was hybrid PVA (2%) with microsteel fiber(0.4%) FRC. By using some microsteel fibers, it was expected that the first crack strength would be improved. Batch #8 was microsteel FRC as control. The contribution of microsteel fibers to strain-hardening behavior would be investigated by comparing batch #2 and batch #7. Batch #9 was hybrid PVA (2%) with hooked flat end steel fiber (0.4%) FRC, while batch #10 was reinforced by hooked flat end steel alone. By using certain amount of long steel fiber, it was hoped that steel fiber would contribute the energy absorption by providing more resistance to the pull out.

Batch #11 and batch #12 were two batches with exactly same matrix with 1% PVA fiber volume. Batch #12 was hybrid system with microsteel fiber with a content of 0.4%. The effect of PVA content on strain-hardening behavior would be investigated by

comparing batch #2 with batch #12. And again, microsteel fiber contribution would be examined under the condition of less PVA fibers in FRC.

### 4.2.3 Normal strength mixture proportion with 30mm PVA fiber

In this series, for the purpose of those applications in bridge deck overlays and pavements, a normal strength matrix was designed. The purpose was to see if it was possible to obtain strain-hardening behavior with a normal strength mix with less cement content. Designed compressive strength was around 40MPa. The mix design proportions are given in Table 4.6 and 4.7.

Four batches were studied. Batch #13 was PVA FRC with 2% PVA of 12mm long, and batch #14 was exactly the same as that of batch #13 except that longer PVA fiber (30mm long) was used in order to investigate the fiber length effect on strain hardening behavior. Furthermore, hybrid concept was used here again. Batch #15 was PVA FRC (2%) with hooked flat end steel (0.4%), and batch #16 was reinforced with hooked flat end steel fiber (0.4%) only. The contribution of PVA and steel fiber to strain-hardening behavior was investigated in a normal strength matrix with 445 $Kg/m^3$ cement.

## 4.3 Experiments for performance evaluation

### 4.3.1 Tests on properties of fresh concrete and compressive strength

Properties of fresh concrete, such as slump and air content were measured according to ASTM C143 & ASTM C231. The test performed for all the batches.

Compression tests followed ASTM C39. Small cylinders with diameter of 50mm and length of 100mm were cast and tested in compression at the age of 28 days. The small

size of specimen was chosen because of the use of small size of coarse aggregate. Three cylinders were tested for each batch. The compression tests were conducted on a MTS testing machine and the loading rate was constantly 0.2 mm/min till failure. The tests were performed for batch #1 to batch #12.

### 4.3.2 Four point bending tests and flexural toughness

Four point bending test was used to examine the strain-hardening behavior of FRC. At least three samples for each batch were tested on a span of 304-mm referred by ASTM method. The specimens were dried and placed in the 4-point flexure-testing setup. The LVDT was placed at midspan in the centre of the bottom surface to measure the displacement during flexure, and mid-deflections were then obtained. The flexural test was performed for all the batches. However, the specimens had different thickness. Batch #1 to #12 had a thickness of 25mm to simulate the thin repair of concrete structure using the SHFRC; size of 50mm thick, 75 mm wide and 350 mm long were cast for batch #13 to batch #16. Batch #13 to #16 were of 50mm thick in order to find application in bridge deck overlays and pavements using the SHFRC.

To quantify the strain-hardening behavior, the flexural toughness concept was used. JCI SF4 was firstly used to quantify the flexural toughness in this research. In JCI method, $T_{JCI}$ is defined in absolute terms as the energy required bending the fiber-reinforced beam that is defined under the load-deflection curve to a midpoint-deflection of L/150 of its span.

As applied as thin repair and bridge deck overlays and pavements, whether the new system can maintain its strain-hardening behavior under severe exposed condition or not

become major concern. To examine the durability response of these FRCs under severe condition, two experiments were conducted for examining durability purpose: freeze-thaw tests (under freeze- thaw cycling) and drying shrinkage test (under drying environment).

### 4.3.3 Freeze-thaw tests

Samples of 25mm thick, 75 mm wide and 350 mm long from batch #1 to #12 were tested under freeze-thaw cycles. After 14 days curing in moisture room, three samples for each batch were placed in freeze – thaw cabinet for cycling and three remained in standard curing chamber at ambient temperature. According to ASTM C666, Procedure A, samples were saturated in water and cycled between +5 °C to –17 °C. Each cycle took about 3-4 hours to complete. After the freeze – thaw cycles reached to 200, the cycled and uncycled specimens were evaluated at the same age of 56 days by four point bending tests as described above. Freeze-thaw test was only performed for first series and second series (including batch #1 to batch #12), since the design of third series used the same concept as the first two series, and it was not necessary to repeat the freeze-thaw test.

### 4.3.4 Drying shrinkage tests

Based on the previous studies, fiber reinforced concrete had shown beneficial effects in counterbalancing the movements arising from volume changes taking place in concrete during drying, and fibers tended to reduce the movements at early age of concrete when compared to plain concrete.

Therefore, free shrinkage test was performed in accordance with ASTM C341 on 400mm long specimens with a 100mm square cross section. Two Specimens for each batch were tested. Samples were covered with plastic to prevent water loss and maintained at standard room temperature after casting for one day. And all specimens were demoulded and stored in environmental chamber at 20-25% relative humidity and at 30° C. The demec points were glued on the surface of specimens to measure the drying shrinkage. The readings were taken twice a day in the early age and everyday in the later age. And the weight losses were also measured simultaneously.

The primary advantage of fibers in relation to shrinkage is their effect in reducing the adverse width of shrinkage cracks under restrained condition. When shrinkage cracks arise because the concrete is restrained from shrinkage movements, the presence of fibers delays the formation of first crack, enables the concrete to accommodate more than one crack and reduces the crack width substantially.

To compare the effect of different FRC on the restrained shrinkage characteristics, restrained shrinkage tests using a steel ring was conducted. The steel ring with the inner diameter of 254 mm, the thickness of 25mm was obtained by cutting a round mechanical tube. A cardboard tube with inner diameter of 407mm was used as outer mould. Both of these rings were placed concentrically on a wooden base so that the free space between them could be filled with the concrete mixture. The sketch is shown in Figure 4.6. With these dimensions, it could be shown that the concrete ring was subjected to internal uniform pressure. The outer mould was stripped off 1 day after casting, while the upper side of the concrete ring was sealed off using paraffin wax, so that drying would be allowed only from the outer circumferential surface. The specimen was then put into

chamber for drying at 30°C, 20-25% relative humidity. The specimen was investigated at certain age in order to obtain parameters such as first crack age, crack width and crack numbers.

**Table 4.1 Geometries of fiber used in the study**

| Fiber Type | Length (mm) | Diameter (mm) | Aspect ratio | Tensile Strength (GPa) | Surface Property | Modulus (GPa) |
|---|---|---|---|---|---|---|
| PVA Fiber (12mm) | 12 | 0.2 | 60 | 0.9 | hydrophilic | 29 |
| PVA Fiber (30mm) | 30.0 | 0.66 | 45 | 0.9 | hydrophilic | 29 |
| Flat end steel fiber | 26.0 | 0.7 | 37 | 1.2 | hydrophobic | 200 |
| Hooked Flat end steel Fiber | 32.9 | 0.5 | 66 | 1.2 | hydrophobic | 200 |
| Microsteel Fiber | 16 | 0.25 | 64 | 0.4 | hydrophobic | 200 |

**Table 4.2 Mixture proportions based on volume ratio (batch #1~batch #6)**

| Batch Number | #1 | #2 | #3 | #4 | #5 | #6 |
|---|---|---|---|---|---|---|
| | Control | PVA2 | FSteel2 | MCPVA2 | DMCPVA2 | PVA2 mortar |
| cement | 0.221 | 0.217 | 0.217 | 0.215 | 0.215 | 0.289 |
| sand | 0.250 | 0.245 | 0.245 | 0.245 | 0.245 | 0.327 |
| coarse aggregate | 0.250 | 0.245 | 0.245 | 0.245 | 0.245 | 0 |
| PVA Fiber (12mm) | 0 | 0.020 | 0 | 0.020 | 0.020 | 0.020 |
| Flat end steel Fiber | 0 | 0 | 0.020 | 0 | 0 | 0 |
| water | 0.279 | 0.273 | 0.273 | 0.273 | 0.273 | 0.364 |
| Methylcellulose | 0 | 0 | 0 | 0.002 | 0.002 | 0 |
| Antifoamer | 0 | 0 | 0 | 0 | 0.0002 | 0 |

**Table 4.3 Mixture proportions based on weight ratio (Kg/m$^3$) (batch #1~batch #6)**

| Batch Number | #1 | #2 | #3 | #4 | #5 | #6 |
|---|---|---|---|---|---|---|
| | Control | PVA2 | FSteel2 | MCPVA2 | DMCPVA2 | PVA2 mortar |
| cement | 696.15 | 683.55 | 683.55 | 677.25 | 677.25 | 910.35 |
| sand | 650.00 | 637.00 | 637.00 | 637.00 | 637.00 | 850.20 |
| coarse aggregate | 650.00 | 637.00 | 637.00 | 637.00 | 637.00 | 0.00 |
| PVA Fiber | 0 | 26.00 | 0 | 26.00 | 26.00 | 26.00 |
| Flat end steel fiber | 0 | 0 | 156.00 | 0 | 0 | 0 |
| water | 279.00 | 273.00 | 273.00 | 273.00 | 273.00 | 364.00 |
| Methylcellulose | 0.00 | 0.00 | 0.00 | 3.02 | 3.02 | 0.00 |
| Air entraining Agent | 30ml/100 Kg Cement | 30ml/100 Kg Cement | 30ml/100 Kg Cement | 0 | 0 | 30ml/100 Kg Cement |
| Antifoamer | 0 | 0 | 0 | 0 | 0.68 | 0 |
| W/C (By weight) | 0.4 | 0.4 | 0.4 | 0.4 | 0.4 | 0.4 |

**Table 4.4 Mixture proportions of hybrid batches (by volume ratio)**

| Batch Number | #2 | #7 | #8 | #9 | #10 | #11 | #12 |
|---|---|---|---|---|---|---|---|
| | PVA2 | Microsteel-PVA2 | Microsteel | HFsteel-PVA2 | HFsteel | PVA1 | Microsteel-PVA1 |
| cement | 0.217 | 0.217 | 0.221 | 0.217 | 0.221 | 0.219 | 0.219 |
| sand | 0.245 | 0.245 | 0.250 | 0.245 | 0.250 | 0.248 | 0.248 |
| coarse aggregate | 0.245 | 0.245 | 0.250 | 0.245 | 0.250 | 0.248 | 0.248 |
| PVA Fiber | 0.020 | 0.020 | 0 | 0.020 | 0 | 0.010 | 0.010 |
| Microsteel | 0 | 0.004 | 0.004 | 0 | 0 | 0 | 0.004 |
| Hooked flat end Steel Fiber | 0 | 0 | 0 | 0.004 | 0.004 | 0 | 0 |
| water | 0.273 | 0.273 | 0.279 | 0.273 | 0.279 | 0.276 | 0.276 |

**Table 4.5 Mixture proportions of hybrid batches ($Kg/m^3$)**

| Batch Number | #2 | #7 | #8 | #9 | #10 | #11 | #12 |
|---|---|---|---|---|---|---|---|
| | PVA2 | Microsteel-PVA2 | Microsteel | HFsteel-PVA2 | HFsteel | PVA1 | Microsteel-PVA1 |
| cement | 683.55 | 683.55 | 696.15 | 683.55 | 696.15 | 689.85 | 689.85 |
| sand | 637.00 | 637.00 | 650.00 | 637.00 | 650.00 | 643.50 | 643.50 |
| coarse aggregate | 637.00 | 637.00 | 650.00 | 637.00 | 650.00 | 643.50 | 643.50 |
| PVA Fiber | 26.00 | 26.00 | 0 | 26.00 | 0 | 13.00 | 13.00 |
| Microsteel | 0 | 30.00 | 30.00 | 0 | 0 | 0 | 30.00 |
| Hooked flat end Steel Fiber | 0 | 0 | 0 | 30.00 | 30.00 | 30.00 | 0 |
| water | 273.00 | 273.00 | 279.00 | 273.00 | 279.00 | 276.00 | 276.00 |
| Air entraining Agent | 30ml/100 Kg Cement | 30ml/100 Kg Cement | 30ml/100 Kg Cement | 30ml/100 Kg Cement | 30ml/100 Kg Cement | 30ml/100 Kg Cement | 30ml/100 Kg Cement |
| W/C (By weight) | 0.4 | 0.4 | 0.4 | 0.4 | 0.4 | 0.4 | 0.4 |

**Table 4.6 Mixture proportions with 30mm PVA fibers (by volume ratio)**

| Batch Number | #13 | #14 | #15 | #16 |
|---|---|---|---|---|
| | PVA2 | LPVA2 | HFsteel-LPVA2 | HFsteel |
| cement | 0.141 | 0.141 | 0.141 | 0.141 |
| sand | 0.310 | 0.310 | 0.308 | 0.318 |
| coarse aggregate | 0.310 | 0.310 | 0.308 | 0.318 |
| PVA Fiber Length (mm) | 12 | 30 | 30 | 0 |
| PVA Fiber content | 0.020 | 0.020 | 0.020 | 0 |
| hooked flat ends Steel Fiber | 0 | 0 | 0.004 | 0.004 |
| water | 0.178 | 0.178 | 0.178 | 0.178 |

**Table 4.7 Mixture proportions with 30mm PVA fibers (Kg/m$^3$)**

| Batch Number | #13 | #14 | #15 | #16 |
|---|---|---|---|---|
| | PVA2 | LPVA2 | HFsteel-LPVA2 | HFsteel |
| cement | 445 | 445 | 445 | 445 |
| sand | 807 | 807 | 802 | 828 |
| coarse aggregate | 807 | 807 | 802 | 815 |
| PVA Fiber | 26.0 | 26.0 | 26.0 | 0 |
| PVA Fiber Length (mm) | 12.0 | 30 | 30 | 0 |
| hooked flat ends Steel Fiber | 0 | 0 | 32.9 | 32.9 |
| water | 178 | 178 | 178 | 178 |
| AEA dosage | 35ml/100Kg Cement | 35ml/100Kg Cement | 35ml/100Kg Cement | 35ml/100Kg Cement |
| SP (ml/100Kg cement) | 750 | 750 | 750 | 750 |
| W/C (By weight) | 0.4 | 0.4 | 0.4 | 0.4 |

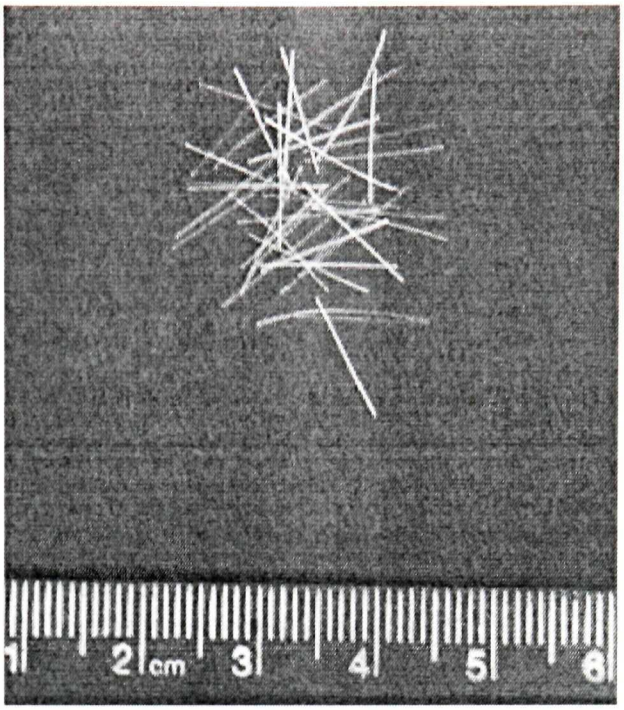


**Figure 4.1 Picture of short PVA fiber (12mm)**

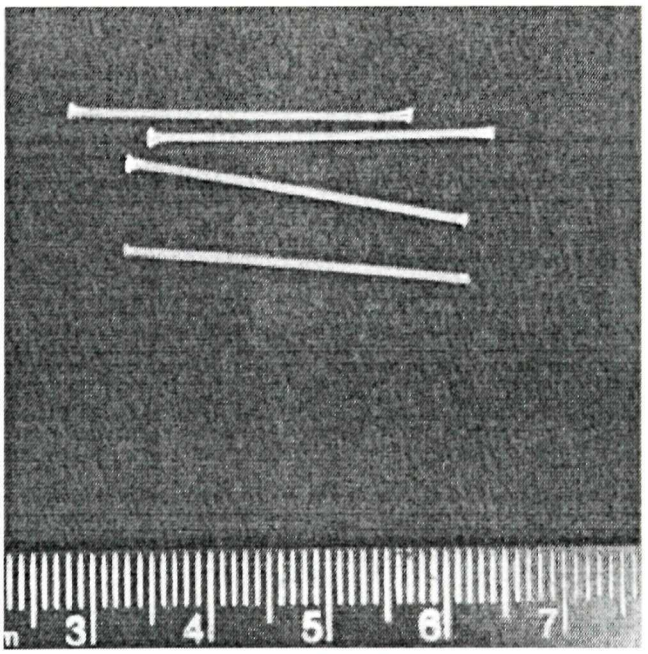


**Figure 4.2 Picture of long PVA fiber (30mm)**

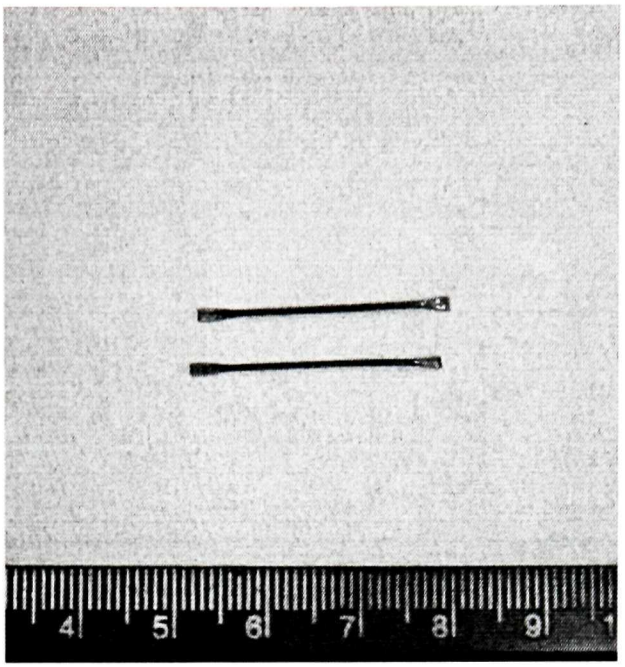


**Figure 4.3 Picture of flat end steel fiber**

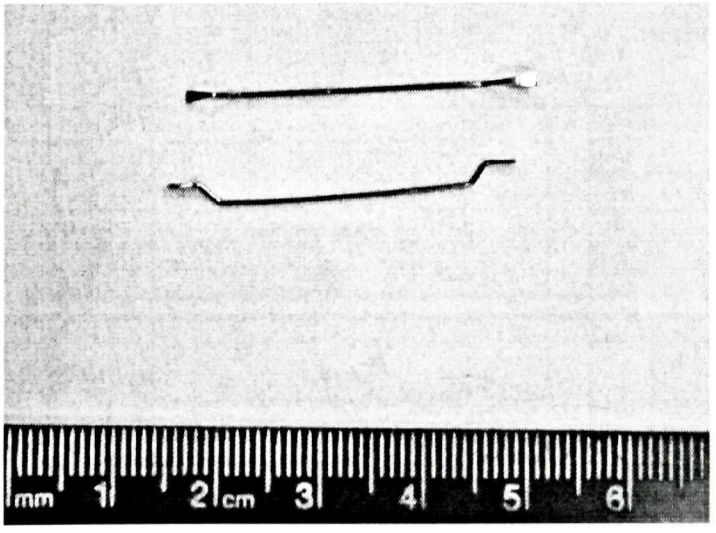


**Figure 4.4 Picture of hooked flat end steel fiber**

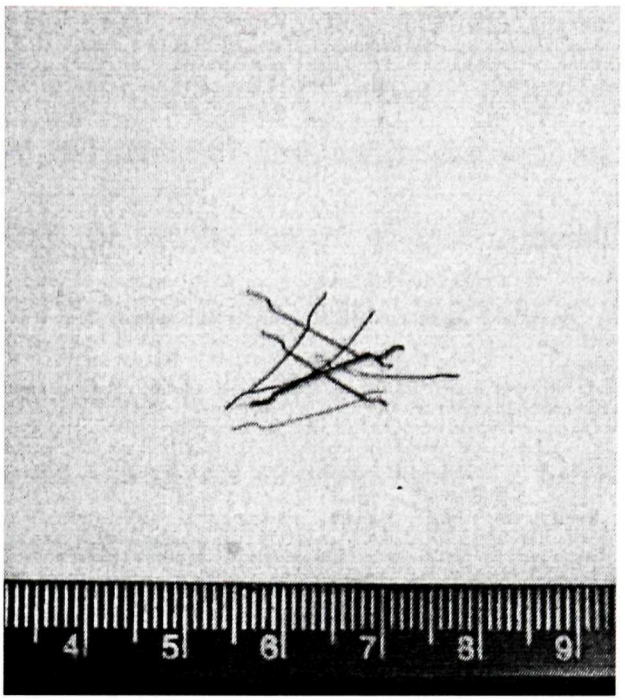


**Figure 4.5 Picture of long Microsteel fiber**

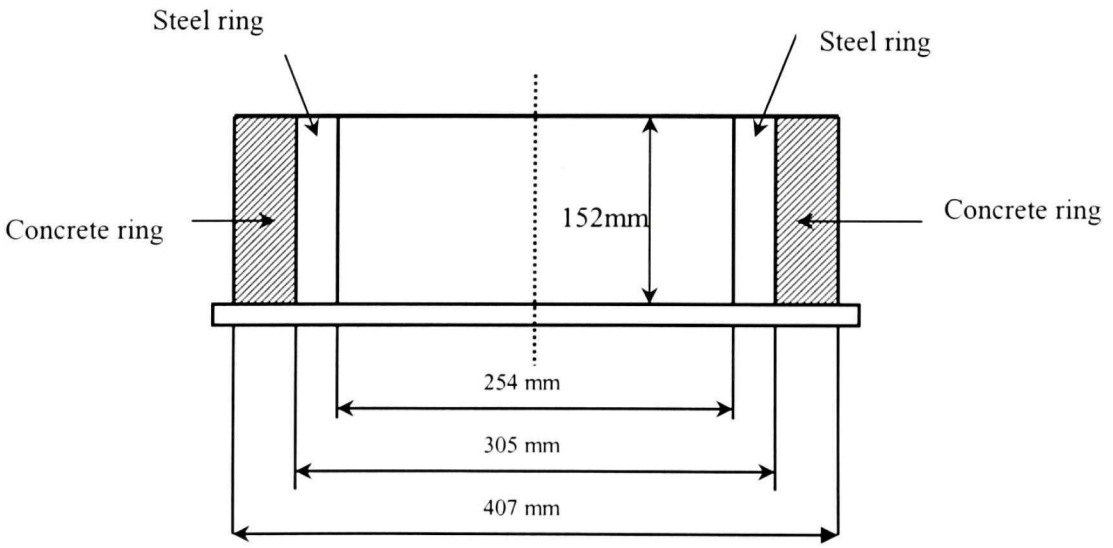


**Figure 4.6 Sketch of restrained shrinkage test**

# Chapter 5 Results

## 5.1 Air content and slump

The results of air content and slump of fresh concrete are shown in Table 5.1. The fiber content had some effects on the air content of fresh concrete. While the plain concrete (batch #1) had shown the least air content, the other batches exhibited higher air content with the fiber reinforcement. Flat end steel fiber and PVA fiber concrete (batch #3 and batch #2) had similar air content. As shown in Table 5.1, batch #4 had extremely high air content because of the methylcellulose addition, and it proved that water soluble polymer had air entraining effect. With the exactly same materials composition as batch #4, antifoamer was added in the batch #5 in the fresh mixture to reduce air content to 5.6% on purpose.

In hybrid systems batch #7 had relatively high air content in this series, and batch #11, FRC with 1% PVA fiber has the least air content. By comparing the fiber type, volume ratio in table 4.3, and fiber geometry in table 4.1, it indicated that not only fiber content but also fiber number has effect on the air content of fresh FRC. With the same rich cement mix, while using same fiber, the higher the volume of the fibers added, the higher the air entrained, based on the comparison between batch #2 and batch #11, batch #7 and batch #12; the more the number of the fibers involved, the higher the air entrained, based on the comparison between batch #8 and #10, batch #7 and #9. All the information of fiber type and ratio for each batch have been listed in chapter 4, table 4.2 to table 4.7.

For batches #13 to #16, steel FRC (batch #16) had the highest air content. Batch #13, FRC with 2% long PVA fibers has the least air content. Air content of batch #13 was

0.5% higher than that of batch #14, and it proved that the more the number of the fibers added, the higher the air content, while using the same volume of fiber in normal strength matrix. However, different fiber has different ability to entrain air in normal strength mix, as concluded by comparison of batch #14 with batch #16.

With the fibers added, it was obvious that slump was decreased. For batch #1 to batch #6 (Table 5.1), except that mortar batch #6 was self flowing, control (batch #1) had the highest slump. Steel FRC (batch #3) had showed high slump because of the smooth surface of steel fiber. PVA FRC with methylcellulose addition (batch #4) had displayed a much higher slump than batch #2 without methylcellulose, probably because methylcellulose entrained a large number of air into concrete, which improved the workability. However, the use of antifoamer in the purpose of reducing air, the slump in Batch #5 reduced by 43% compared to batch #4. For hybrid systems, batch #7 had the lowest slump, and Batch #10 had the highest slump. It is clear that with more fibers (by quantity or by volume) added in matrix, the lower the slump of FRC was expected.

## 5.2 Compressive strength

The compressive strength at 28 days is shown in Table 5.2. The compressive strength of plain concrete (batch #1) was 60MPa. With 2% PVA fibers added (batch #2), the strength reduced 13%. With 2% steel fiber added (batch #3), the strength however increased 7%. Because of methylcellulose entraining more air, batch #4 showed lowest strength in this series by reducing 16% compared to batch #2. With reduced air, batch #5 showed improved strength of 54MPa, which was close to batch #2. However, all the PVA

FRC batches except mortar (batch #6) showed lower strength than plain concrete (batch #1). The results proved that the addition of different fiber has slightly effect on the compressive strength, and fiber addition does not necessary help for improving compressive strength of FRC.

In hybrid system, the compressive strengths of all the fibrous batches were around 50MPa. Hybrid systems which had more fiber volume (#7 and #9) compared to steel FRCs themselves (#8 and #10), had a relatively lower compressive strength.

## 5.3 Flexural strength and Load-deflection curves

The flexural strength of average of three tests are summarized in Figure 5.1 for batch #1 to batch #6, Figure 5.2 for batch #7 to batch #12, and Figure 5.3 for batch #13 to batch #16. The data with deviation are shown in Table 5.3 as well. All the detailed results for each batch are listed in table A.3, A.4 and A.5 in Appendix A. Typical load-deflection curves were obtained by averaging three curves from the tests of same batch. An example is given in figure 5.4 with averaged and original curves of PVA2 FRC. Although averaged curve is not a test result, it could serve the purpose of comparison. The original load-deflection curves for all the batches are attached in Appendix B.

### 5.3.1 The effect of fiber on flexural strength

For uncycled six batches shown in Figure 5.1 (light coloured bar), plain concrete (batch #1) had the lowest flexural strength, PVA FRC (batch #2) had improved flexural strength, and steel FRC (batch #3) had a higher flexural strength than PVA FRC (batch #2). With the methylcellulose addition, the flexural strength of batch #4 and batch #5 were 39% higher than that of #2. It was obvious that PVA fiber contributed to the

increase of flexural strength, and the polymer addition was able to further improve the strength due to better bond between fiber and matrix. On the other side, Batch #6 of fiber reinforced mortar showed extremely high flexural strength. With the same fiber content as batch #2, and without polymer addition, the improvement of flexural strength in mortar matrix composite (batch #6) could be attributed to high content of cement paste.

As shown in Figure 5.2, the flexural strength of hybrid system (batch #7 and batch #9) increased about 20% compared to that of PVA FRC (batch #2). It indicated that the hybrid system could achieve similar flexural strength as PVA FRC with polymer addition (batch #4 and batch #5). With 1% PVA fiber addition, the flexural strength was only 4.5MPa for batch #11 and 4.8 MPa for batch #12, which were 15% lower than that of PVA FRC reference (#2).

In Figure 5.3, it is indicated that length of PVA fiber had effect on the flexural strength. The long PVA FRC (batch #14) was 41% higher in flexural strength than the short PVA FRC (batch #13), although fiber volume ratios were the same for both batches. Furthermore, with addition of hooked flat end steel fiber (batch #15), the flexural strength increased another 9% compared to batch #14. HFsteel FRC (batch #16) as reference had lowest flexural strength in this series because of low amount of steel fiber added.

It should be noticed that in rich cement mix, hybrid system of HFsteel and PVA FRC (batch #9) had 17% of flexural strength increment compared to PVA FRC (batch #2). However, in Figure 5.3, hybrid system Batch #15, with both HFsteel and PVA FRC had only 9% increase in flexural strength if compared to PVA FRC (batch #14). This was indicative that the flexural strength was not necessary to be proportional to the fiber content added.

### 5.3.2 Strain hardening behavior under flexure

***Strain hardening and strain softening behavior*** — Representative load-deflection curves for batch #1 to batch #6 are shown in Figure 5.5. It was obvious that the plain concrete (#1) was brittle. The curve went up till peak strength and dropped vertically. The crack pattern is shown in Figure 5.6.

By comparing the load deflection curves of PVA FRC (batch #2) and flat end Steel FRC (batch #3), it was demonstrated that the PVA fiber concrete(batch #2) with 2% fiber volume ratio displayed a quasi strain-hardening response. On the other hand, steel fiber concrete exhibited a high first crack strength but a postpeak softening behavior even with the same 2% fiber by volume. The cracking pattern of uncycled specimens in Figure 5.7 and Figure 5.8 showed that the flat end steel FRC (batch #3) was accompanied by a single widely-opened crack, while the PVA FRC (batch #2) instead by a number of distributed multiple cracks. The high first crack strength of steel FRC was likely attributed to the high tensile strength of fibers and the post peak energy absorption capacity was to the long fiber length. Nevertheless, the contribution to the multiple cracking in PVA FRC was due to the better chemical adhesive bond of PVA fibers with concrete, and the strong ability of PVA fiber bearing and transferring the load. And it was apparent that fiber type is critical. With the same amount of fibers, different types of fiber could generate different postpeak response.

***The effect of aggregates on strain hardening response*** — The effect of aggregate content was observed in Figure 5.5. In PVA fiber concrete (batch #2), the aggregates to paste ratio was 1.0, and in PVA mortar (batch #6), this ratio was 0.5. It was clear that the more the cement paste was used as binder, the higher the energy that could be absorbed.

Therefore, the energy absorption of fiber reinforced concrete decreased with an increase of aggregate content and size. The multiple cracks in PVA mortar (batch #6) (Figure 5.9) was indicative of a strain-hardening behavior.

***The effect of polymer addition on strain hardening response*** — The effect of methylcellulose modification was revealed by comparing the load-deflection curves of batch #2 with #4 and #5 in Figure 5.5. The methylcellulose addition to PVA FRC (batch #4 and #5) improved significantly not only the first crack strength but also the energy absorption compared to PVA FRC without methylcellulose addition (Batch #2). Batch #5, PVA FRC with methylcellulose and antifoamer agent showed better strain-hardening behavior than batch #4 without antifoaming agent. The multiple cracking was observed in both cases (Figures 5.10 and 5.11). It indicated that additional air content did not help strain-hardening response, since more pores broke the bridging of fiber and matrix and interrupted the transfer of the load under flexure. In general, it could be concluded that methylcellulose as polymer addition was an effective approach to achieve and improve strain hardening behavior.

***The effect of PVA fiber content on strain hardening response*** — When only 1% PVA fiber was added to rich cement mix (batch #11), the energy absorption was sharply reduced, compared to PVA FRC with 2% fiber content (batch #2), as is shown in Figure 5.12. The strain-hardening response did not exist in the batch #11, instead, a strain-softening behavior was seen. A close look on the sample surface showed a single

localized crack (Figure 5.13). A minimum amount of PVA fiber volume fraction between 1% to 2% is necessary to achieve quasi strain-hardening behavior with multiple cracking.

***The effect of hybrid system on strain hardening response in rich cement mix*** — The effect of hybrid system on strain hardening response in rich cement mix are shown in Figures 5.14 to 5.16. Figure 5.14 compares three curves, #2 as PVA FRC, #7 as hybrid of microsteel and PVA FRC, and #8 as microsteel FRC. With small quantity microsteel fibers only, the FRC in batch #8 demonstrated a strain-softening behavior with improved peak strength compared to plain concrete. However, when this quantity of microsteel fibers was added to PVA FRC, the hybrid composite(#7) showed not only an improved first crack strength, but also a better strain-hardening behavior with multiple cracking (Figure 5.17). It was noticed that there was almost no load drop when first crack strength was reached, compared to PVA FRC (#2) which was usually accompanied by a dip after first crack strength and before the start of its strain hardening.

While the above phenomenon was observed with the use of microsteel fibers, more batches were investigated by adding other type of steel fiber. Figure 5.15 compares curves of #9 as hybrid composite with hooked flat end steel and PVA FRC, #10 as hooked flat end steel FRC and #2 as PVA FRC. The length of hooked flat end steel fiber was 32.9mm. It was interesting to find that steel FRC with hooked flat end fibers at 30Kg/m$^3$ displayed certain strain-hardening behavior with multiple cracking (Figure 5.18). This was not achieved in batch #3 steel FRC even with 2% by volume flat end steel fibers. It was therefore possibly to conclude that the strain-hardening response of fiber reinforced concrete was dependent not only on the fiber type but also the end

conditions of the fiber. Moreover, it revealed again the phenomenon that the hybrid system could smoothly transfer the load from first crack to strain hardening. Steel fiber in hybrid FRC not only improved the first crack strength and energy absorption regarding the fiber length and fiber end shape, but also affected the energy dissipation under flexure and suppressed the unloading after first crack generates.

For batches of #8, #11 and #12 in Figure 5.16, all the curves show the strain-softening behaviour with 1% PVA fibers. PVA FRC (#11) and hybrid system (#12) resulted in very similar first crack strength with a strain-softening behavior. Single cracking pattern was seen in both specimens, as shown in Figure 5.13 and figure 5.19. It indicated that 1% PVA fiber did not create strain-hardening response in concrete, even in the hybrid system with certain quantity of microsteel fibers. Microsteel fiber had almost no effect on flexural behavior of FRC with 1% PVA fiber, neither the first crack strength nor the change of energy absorption.

***Fiber length effect on the strain-hardening response in normal strength mix*** — In the normal strength mix, only 445 $Kg/m^3$ cement was used. Figure 5.20 compares the flexural curves of the PVA FRC with 2% of 12mm long PVA fiber (batch #13), the PVA FRC with 2% of 30mm long PVA fiber (batch #14), the hybrid system with 2% of long PVA fiber and 0.4% of hooked flat end steel fiber (batch #15), and the FRC with 0.4% of hooked flat end steel fiber (batch #16) only. The matrix design was for normal strength concrete with a paste to aggregate ratio of 0.51 by volume. The PVA fiber in normal strength mix (batch #13) was the same as that was used in rich cement mix (batch #2). However, the batch #2 with a paste to aggregate ratio of 1.0 by volume showed a strain

hardening behavior with multiple cracking, while the batch #13 with a paste to aggregate ratio of 0.51 exhibited the strain-softening response with early localized single cracking, suggesting that the cement paste content was one of the important parameters to achieve the strain-hardening behavior and multiple cracking.

With the use of the same amount of long PVA fiber as in batch #13, batch #14 showed improved first crack strength and different flexural behavior, that is, strain-hardening behavior with multiple cracking. It could be concluded that the length of PVA fiber affected the flexural behavior of FRC. The long PVA fiber would lead to a high first crack strength and peak strength, a large energy absorption capacity, and a strain hardening response with multiple cracking.

***Effect of hybrid system on strain hardening response in normal strength mix*** — The hybrid design concept was also applied in normal strength mix. The load-deflection curves of long PVA FRC (batch #14), Hybrid system with long PVA fiber and hooked flat end steel fiber (batch #15) and FRC with hooked flat end steel fiber only (batch #16) shown in Figure 5.20 were investigated.

Batch #16, with only 30Kg/m$^3$ of hooked flat end steel fiber, although showed certain strain hardening response in rich cement mix (batch #10), resulted in strain-softening response in normal strength mix. It implied again that the amount of cement paste as binder was a very important parameter to a strain hardening response.

When 30mm PVA fibers combined with 32.9 mm long steel fibers, the hybrid system (batch #15) displayed a strain hardening behavior with a smooth load-deflection curve

again, the steel fibers suppressed the load drop after the first crack, and assisted an ascending postpeak hardening.

## 5.4 Freeze-thaw resistance of strain hardening FRC

### 5.4.1 The effect of freeze-thaw cycling on PVA FRC

The flexural strengths of FRC specimens underwent 200 freeze-thaw cycles are compared with those uncycled in Figure 5.1. The flexural strength of plain concrete (batch #1) increased after cycling by 10%. With PVA fiber added, PVA FRC (batch #2) and PVA mortar (batch #6) underwent a similar loss in strength after freeze-thaw cycling, the deterioration were 15% and 22%, respectively. In the contrary, there was a flexural strength gain for flat end steel FRC (batch #3) by 19% after freeze-thaw cycling. Moreover, with methylcellulose addition in PVA FRC in batches #4 and #5, the flexural strength was maintained around 6.2MPa and 6.7MPa after freeze-thaw cycling, with a difference of -1.5% and 3% before and after cycling, respectively.

The load-deflection curves of each batch (batch #1 to batch #12) before and after cycling were plotted separately in Figure 5.21 to Figure 5.32. The cracking patterns of freeze-thaw cycled concretes after flexural tests were compared with those of uncycled specimens in Figure 5.6 (batch #1), Figure 5.7 (batch #2), figure 5.8 (batch # 3), Figures 5.9 (batch # 6), Figures 5.10 (batch # 4), Figures 5.11 (batch # 5), Figures 5.13 (batch # 11), Figures 5.17 (batch # 7), Figures 5.18 (batch # 10), Figures 5.19 (batch # 12), Figure 5.33 (batch #9) and Figure 5.34 (batch #8).

Plain concrete in Figure 5.21 showed almost no change before and after freeze-thaw cycling. PVA FRC (batch #2) and PVA mortar (batch #6) experienced loss of energy

absorption ability after cycling, as are shown in Figure 5.22 and Figure 5.26. However, it is shown from Figure 5.24 and Figure 5.25 that PVA FRC with methylcellulose (batches #4 and #5) exhibited the similar strain hardening curves before and after cycling, and had almost no loss of toughness after freeze-thaw cycling. The flat end steel FRC (batch #3) instead demonstrated a strength gain and enhanced energy absorption ability by having a large postpeak area (shown in Figure 5.23), owing to the fact that the energy absorption of steel fiber concrete was controlled by fiber pullout.

Concerning these phenomena, it was likely that the loss of energy absorption capacity in PVA FRC and mortar was related to two possibilities: One was the deterioration of the interfacial bond. It caused by difference in thermal expansion coefficients between PVA fiber and concrete matrix under freeze – thaw cycling. This mismatch could lead to the debonding or gap between fiber and matrix under severe cycling. The other possible mechanism was likely the brittleness of PVA fiber created by freezing. The change of its properties not only would damage the chemical bond between fiber and matrix interface, it affected its ability of stretching and transferring the load as well.

In the contrary, steel fiber remained its properties during freeze-thaw cycling. It is likely that there is no deterioration of the concrete (matrix) under freeze-thaw cycling if enough air is available; however, matrix got more strength because of the ageing. This could be proved by the comparison of the flexural strength and flexural behavior of plain concrete (batch #1) before and after freeze-thaw cycling, which is shown in table 5.3 and Figure 5.21. Moreover, steel fiber had similar thermal coefficient as concrete matrix, and also it was the mechanical anchor, not the adhesive bond made no bond deterioration between steel fiber and matrix as PVA fiber FRC had. Therefore, steel FRC

actually get a better behavior under frost action by gaining more strength and higher energy absorption.

Another evidence was that, with methylcellulose addition, the properties of matrix were changed to have the better internal cohesiveness and better connection to fiber, hence enhanced interfacial bond between fiber and matrix. Therefore, these FRCs maintained their flexural strength and flexural behavior.

Therefore, it was clear that either PVA fiber or interfacial bond between PVA fiber and matrix would deteriorate during freeze-thaw cycling. With the addition of polymer, the PVA FRC could have better freeze-thaw resistance to maintain the strain-hardening response.

### 5.4.2 The effect of freeze-thaw cycling on hybrid system

As is shown in Figure 5.2, the flexural strengths of steel FRC including microsteel FRC (batch #8) and hooked flat end steel FRC (batch #10) had almost no change after 200 freeze-thaw cycling. However, when 2% of PVA fibers were used in the hybrid system in batch #7 and batch #9, there were 16% losses of flexural strength. The percentage of loss was close to that of only PVA fiber concrete (batch #2) under cycling. The hybrid system did not seem to help reduce the strength loss caused by the deterioration of PVA fiber.

## 5.5 Flexural toughness (JCI)

To quantify the flexural toughness of all the fiber reinforced concrete, JCI SF4 method was used. JCI toughness index was defined as area under load-deflection curves

up to 2mm. It should be pointed that the specimens used in this research were not standard size of 100mm by 100mm by 400mm. Instead, they were 25mm by 75mm by 350mm, and 50 mm by 75mm by 350mm. JCI toughness method was used only for relative comparison.

The average and deviation of flexural toughness for batch #1 to #12 were listed in Table 5.4. They were also compared in Figures 5.35 and 5.36 for al the batches before after freeze-thaw cycling. The flexural toughness results for batch #13 to batch #16 are shown in Figure 5.37.

By comparing Figure 5.35 and Figure 5.36, it was found that JCI method could not reflect the strain hardening behavior. And it could only quantify the flexural behavior at certain extent. The energy absorption after deflection of 2mm was not considered. And strain hardening behavior was neglected. For instance, PVA mortar (batch #6) had much more energy absorption than PVA FRC (batch #2) in load-deflection curves as is shown in Figure 5.5. However, $T_{JCI}$ was only 1.60 KN•mm for PVA mortar (batch #6) compared to $T_{JCI}$ of 1.46 KN•mm for PVA FRC (batch #2), which did not show much difference. One more example was batches #5 and #4, batch #5 had higher energy absorption with continuously increased flexural curve after deflection of 2mm than batch #4 which had softening behavior after defection of 2mm. However, based on JCI method, they had closed $T_{JCI}$ as 1.66 KN•mm and 1.63 KN•mm, respectively. Another example was the comparison of two hybrid system, batch #7 and batch #9, although they had much different fiber pull-out process, both of them showed similar $T_{JCI}$ in Figure 5.36.

Therefore, JCI method is not an effective method to quantify the stain-hardening response. Another difficulty is that it is impossible at this point to use one parameter to

express the energy absorption capacity and multiple cracking patterns. More research work was needed to relate the flexural behavior such as the shape of flexural curve to multiple cracking phenomena. And this parameter should be either separated or involved into energy absorption capacity. More discussion would be carried out in Chapter 6.

## 5.6 Drying shrinkage test

### 5.6.1 The effect of fiber on free shrinkage under severe drying environment

The results of free shrinkage tests for batch #1 to batch #6 are shown in Figure 5.38. Without coarse aggregates, PVA mortar (batch #6) exhibited the highest shrinkage, and the strain curve had a much steep slope compared with other batches. PVA fiber concrete with methylcellulose (batch #4) also showed significant free shrinkage compared to the other concrete batches. The shrinkage strain at the age of 60 days was approximately 1.5 times that of the PVA fiber concrete (#2). This was possibly related to the excessive air entrained by methylcellulose. In the severe drying environment, during the movement of free water and capillary water, the additional internal free space could result in more shrinkage. With the antifoamer agent and the removal of entrained air by polymer, the free shrinkage was reduced in batch #5 to a level close to the control.

PVA FRC (batch #2), experienced the similar free shrinkage as the control (batch #1), while steel FRC showed slightly decreased deformation (batch #3). It seemed that the fibers did not substantially suppress the free shrinkage under severe drying condition.

Weight loss is another indicator for drying shrinkage. It is shown in Figure 5.39. The trend of weight change curves was similar to that of shrinkage results. The more the drying shrinkage, the higher the weight loss. PVA mortar (batch #6) had the highest weight loss,

polymer modified PVA FRC (batch #4) was the second, while the control concrete showed the lowest. In this test, PVA FRC (batch #2) had higher weight loss than plain concrete (batch #1) and steel FRC (batch #3), while the drying shrinkage deformations of the three were close to each other.

### 5.6.2 The effect of fiber on restrained shrinkage under severe drying condition

Table 5.5 shows the restrained shrinkage test results with first crack age, crack numbers, and maximum crack width for batches #1 to #6. The typical restrained shrinkage cracks on the ring specimens are displayed in Figure 5.40.

Compared to the control concrete, all the fiber reinforced concretes demonstrated the ability to delay crack initiation to control crack opening and reduce the total crack area significantly.

Steel fiber which was longer and stiffer than PVA fiber, performed best in controlling shrinkage under restrained condition by showing the delayed first crack, smaller crack width.

Without coarse aggregates to prevent the shrinkage, PVA mortar (batch #6) ring cracked earlier with larger crack width, compared to PVA FRC (batch #2).

Polymer modified PVA FRC (batch #4) which showed more free shrinkage exhibited early first crack due to the addition of polymer. However, the maximum crack width of batch #4 was 0.1mm smaller than that of PVA FRC (batch #2). And the individual crack width was well controlled by multiple cracking due to the enhanced bond between fiber and matrix. Batch #5 with reduced air showed delayed first cracking age with less cracks and controlled crack width.

**Table 5.1 Air content and slump of fresh concrete**

| Batch Number | #1 | #2 | #3 | #4 | #5 | #6 |
|---|---|---|---|---|---|---|
| Batch | Control | PVA2 | FSteel2 | MCPVA2 | DMCPVA2 | PVA2 mortar |
| Air content (%) | 4.4 | 5.6 | 5.1 | 11.0 | 5.6 | 4.9 |
| Slump (mm) | 211 | 71 | 183 | 140 | 80 | Self flow |
| Batch Number | #7 | #8 | #9 | #10 | #11 | #12 |
| Batch | Microsteel-PVA2 | Microsteel | HFsteel-PVA2 | HFsteel | PVA1 | Microsteel-PVA1 |
| Air content(%) | 7.0 | 6.4 | 6.5 | 5.6 | 5.2 | 6.6 |
| Slump(mm) | 51 | 164 | 55 | 175 | 125 | 97 |
| Batch Number | #13 | #14 | #15 | #16 | | |
| Batch | PVA2 | LPVA2 | HFsteel-PVA2 | HFsteel | | |
| Air content(%) | 5.3 | 4.8 | 5.5 | 6.0 | | |
| Slump (mm) | 10 | 19 | 12.5 | 162 | | |

**Table 5.2 Compressive strength**

| Batch Number | Batch Name | Stress |
|---|---|---|
| | | MPa |
| #1 | Control | 60.21 ± 4.05 |
| #2 | PVA2 | 52.12 ± 1.16 |
| #3 | Fsteel2 | 64.54 ± 0.64 |
| #4 | MCPVA2 | 43.72 ± 2.79 |
| #5 | DMCPVA2 | 54.06 ± 1.03 |
| #6 | PVA2 Mortar | 64.36 ± 2.29 |
| #7 | Microsteel-PVA2 | 51.10 ± 5.59 |
| #8 | Microsteel | 50.52 ± 2.07 |
| #9 | HFsteel-PVA2 | 43.67 ± 7.02 |
| #10 | HFsteel | 51.58 ± 10.29 |
| #11 | PVA1 | 50.10 ± 4.97 |
| #12 | Microsteel-PVA1 | 39.5 ± 1.79 |

**Table 5.3 Flexural strength under four point bending test**

| Batch number | Batch Name | Condition | Stress |
|---|---|---|---|
| | | | MPa |
| #1 | Control | Cycled | 4.2 ± 0.25 |
| | | Uncycled | 3.8 ± 0.36 |
| #2 | PVA2 | Cycled | 4.5 ± 0.15 |
| | | Uncycled | 5.3 ± 0.35 |
| #3 | Fsteel2 | Cycled | 7.6 ± 0.93 |
| | | Uncycled | 6.4 ± 0.44 |
| #4 | MCPVA2 | Cycled | 6.2 ± 0.31 |
| | | Uncycled | 6.3 ± 0.39 |
| #5 | DMCPVA2 | Cycled | 6.7 ± 0.36 |
| | | Uncycled | 6.5 ± 0.24 |
| #6 | PVA2 Mortar | Cycled | 6.0 ± 1.27 |
| | | Uncycled | 7.7 ± 0.20 |
| #7 | Microsteel-PVA2 | Cycled | 5.1±0.43 |
| | | Uncycled | 6.1±0.77 |
| #8 | Microsteel | Cycled | 4.5±0.25 |
| | | Uncycled | 4.7±0.50 |
| #9 | HFsteel-PVA2 | Cycled | 5.2±0.84 |
| | | Uncycled | 6.2±1.86 |
| #10 | HFsteel | Cycled | 4.7±0.61 |
| | | Uncycled | 4.7±1.11 |
| #11 | PVA1 | Cycled | 4.3±0.55 |
| | | Uncycled | 4.5±0.34 |
| #12 | Microsteel-PVA1 | Cycled | 4.4±0.45 |
| | | Uncycled | 4.8±0.50 |
| #13 | PVA2 | Uncycled | 4.60 ± 0.20 |
| #14 | LPVA2 | Uncycled | 6.46 ± 0.98 |
| #15 | HFsteel-LPVA2 | Uncycled | 7.06 ± 1.15 |
| #16 | HFsteel | Uncycled | 4.46 ± 0.25 |

**Table 5.4 JCI Flexural toughness under four point bending test**

| Batch Number | Batch | Condition | $T_{JCI}$ |
|---|---|---|---|
| | | | mm • KN |
| #1 | Control | Cycled | 0.2041 ± 0.015 |
| | | Uncycled | 0.1813 ± 0.024 |
| #2 | PVA2 | Cycled | 1.2370 ± 0.035 |
| | | Uncycled | 1.4552 ± 0.103 |
| #3 | Fsteel2 | Cycled | 2.0058 ± 0.241 |
| | | Uncycled | 1.6893 ± 0.098 |
| #4 | MCPVA2 | Cycled | 1.6185± 0.064 |
| | | Uncycled | 1.6587 ± 0.132 |
| #5 | DMCPVA2 | Cycled | 1.6221±0.089 |
| | | Uncycled | 1.6318±0.085 |
| #6 | PVA2 Mortar | Cycled | 1.4491 ± 0.271 |
| | | Uncycled | 1.6002 ± 0.120 |
| #7 | Microsteel-PVA2 | Cycled | 1.4569 ± 0.119 |
| | | Uncycled | 1.7637 ± 0.239 |
| #8 | Microsteel | Cycled | 0.3669 ± 0.082 |
| | | Uncycled | 0.3938 ± 0.085 |
| #9 | HFsteel-PVA2 | Cycled | 1.4101 ± 0.149 |
| | | Uncycled | 1.6729 ± 0.343 |
| #10 | HFsteel | Cycled | 1.1976 ± 0.042 |
| | | Uncycled | 1.2540 ± 0.365 |
| #11 | PVA1 | Cycled | 0.9266 ± 0.139 |
| | | Uncycled | 0.9113 ± 0.026 |
| #12 | Microsteel-PVA1 | Cycled | 0.4744 ± 0.021 |
| | | Uncycled | 1.0479 ± 0.069 |
| #13 | PVA2 | Uncycled | 4.1273 ± 1.017 |
| #14 | LPVA2 | Uncycled | 5.8560 ± 1.126 |
| #15 | HFsteel-LPVA2 | Uncycled | 7.5455 ± 1.060 |
| #16 | HFsteel | Uncycled | 3.4084 ± 1.150 |

**Table 5.5 Cracking characteristic under restrained shrinkage**

| Batch | #1 | #2 | #3 | #4 | #5 | #6 |
|---|---|---|---|---|---|---|
| | Control | PVA2 | Fsteel2 | MC PVA2 | DMC PVA2 | PVA2 Mortar |
| First crack age (days) | 2 | 8 | 21 | 4 | 5 | 4 |
| Crack Number (60 days) | 1 | 5 | 9 | 11 | 3 | 6 |
| Maximum Crack Width (mm) | 3.5 | 0.25 | 0.08 | 0.15 | 0.20 | 0.60 |

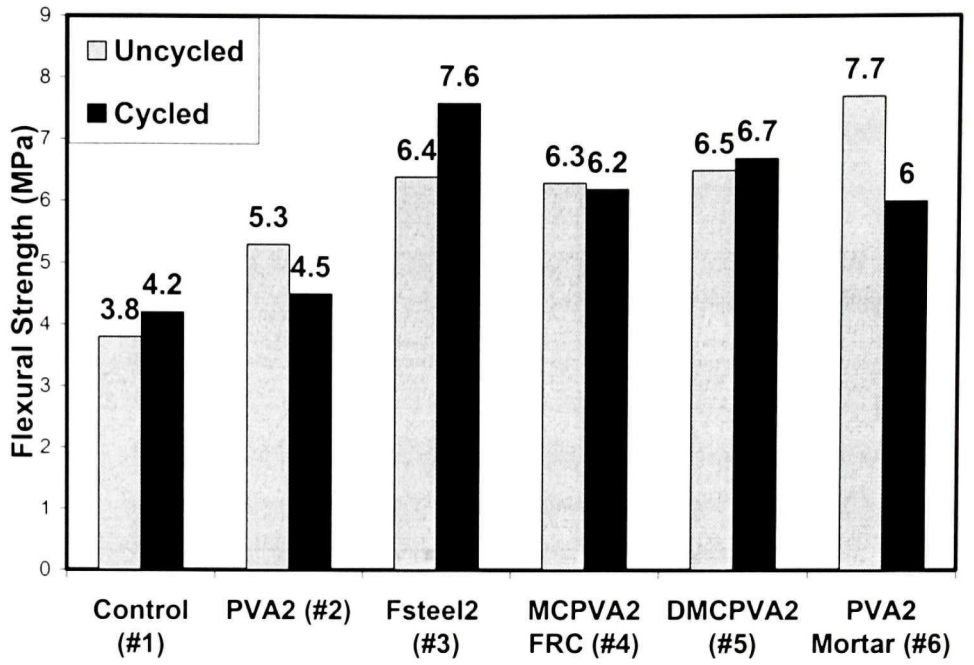


**Figure 5.1 Comparison of Flexural strength (#1~#6)**

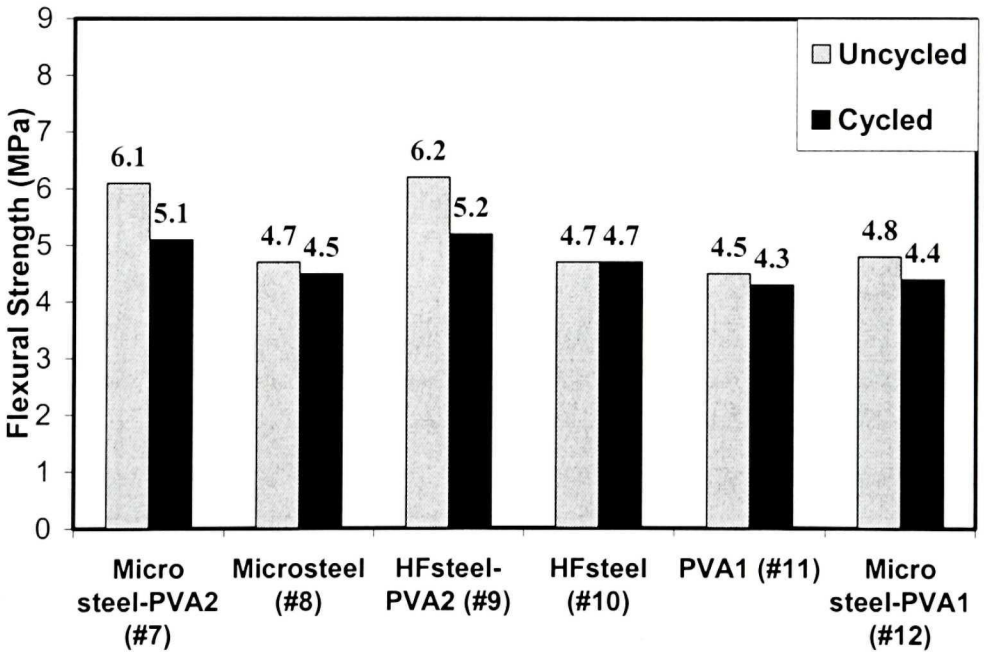


**Figure 5.2 Comparison of Flexural strength (#7~#12)**

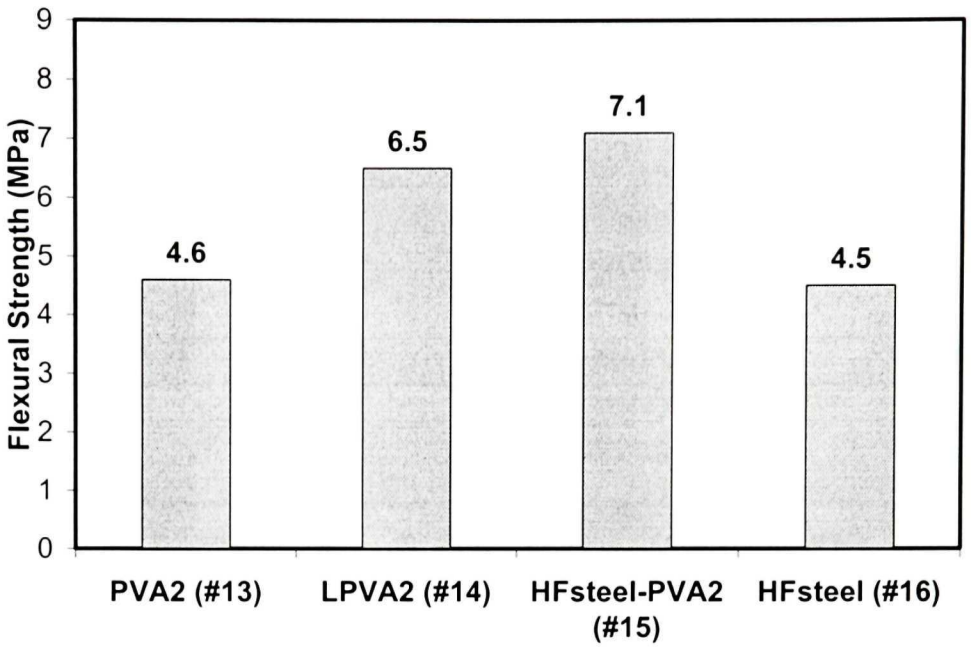


**Figure 5.3 Comparison of Flexural strength (#13~#16)**

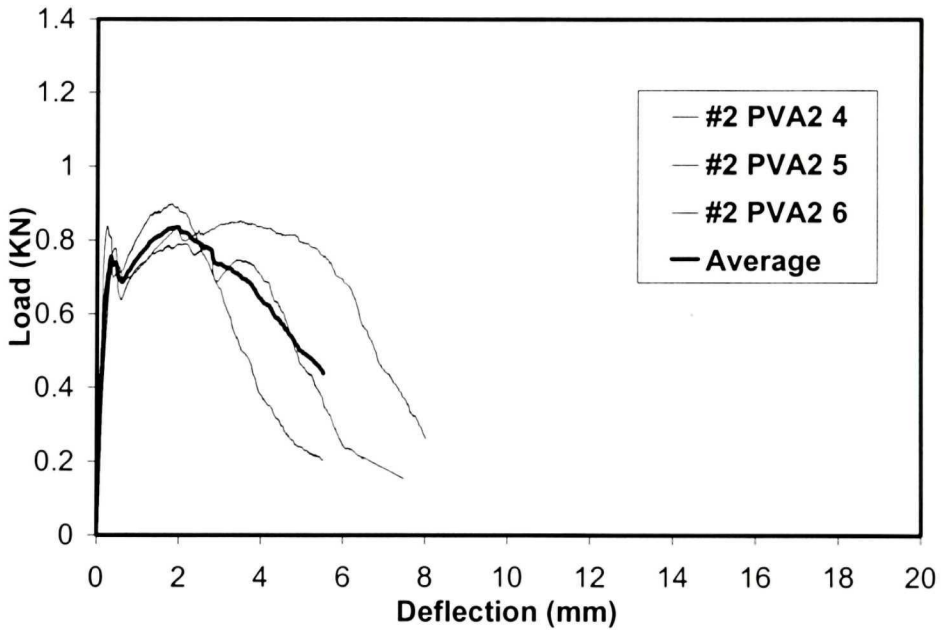


**Figure 5.4 Average of three curves as typical curve**

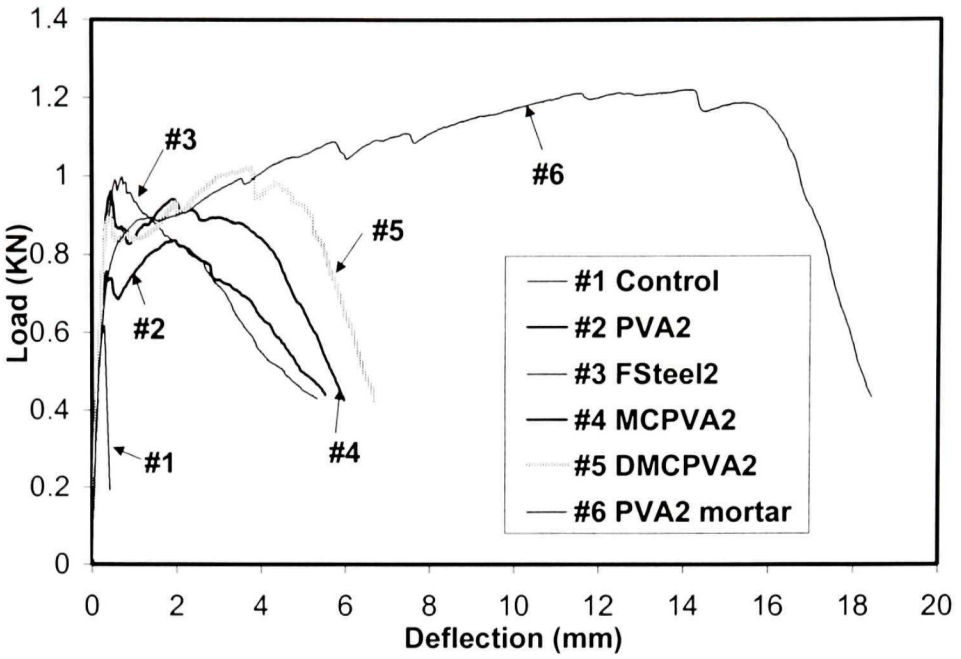


**Figure 5.5 Effect of polymer addition & aggregate content on hardening behavior**

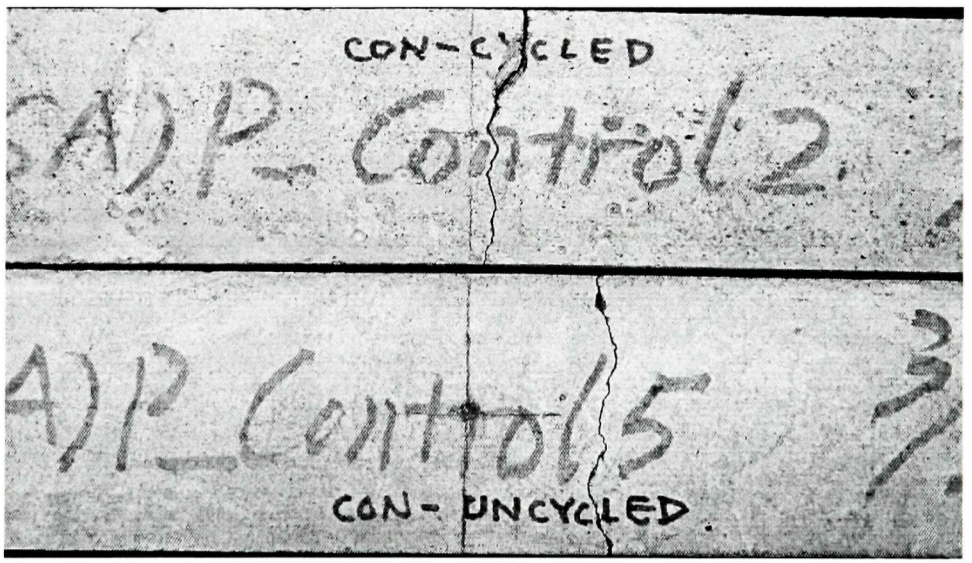


**Figure 5.6 Cracking pattern of Control (batch #1)**
**Top: Cycled; Bottom: Uncycled**

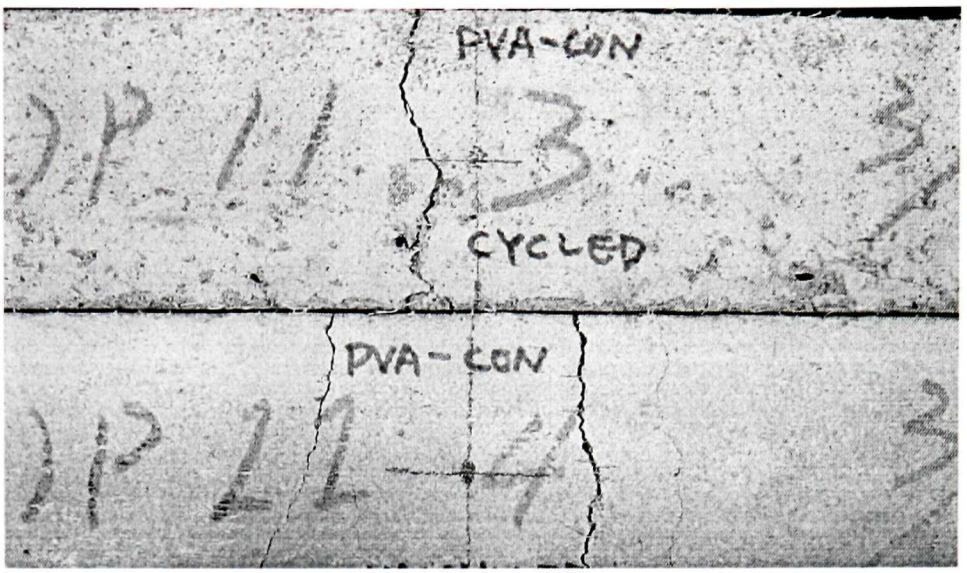


**Figure 5.7 Cracking pattern of PVA2 FRC (batch #2)**
**Top: Cycled; Bottom: Uncycled**

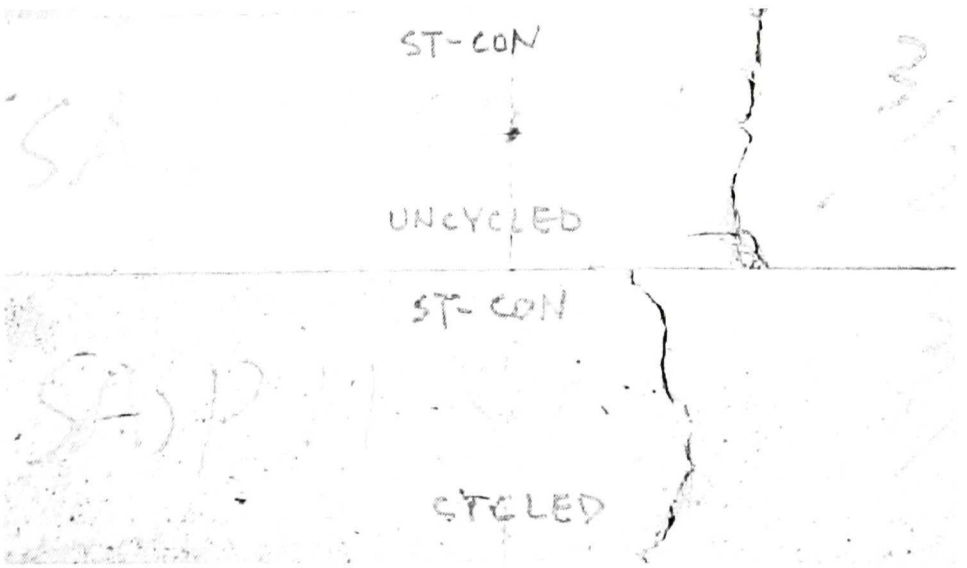


**Figure 5.8 Cracking pattern of Fsteel FRC (batch #3)**
**Top: Uncycled; Bottom: Cycled**

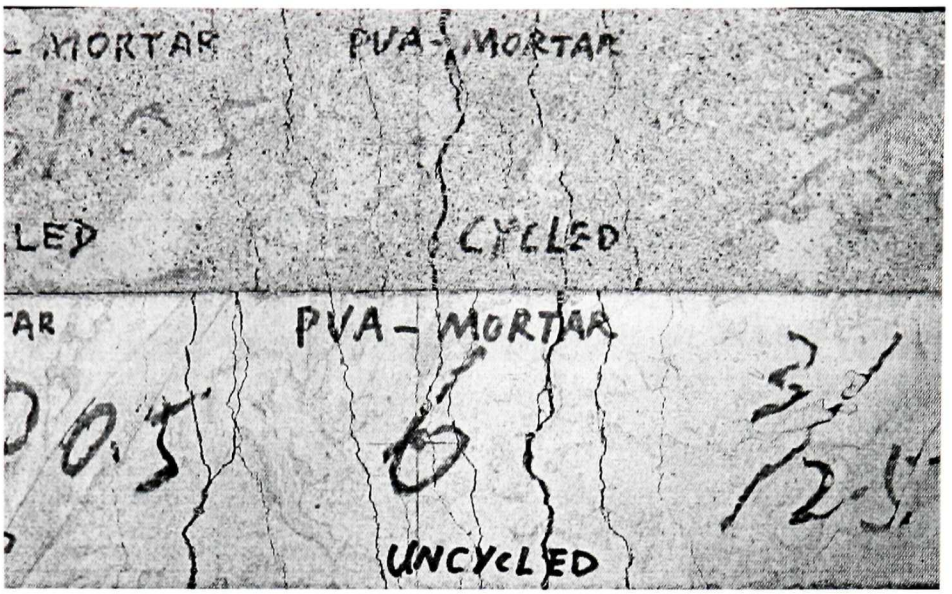


**Figure 5.9 Cracking pattern of PVA2 mortar (batch #6)**
**Top: Cycled; Bottom: Uncycled**

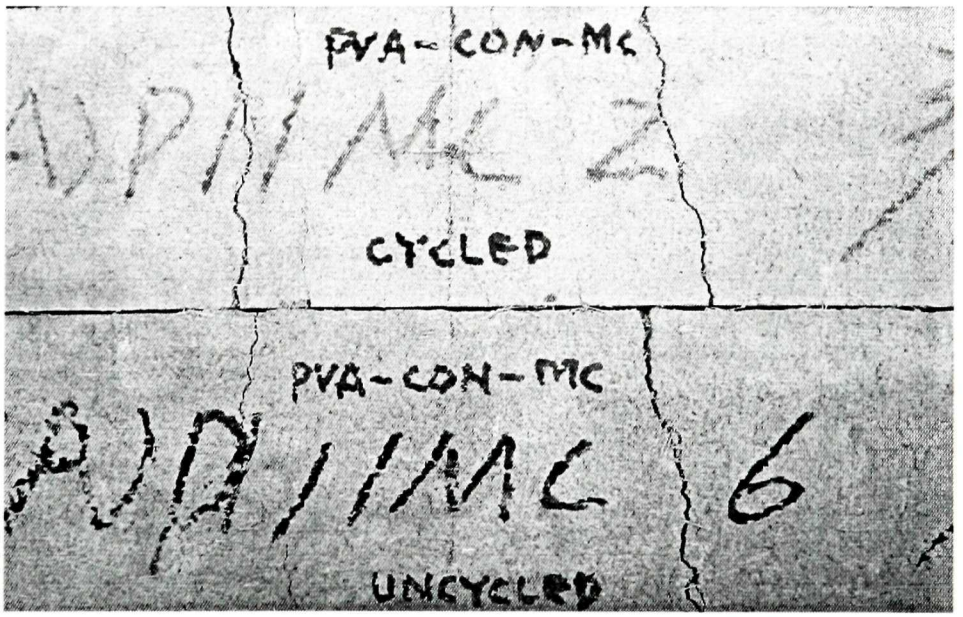


**Figure 5.10 Cracking pattern of MCPVA2 FRC(batch #4)**
**Top: Cycled; Bottom: Uncycled**

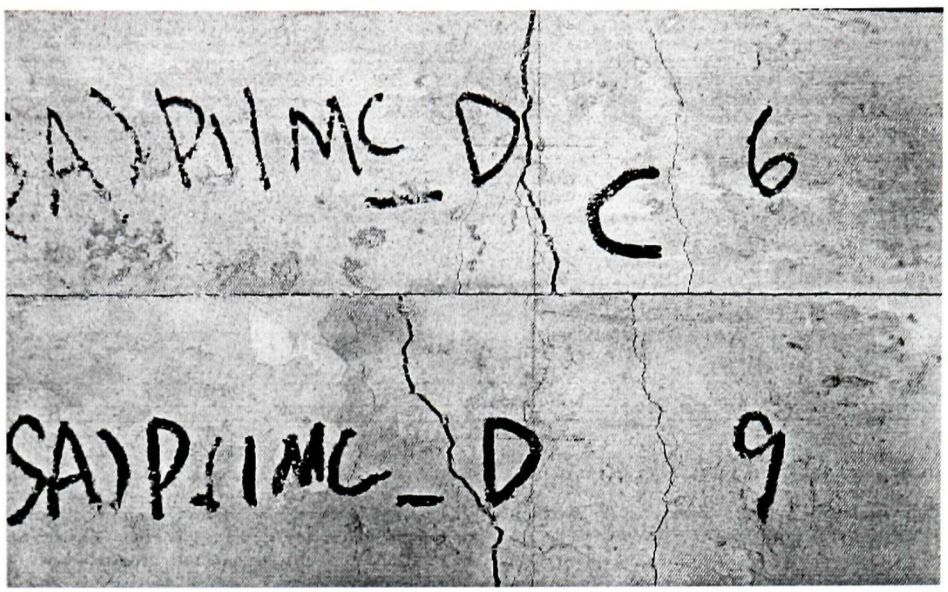


**Figure 5.11 Cracking pattern of DMCPVA2 (batch #5)**
**Top: Cycled; Bottom: Uncycled**

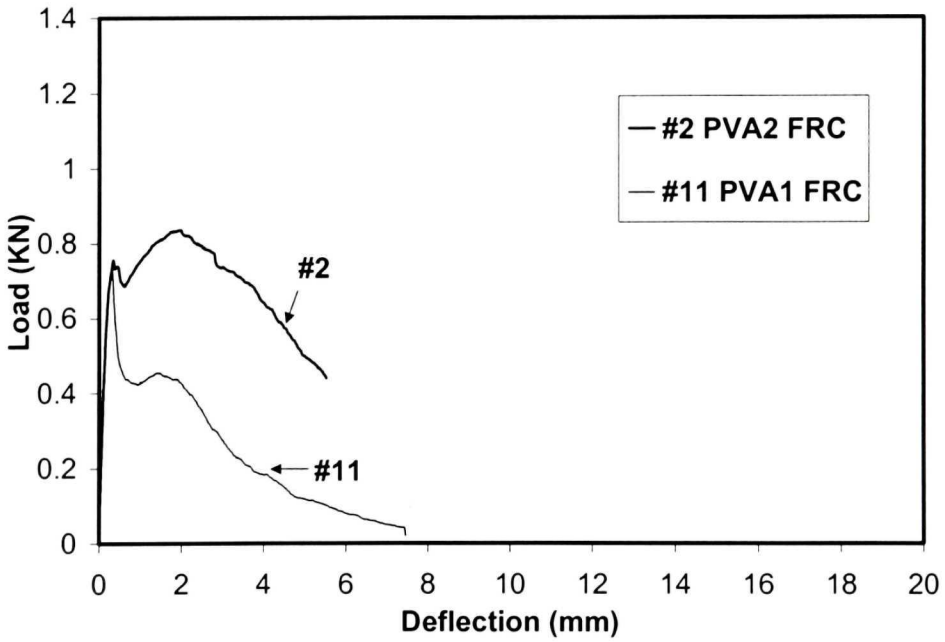


**Figure 5.12 Effect of fiber content on hardening behavior**

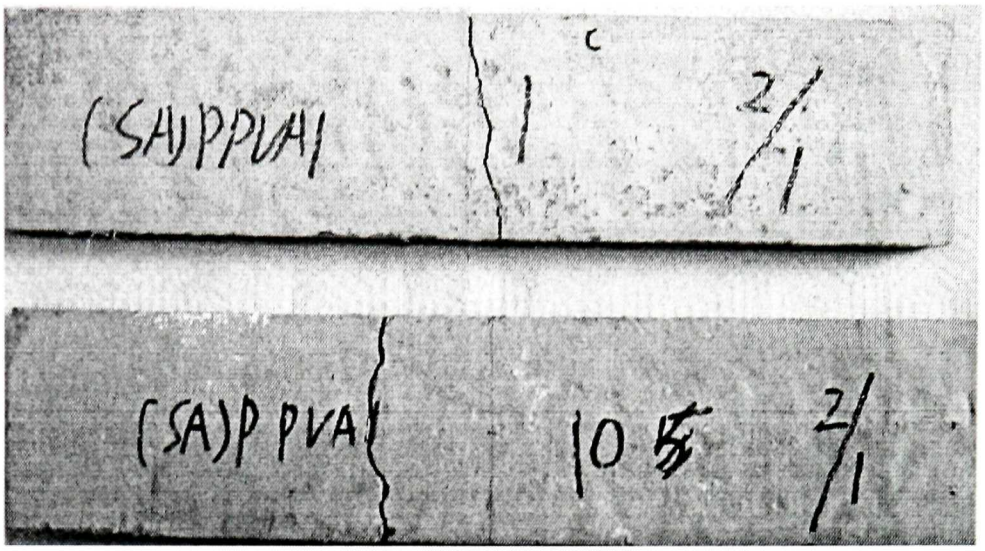


**Figure 5.13 Cracking pattern of PVA1 FRC (batch #11)**
**Top: Cycled; Bottom: Uncycled**

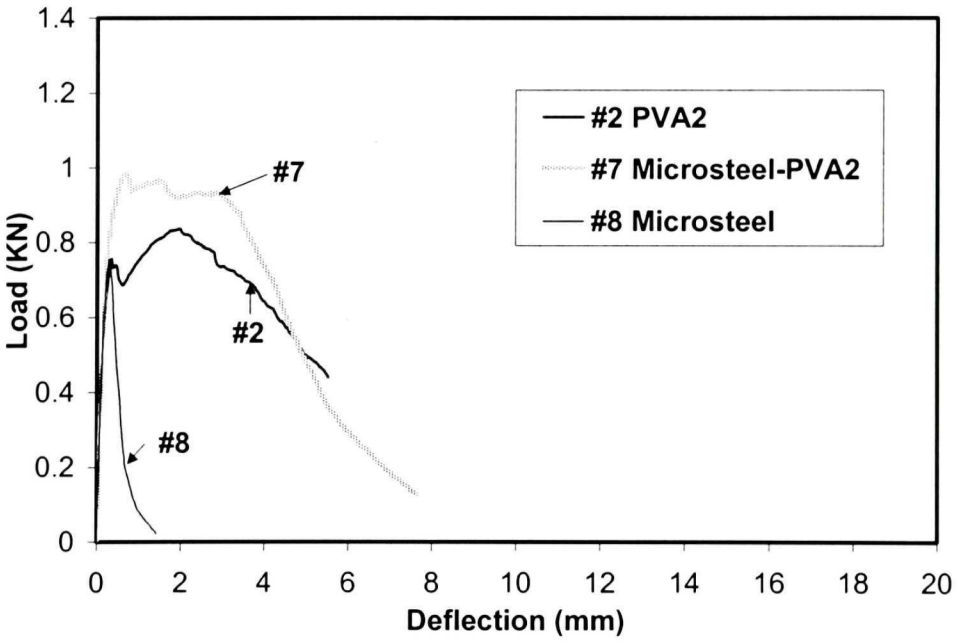


**Figure 5.14 Effect of hybrid reinforcing on hardening behavior (#2, #7, #8)**

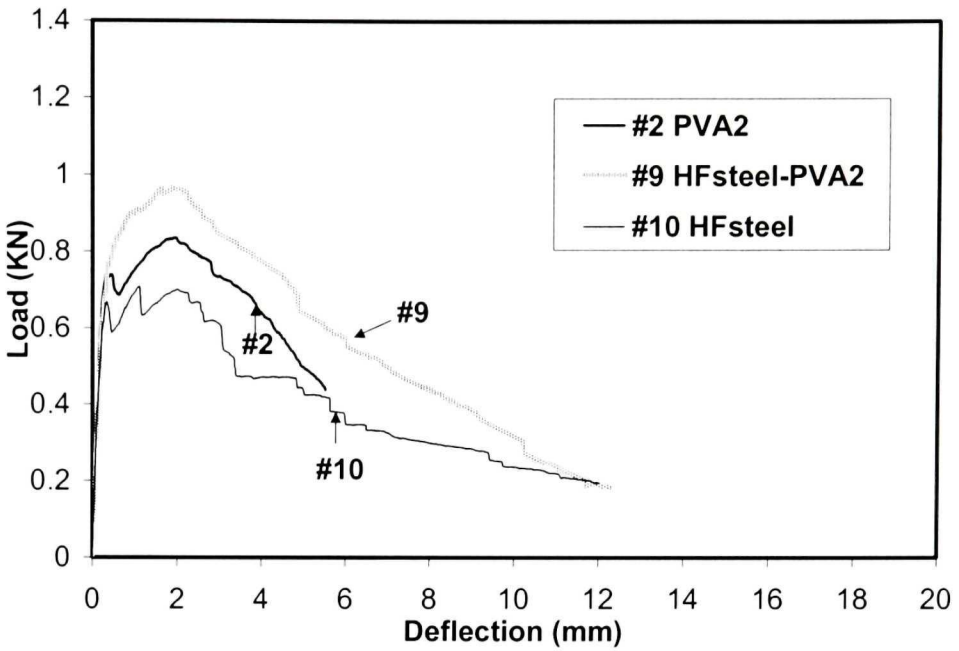


**Figure 5.15 Effect of hybrid reinforcing on hardening behavior (#2, #9, #10)**

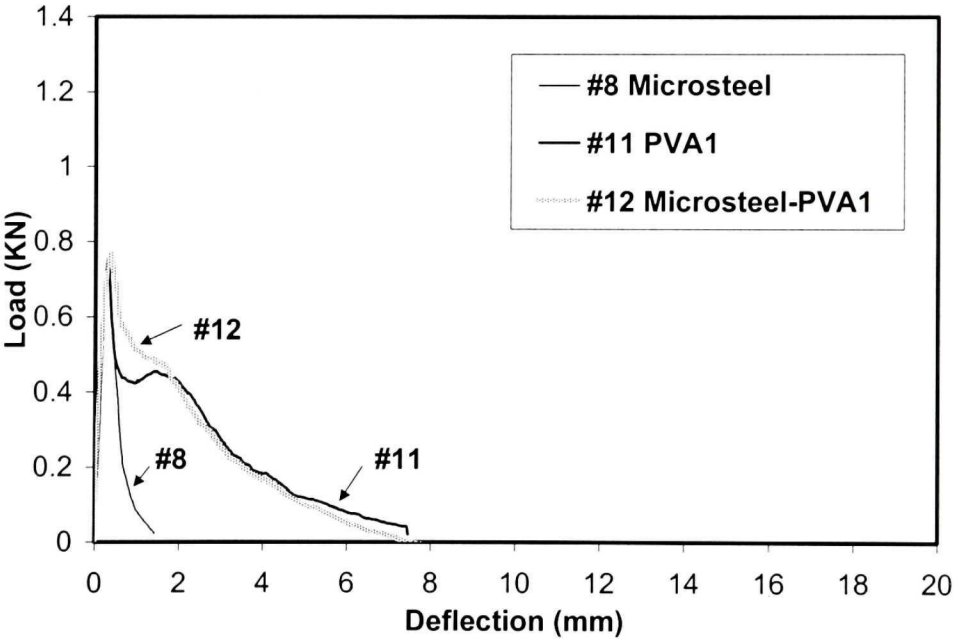


**Figure 5.16 Effect of hybrid reinforcing on hardening behavior (#8, #11, #12)**


**Figure 5.17 Cracking pattern of Microsteel-PVA2 FRC (batch #7)**
**Top: Cycled; Bottom: Uncycled**

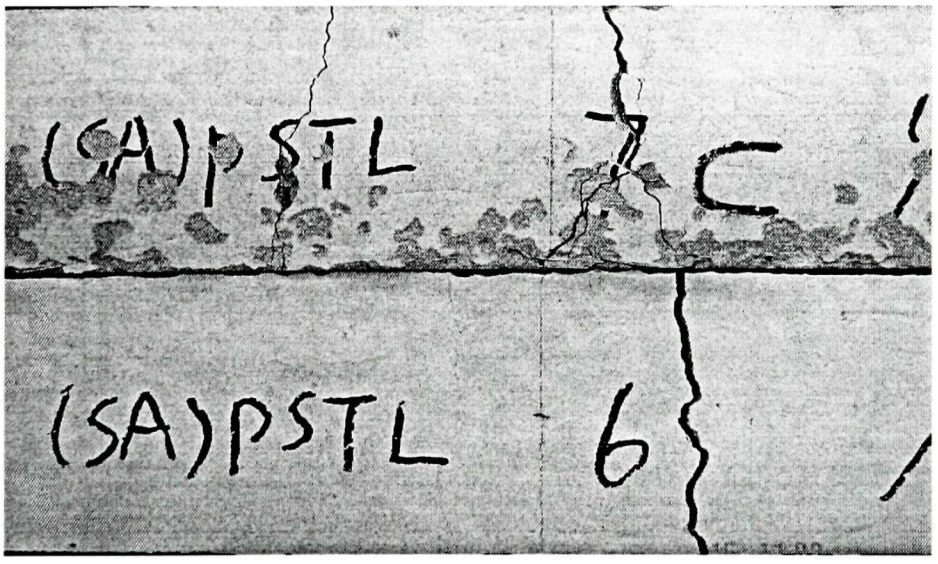


**Figure 5.18 Cracking pattern of HFsteel FRC (batch #10)**
**Top: Cycled; Bottom: Uncycled**


**Figure 5.19 Cracking pattern of Microsteel-PVA1 FRC (batch #12)**
**Top: Cycled; Bottom: Uncycled**

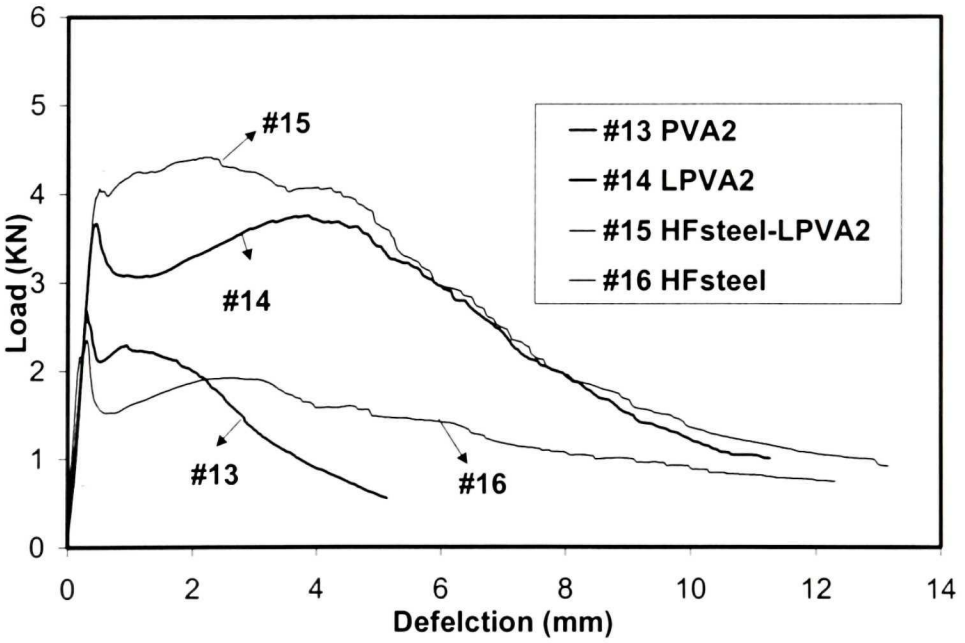


**Figure 5.20 Effect of fiber length &hybrid reinforcing on hardening behavior**

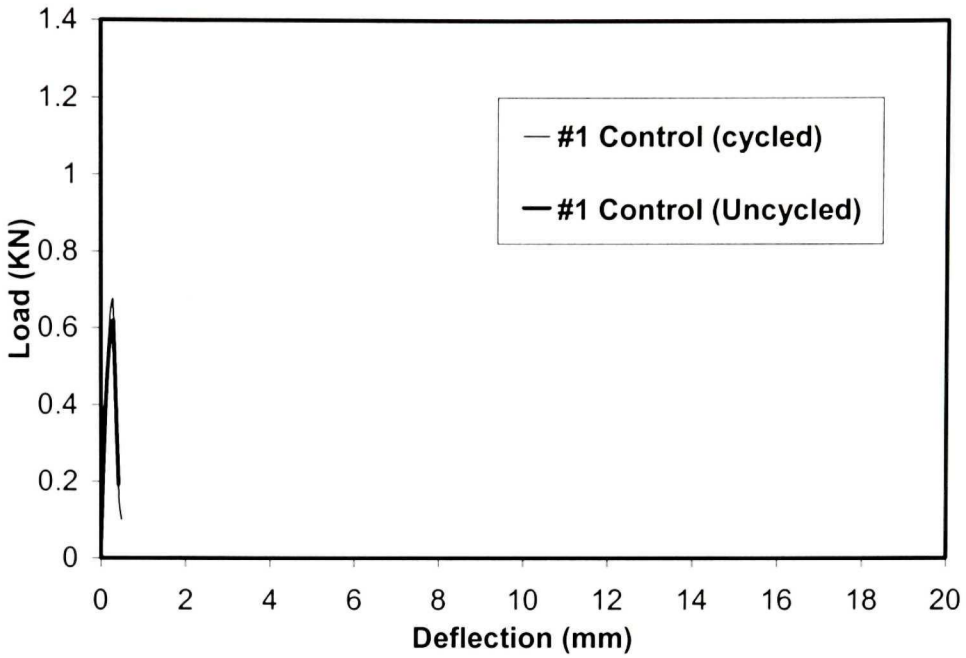


**Figure 5.21 Load-deflection curves before and after freeze-thaw cycles (#1)**

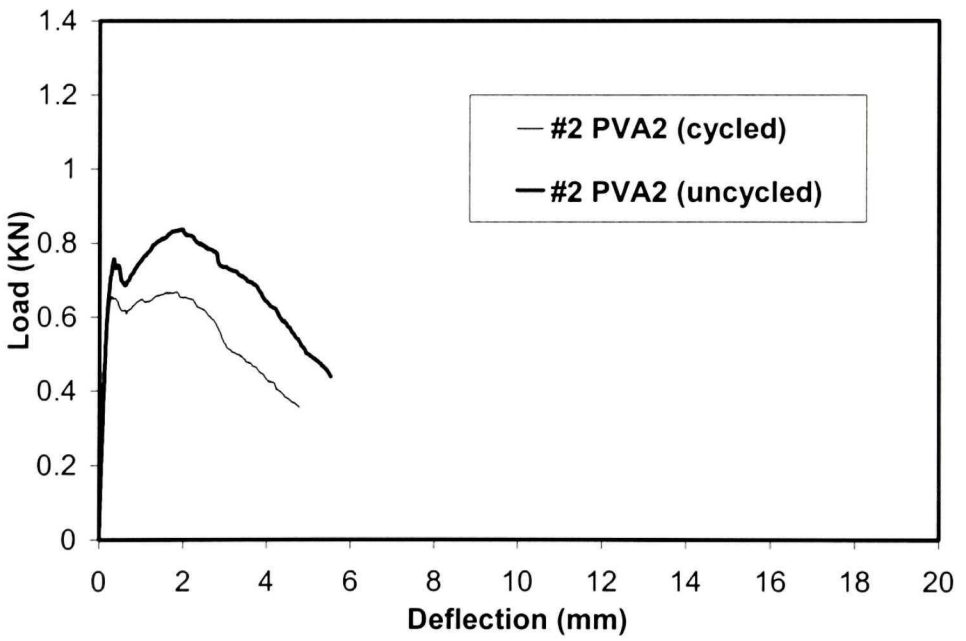


**Figure 5.22 Load-deflection curves before and after freeze-thaw cycles (#2)**

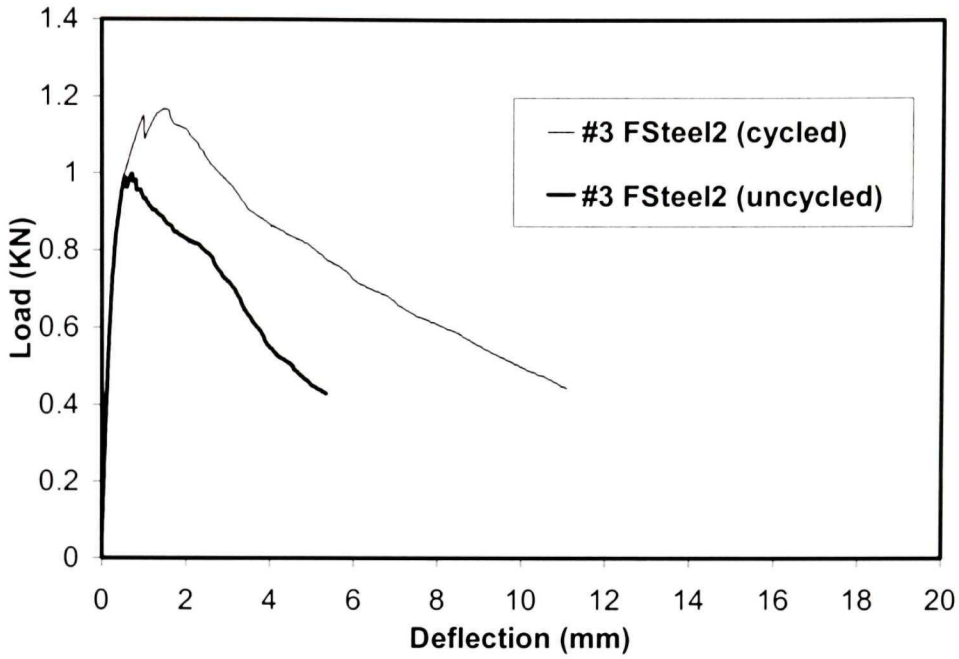


**Figure 5.23 Load-deflection curves before and after freeze-thaw cycles (#3)**

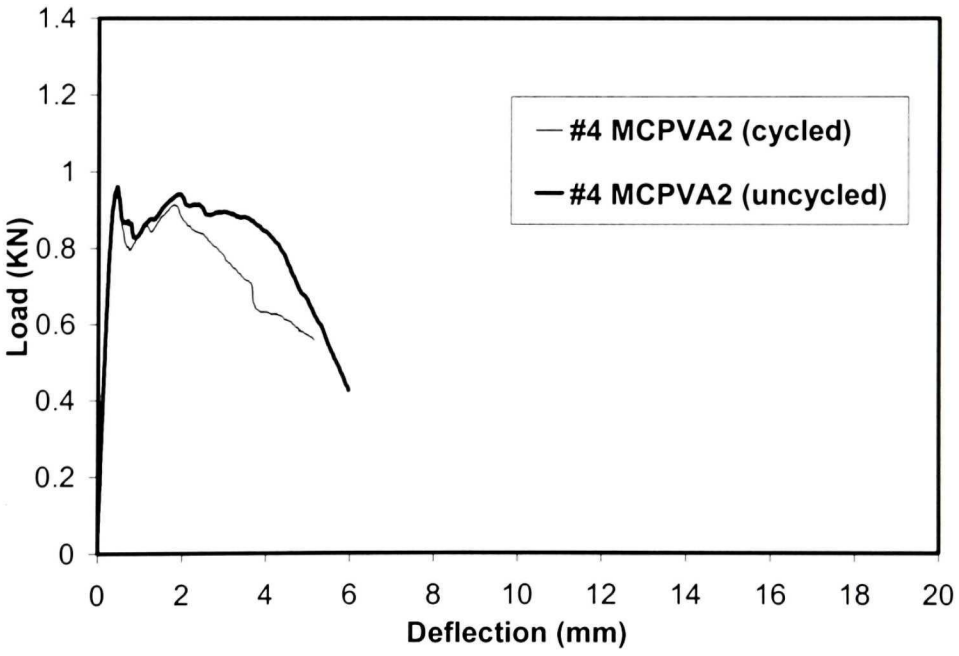


**Figure 5.24 Load-deflection curves before and after freeze-thaw cycles (#4)**

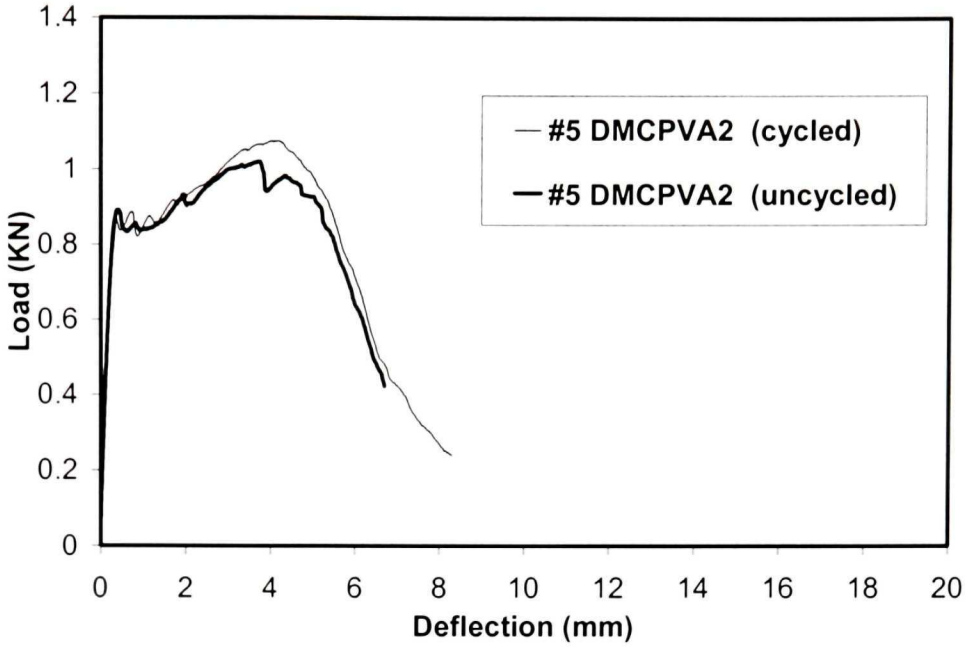


**Figure 5.25 Load-deflection curves before and after freeze-thaw cycles (#5)**

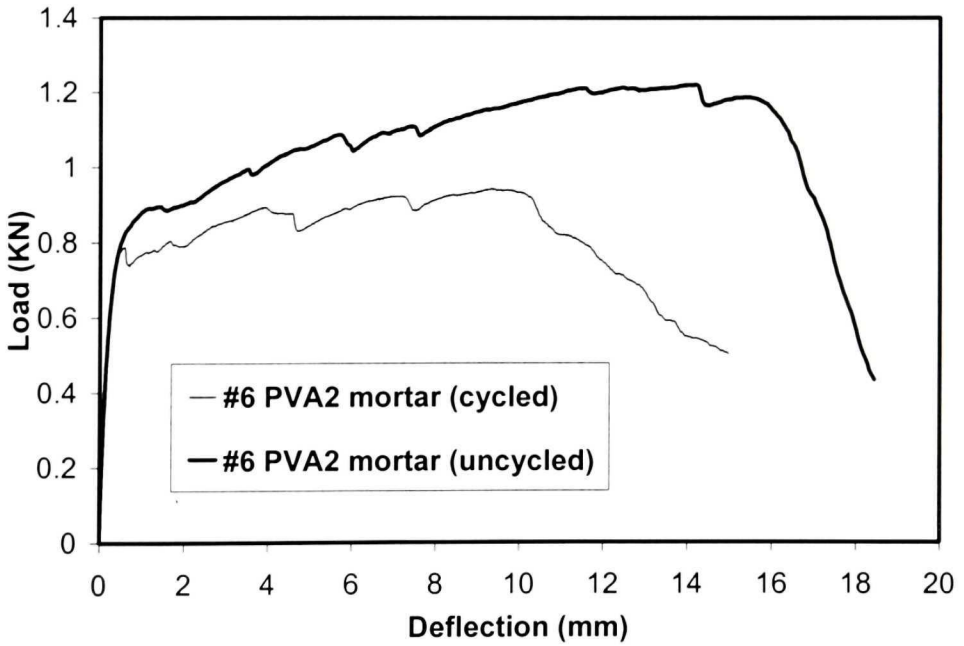


**Figure 5.26 Load-deflection curves before and after freeze-thaw cycles (#6)**

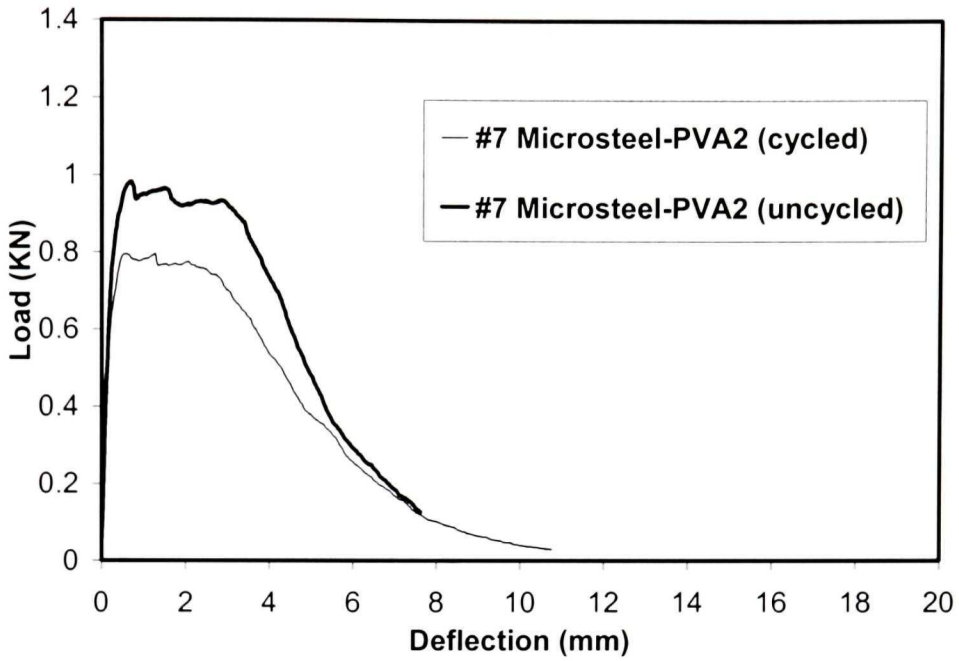


**Figure 5.27 Load-deflection curves before and after freeze-thaw cycles (#7)**

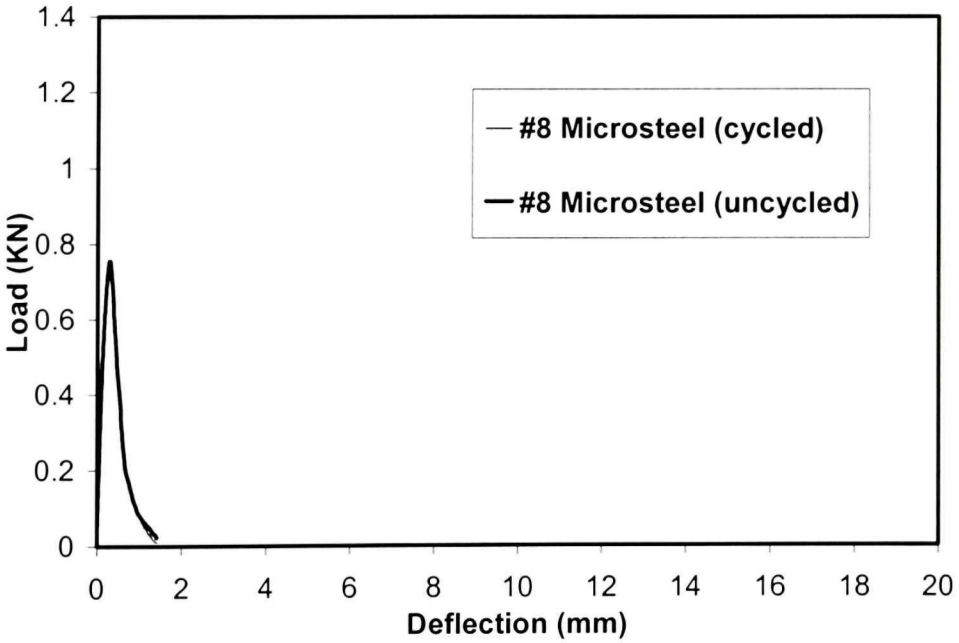


**Figure 5.28 Load-deflection curves before and after freeze-thaw cycles (#8)**

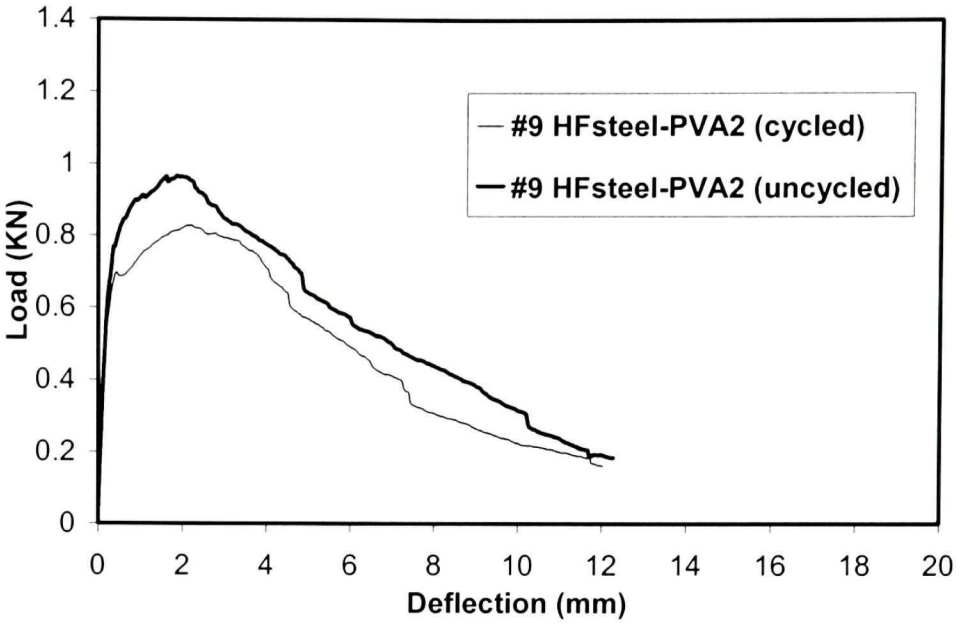


**Figure 5.29 Load-deflection curves before and after freeze-thaw cycles (#9)**

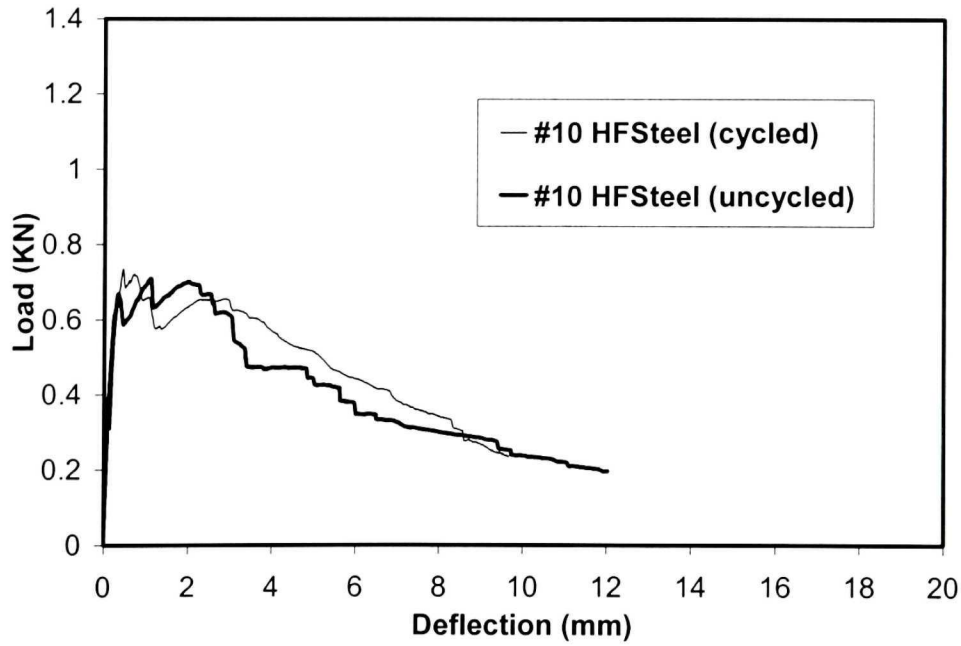


**Figure 5.30 Load-deflection curves before and after freeze-thaw cycles (#10)**

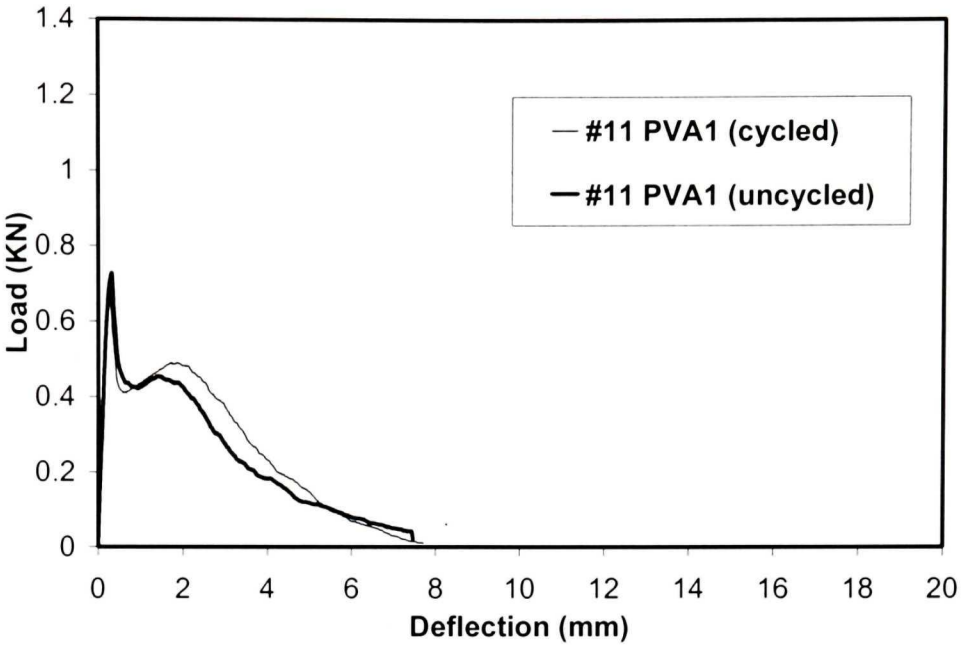


**Figure 5.31 Load-deflection curves before and after freeze-thaw cycles (#11)**

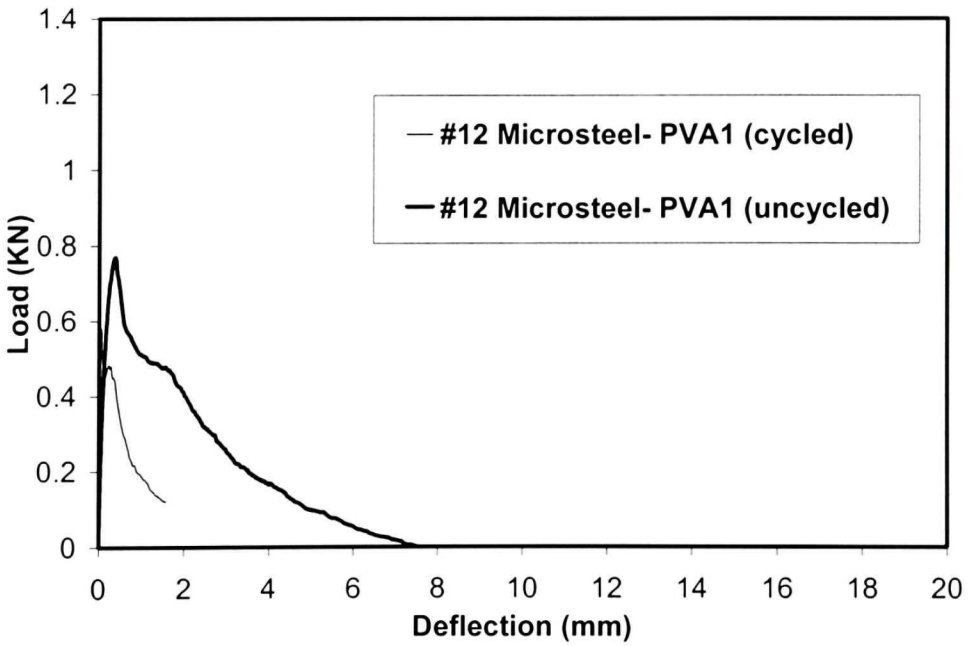


**Figure 5.32 Load-deflection curves before and after freeze-thaw cycles (#12)**

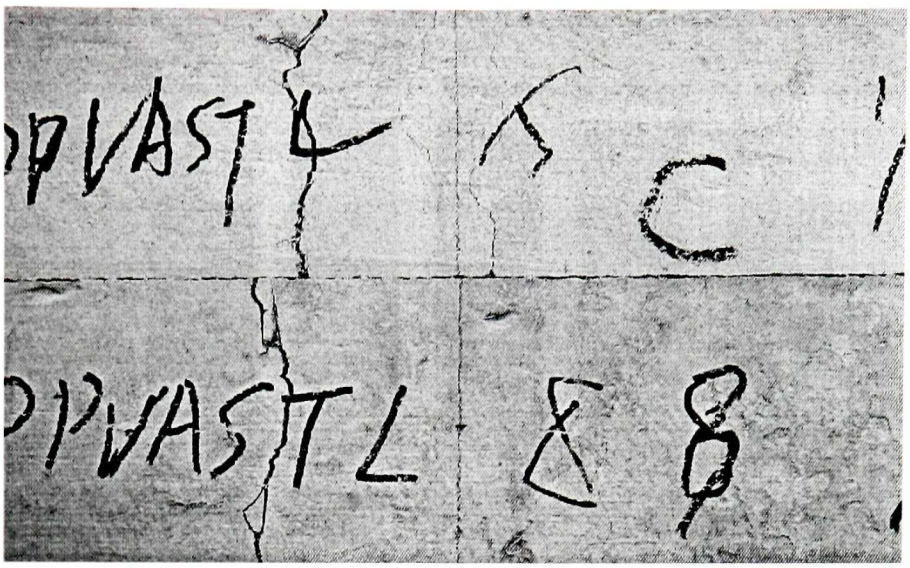

**Figure 5.33 Cracking pattern of HFsteel –PVA2 FRC (batch #9)**
**Top: Cycled; Bottom: Uncycled**

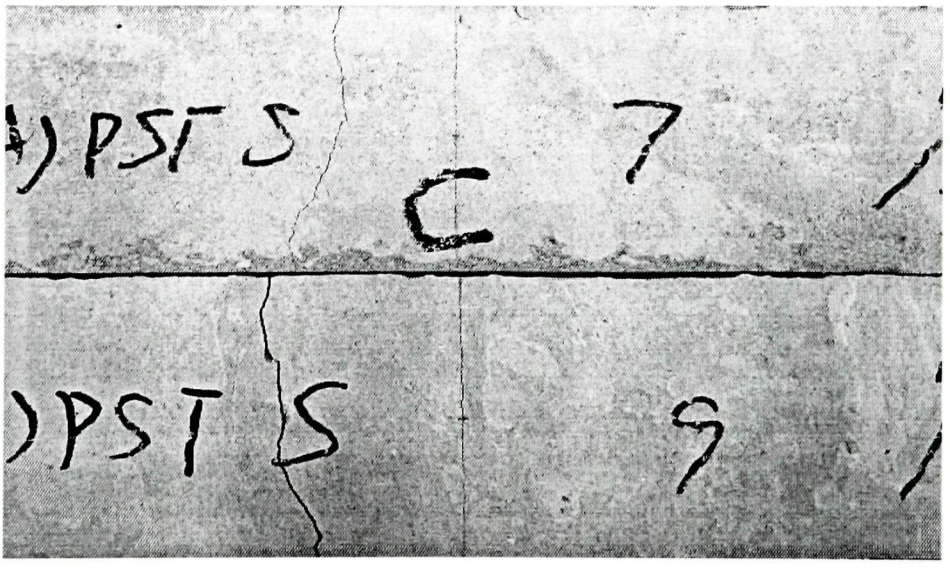

**Figure 5.34 Cracking pattern of Microsteel FRC (batch #8)**
**Top: Cycled; Bottom: Uncycled**

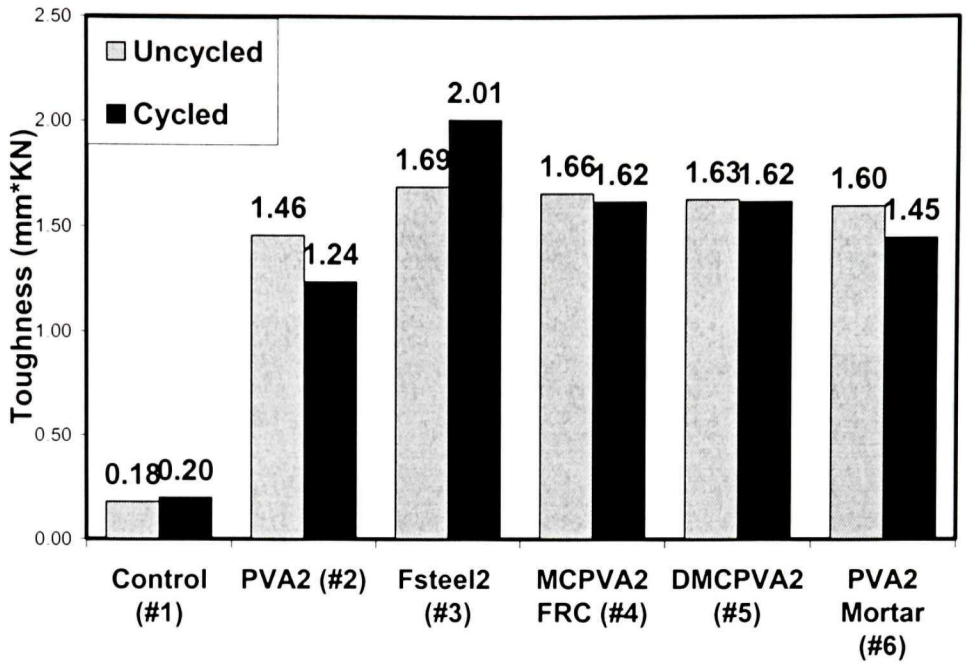


**Figure 5.35 Comparison of $T_{JCI}$ under freeze-thaw cycles (#1~#6)**

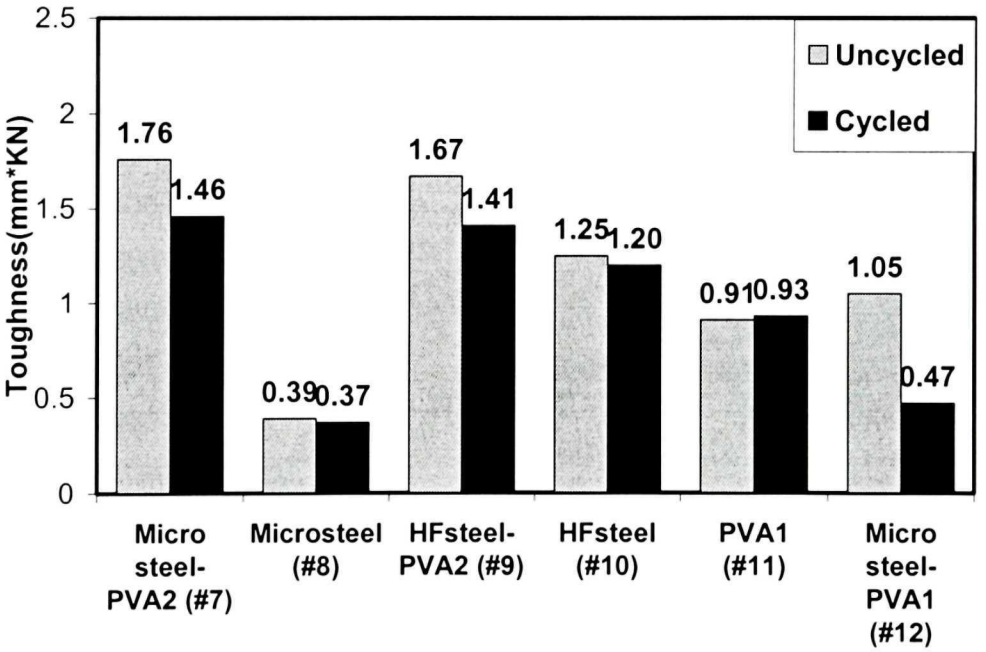


**Figure 5.36 Comparison of $T_{JCI}$ under freeze-thaw cycles (#7~#12)**

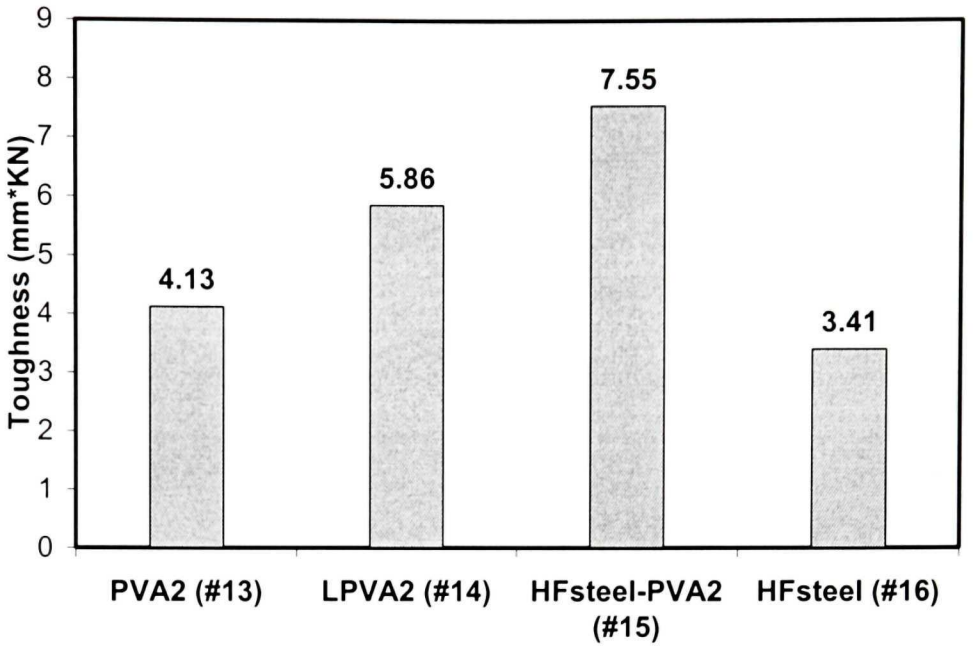


**Figure 5.37 Comparison of $T_{JCI}$ under flexure (#13~#16)**

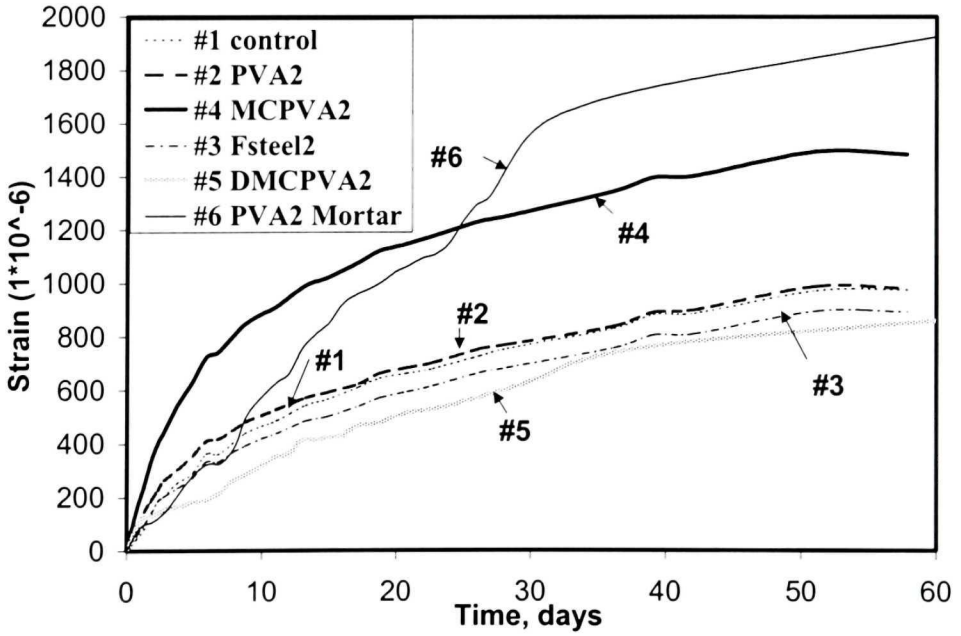


**Figure 5.38 Effect of Fiber & polymer addition on free shrinkage under drying**

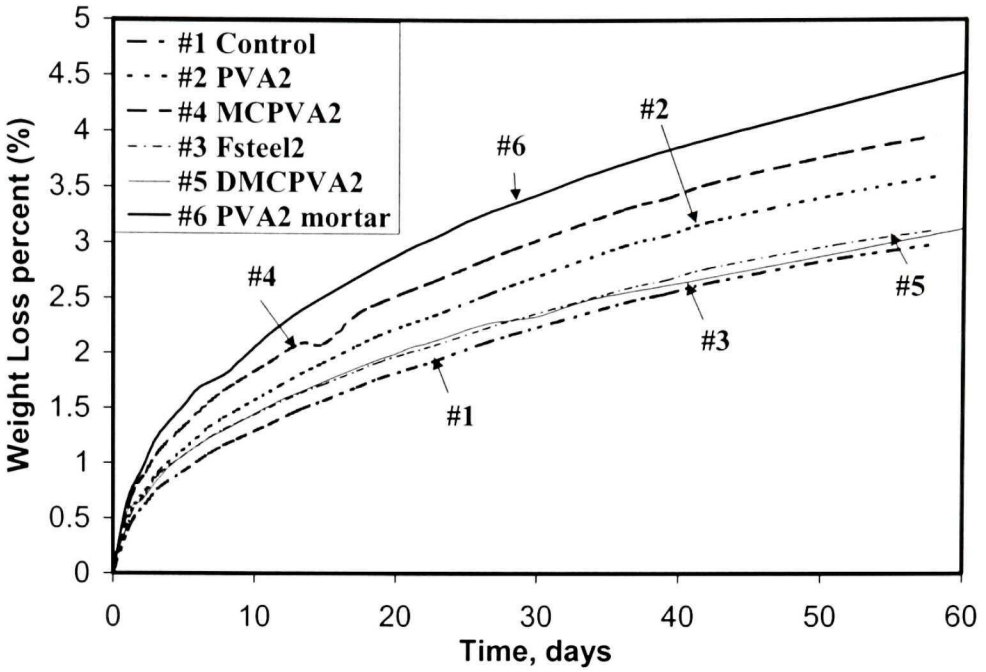


**Figure 5.39 Effect of Fiber & polymer addition on weight loss under drying**

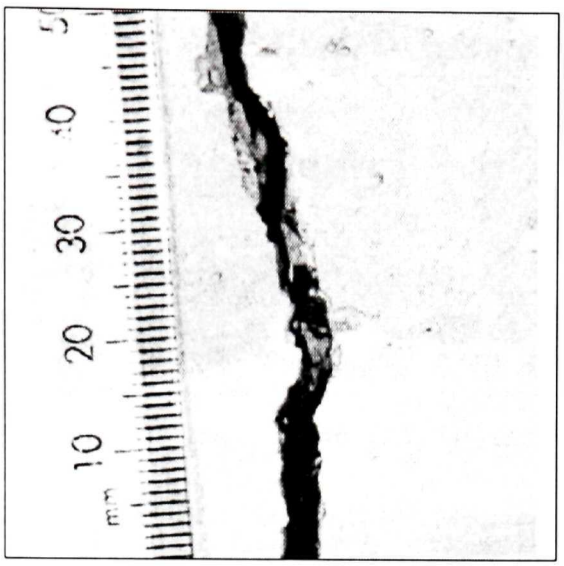

a: Control (#1)

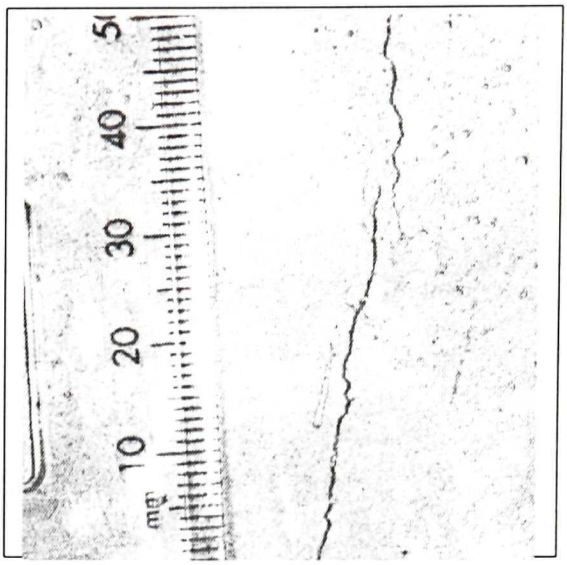

b : PVA2 FRC (#2)

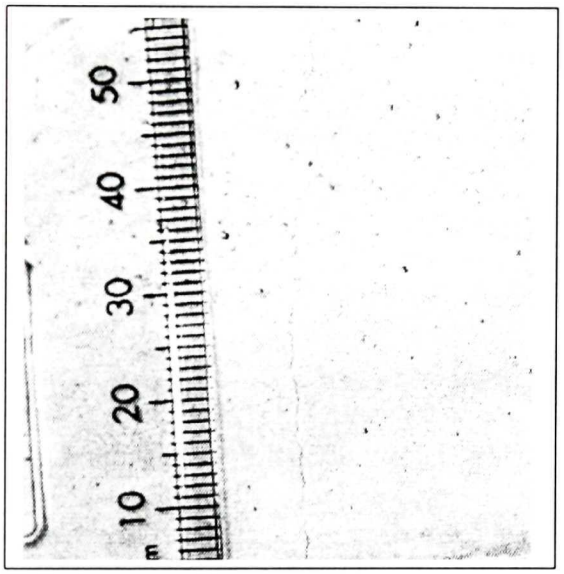

c : Fsteel2 FRC (#3)

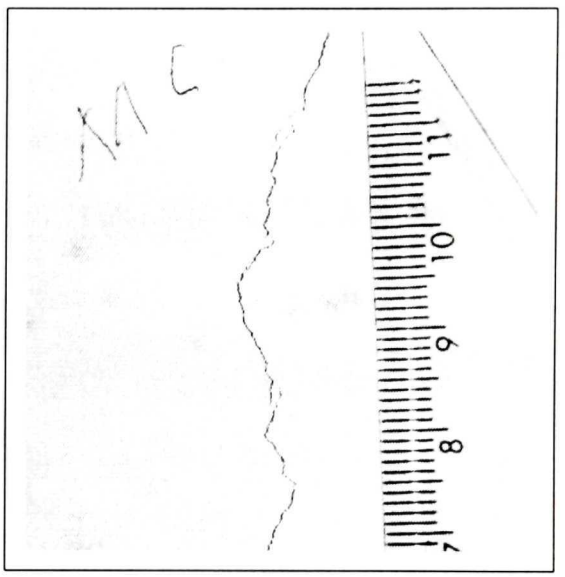

d : MCPVA2 FRC (#4)

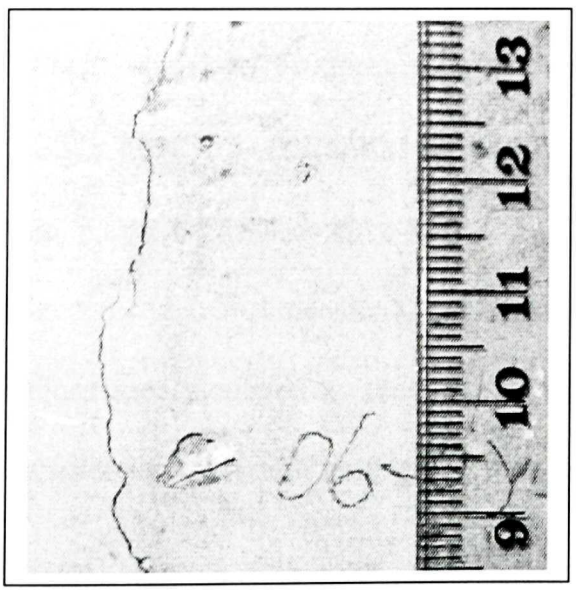

e: DMCPVA2 FRC (#5)

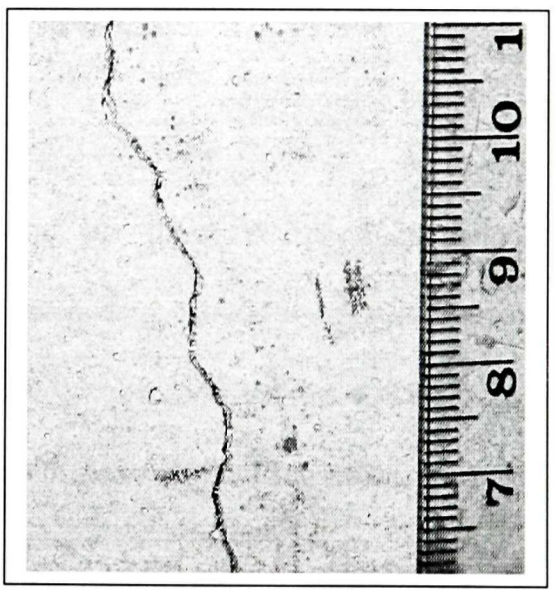

f: PVA2 Mortar (#6)

**Figure 5.40: Typical cracking on the ring specimen under restrained drying condition**

# Chapter 6 Quantification of Toughness in Strain Hardening Fiber Reinforced Concrete

## 6.1 General Concept of Toughness

The enhanced performance of fiber reinforced concrete over its unreinforced counterpart comes from its improved capacity to absorb energy during fracture. While a plain concrete fails in a brittle manner under loading and cracking, the ductile fibers in reinforced concrete continue to carry stresses beyond matrix cracking which helps maintain structural integrity. At the same time, ductile fibers transfer the loads from one location to another, which help structural cohesiveness in the materials, controls crack width and enhance energy absorption capacity. Under flexural tests, the energy absorption attribute of FRC is often termed as "toughness". Generally, Toughness, defined as a measure of energy absorption capacity, is used to characterize fiber reinforced concrete's ability to resist fracture when subjected to static strains or to dynamic or impact loads.

## 6.2 Current Standard Toughness Evaluation

### 6.2.1 ASTM C 1018 — Standard Test Method of Toughness Index

In this method [ASTM 1018-97], toughness of the fiber reinforced concrete is characterized using non-dimensional performance parameters called "toughness indices." These indices are calculated as the ratio of the energy absorbed by the specimen to a specified deflection (a certain multiple of the first crack deflection) to the energy absorbed

up to the first crack. Toughness indices, $I_5$, $I_{10}$, $I_{20}$, and $I_{30}$ are thus related to 3, 5.5, 10.5, 15.5 times the first-crack deflection, respectively. The method is shown in Figure 6.1.

It could be expressed in general terms:

$$I_N = \frac{Energy \cdot absorbed \cdot up \cdot to \cdot a \cdot certain \cdot multiple \cdot of \cdot first \cdot crack \cdot deflection}{Energy \cdot absorbed \cdot up \cdot to \cdot the \cdot first \cdot crack} \quad [1]$$

The subscript N in the index is based on the elasto-plastic analogy such that, for a perfectly elasto-plastic material, the index $I_N$ would have a value equal to N.

The strength remaining in the cracked material is characterized by the residual strength factor R derived from the toughness indexes. It represents the average strength after first crack with the reference to the first crack strength at a given deflection interval. The residual strength factor $R_{10,30}$ was recommended by ASTM, and $R_{10,50}$ was also often used for fiber reinforced concrete in pavement application and its value varied widely from approximately 0.4 to 1.0.

In general:

$$R_{a,b} = 100\% \times (I_b - I_a)/(b - a) \quad [2]$$

More specifically:

$$R_{10,30} = 100\% \times (I_{30} - I_{10})/(30 - 10)$$

$$R_{10,50} = 100\% \times (I_{50} - I_{10})/(50 - 10)$$

For index $I_N \geq N$, such as $I_5 \geq 5$, $I_{10} \geq 10$, $I_{30} \geq 30$, $I_{50} \geq 50$, it is an indication of strain hardening behavior. Moreover, the farther the sequence can be extended, the more ductile the material seems to be.

### 6.2.2 ASTM C 1399 — Residual Strength Test Method (RSTM)

A new RSTM technique has been proposed by Banthia et al. [1999] and approved to be standard method in ASTM C1399. This method is designed for the fiber reinforced concrete with low fiber volume fractions of steel or synthetic fiber [Banthia et al. 2000]. For such composites, the postpeak response obtained from open-loop testing machines tends to be very unreliable given the sudden release of energy in these machines at the occurrence of the peak load. Therefore, a new RSTM method was developed to provide a valid postpeak response using such machinery. In this method, a stable narrow crack is first created in the specimen by applying a flexural load in parallel with a steel plate under controlled conditions. The plate is then removed, and the specimen is tested in a routine manner in flexural to obtain the postcrack load-displacement response [ASTM C1399]. The residual strength (RS) could be obtained using the following equation:

$$RS = \frac{L}{bd^2}\left[\frac{P_{0.5} + P_{0.75} + P_{1.0} + P_{1.25}}{4}\right] \qquad [3]$$

Where, L = beam span; b = beam width; h= beam depth; $P_i$ = Load value at the deflection of i mm. Therefore, $P_{0.5}$, $P_{0.75}$, $P_{1.0}$, $P_{1.25}$ represent the load at the deflection of 0.5mm, 0.75mm,1.0mm,1.25mm in the load-deflection curve, respectively.

It was reported that this new technique could avoid the error obtained from open-loop testing machines, and was capable of identifying the influence of various fiber characteristics such type, length, volume fraction, etc [Banthia et al. 1999] .

### 6.2.3 JCI SF4 and JSCE SF4 — Japan Society of Civil Engineers Standard SF-4 method of FRC Toughness Characterization

These two methods are identical: Toughness $T_{JCI}$ is defined in absolute terms of the energy required to bend the fiber-reinforced beam to a midpoint-deflection of L/150 of its span, as shown in Figure 6.2. Expressed as:

$$T_{JCI} = Area \cdot under \cdot load \cdot deflection \cdot curve \cdot till \cdot deflection \cdot of \cdot (L/150) \quad [4]$$

The energy absorption of fiber reinforced concrete was analyzed and calculated by this method in Chapter 5.

And JSCE SF4 describes the flexural toughness factor (FT):

$$FT = \frac{Area \cdot under \cdot load \cdot deflection \cdot curve \cdot till \cdot deflection \cdot of \cdot (L/150) \times L}{(L/150) \times b \times h^2} \quad [5]$$

It is noticed that the flexural toughness factor (FT) has the unit of stress, which indicates the post-matrix residual strength of the materials when loaded to an arbitrary deflection of span/150.

### 6.2.4 ACI 544

In this method [ACI Committee 544], both of the unreinforced matrix beam and fiber reinforced concrete beam are tested by ASTM C1018 bending method to obtain the load-deflection curves. The toughness index $I_t$ could be described as the ratio of area under the whole load-deflection curve of fiber reinforced beam to the area under the whole load-deflection curve of unreinforced matrix beam. Therefore, $I_t$ is a measure of the improvement in toughness relative to the unreinforced matrix. The method is shown in Figure 6.3.

## 6.3 Comments on Standard Toughness Measurement Methods for Strain Hardening Fiber Reinforced Concrete

### 6.3.1 ASTM C1018 Method

ASTM C1018 method has rigorous requirement during the testing and calculation. The difficulty is to define the deflection of first crack initiation. The calculations of toughness indexes require an accurate assessment of the first-crack energy which constitutes the denominator in the definition of the various indexes. The most significant problem is any error in the first –crack energy will lead to a significant deviation in the value of the various indexes.

The definition of first crack is still arbitrary even in the specification. An example is shown in Figure 6.4. As defined in ASTM C1018, first crack is "the point load-deflection curve at which the form of the curve first becomes nonlinear (approximates the onset of cracking in the concrete matrix)". Based on this, the first cracking in the matrix may be placed at Point A. However, as written in the standard, "if the load-deflection curve is slightly convex upwards throughout its initial portion, first crack is the point at which the curvature first increases sharply and the slope of the curve a definite change." According to this definition, the first cracking in the matrix may be placed at Point B. However, since there is no sharp curvature change in this case, the initial cracking could generate any point from B to C. Therefore, it is very difficult to define the first crack displacement in the fiber reinforced concrete. Moreover, in the fiber reinforced concrete, when a strain hardening behavior leads to a load transfer from first crack to the hardening response, it is especially difficult to define an accurate first crack displacement.

Limitation of the ASTM C1018 toughness indexes can be further demonstrated by load-deflection curves shown in Figure 6.5. In this example, the characterization of toughness index may be insufficient to differentiate between two composites [Naaman et al.1995]. In figure 6.5, Composite B exhibits a toughness index $I_{1B,\ 5B}$=5, whereas composite A has an index $I_{1A,\ 5A}$ =6. The toughness index by itself could not tell which composite is better.

By using the residual factor R into example (Figure 6.5), it is obtained $R_B = (5-1)/4 = 1$, and $R_A = (6-1)/4 = 1.25$. Thus, $R_B < R_A$. The shapes of load-deflection curves A and B were reflected, but the question is still there. Unless one sees the load-deflection response, it is difficult to decide. The factor was composites B absorbed more than four times energy of composites A. In addition, concerning the difficult in determining the first crack displacement, the error would be doubled during the calculation of residual strength factor R through the toughness index I.

### 6.3.2 ASTM C 1399 — Residual Strength Test Method (RSTM)

This new technology is mainly developed for fiber reinforced concrete with low volume fraction of fibers, and not suitable for strain hardening fiber reinforced concrete, since there is no sudden release of energy in strain hardening materials. Moreover, the technology is complicated, and is more suitable to study the critical cracking zone. In addition, the maximum deflection of 1.25mm is computed in residual strength method, thus the large postpeak response of strain hardening response of FRC could not be reflected.

### 6.3.3 JCI SF4 Method

As discussed in chapter 5, JCI method is not an effective method to quantify the stain-hardening response, since only the area under load-deflection curve up to 2 mm (if span equals to 300mm) is used in calculation. The strain-hardening FRC could have much large deflection with a peak load higher than the first crack strength.

The JCI flexural toughness factor (FT) has the unit of stress, which is similar to the residual strength factor $R_{a,b}$ of ASTM C1018. And again with the limitation of (L/150) m, this strength-based factor will not show the difference if strain-hardening materials have larger deflection than (L/150) m.

The JCI toughness method was used in chapter 5 to evaluate the flexural toughness of all the batches. However, it did not truly be represent the strain-hardening response.

### 6.3.4 ACI 544 method

The method proposed by ACI Committee 544 for evaluate toughness, however, is also limited, since in many cases with fibers of long length, the load will never drop to the zero. The energy could not be calculated accurately due to the long postpeak tail with small slope.

## 6.4 Other Proposed Toughness Methods

In addition to the standard methods, some other special methods to evaluate toughness of fiber reinforced concrete were also developed in order to overcome the difficulties in quantification.

### 6.4.1 Post-Crack Strength ($PCS_m$) Method

This method was developed based on residual strength concept. To avoid the human error on measuring the first crack displacement, the peak load displacement was chosen. Basically, the method considers the post-peak area under the load versus deflection curve for the computation of $PCS_m$. The method is illustrated in Fig. 6.6 [Banthia et al. 1995] and the $PCS_m$ measured at a deflection of L/m, is defined as follows:

$$PCS_m = \frac{(E_{post,m})L}{[(L/m) - \delta_{peak}]bh^2} \qquad [6]$$

Where, $PCS_m$ = post-crack strength at a deflection of L/m; $E_{post,m} = E_{total} - E_{pre}$ = area under the load-deflection curve until a serviceability limit – area up to peak; L = beam span; b = beam width; h= beam depth; $\delta_{peak}$ = deflection at the peak load; L/m = application specific serviceability limit deflection.

The advantage of the method is that $E_{post,m}$ is obtained by subtracting $E_{pre}$ from the total energy $E_{total, m}$(unlike the ASTM technique, where division by the first-crack energy is involved) and as such the resulting $PCS_m$ values are not sensitive to small errors made in the calculation of the prepeak energy $E_{pre}$.

However, fiber reinforced concrete with strain-hardening response may involve several peaks. A typical example is shown in Figure 6.7. In this case, it is point A not point B which should be chosen as peak load to calculate the $E_{post,m}$, since point A is the first peak.

### 6.4.2 Absolute Toughness Value Method

This method was developed based on ASTM C1018. Instead of using actual deflection $\delta_f$ at first crack which could not be accurately identified, the toughness index

was computed using $\phi\delta_f$, the erroneous deflection at first crack which included actual deflection plus elastic and inelastic extraneous deformations. So, from figure 6.8, the typical toughness indexes $I_{me}$ ( m = 5, 10, 20, 30) based on the erroneous load-deflection response, could be computed from simple geometry [Gopalaratnam et al. 1991] as:

$$I_{me} = \frac{0.5P_f(\phi\delta_f) + \gamma_{me}P_f(\frac{m-1}{2})(\phi\delta_f)}{0.5P_f(\phi\delta_f)} = 1 + (m-1)\gamma_{me} \qquad [7]$$

When : $\gamma_{me} = 1 - \frac{k_{de}}{K_{ae}}(\frac{m-1}{4})$

Where $K_{de}$ = slope of the erroneously measured load-deflection response, and $k_{ae}$ = initial or precracking slope of the erroneous load deflection response = $P_f/(\phi\delta_f)$.

With a large number of parameters involved, this method is not simple and could not be used directly at any situation. Moreover, according to concept, this method is mainly to solve the problem of the uncertain first crack displacement.

## 6.5 Ductility Factor — A Toughness Measurement of Strain Hardening Response

### 6.5.1 Ductility Factor

Based on the review of the toughness methods, a ductility factor is used to quantify and compare the strain hardening behavior of fiber reinforced concrete.

The post crack strength ($PCS_m$) proposed by Banthia et al [1995] seemed to be a good indicator of the effectiveness of fiber toughening mechanisms. It was defined as "Post-crack strength", that is, load-carrying capacity after first crack. It was also called "residual strength". The expression is as follows:

$$\sigma_{pcs} = PCS_m = \frac{(E_{post,m})L}{[(L/m) - \delta_{peak}]bh^2} \quad [6]$$

Where, $\sigma_{pcs}$ = post-crack strength at a deflection of L/m; $E_{post,m}$ = area under the load-deflection curve in the post-peak region until a serviceability limit; L = beam span; b = beam width; h= beam depth; $\delta_{peak}$ = deflection at the peak load; L/m = application specific serviceability limit deflection.

The schematic of $E_{post,m}$ is shown in Figure 6.6. $E_{post,m}$ represents the energy absorption capacity after the first peak load and can be used to reflect postpeak hardening or softening. Moreover, $E_{post,m}$ is also dependent on L/m, which is in favor of the hardening materials. A net deflection (L/m - $\delta_{peak}$ ) value according to application specific serviceability limit (L/m) should be determined. This value is more likely a variable depending on the design requirement and experimental program. Usually, in bridge design, m =300; in FRP composite design, m = 60. For strain hardening FRC used in the special application involving large energy absorption, m could be defined flexibly by the designer. This concept is similar to the subscript N in ASTM C1018 and could be further extended to any net deflection along the load-deflection curve. The post-crack strength method avoid the difficulty in identifying the first crack displacement of ASTM toughness method

However, the post crack strength still cannot distinguish the difference between strain-softening behavior and strain-hardening behavior, and the level of the hardening. A strain-hardening fiber reinforced concrete with a low flexural stress and a strain-softened fiber reinforced concrete with a high flexural stress may show the similar toughness value. Therefore, a ductility factor, D, is defined as follows:

$$D = \frac{\sigma_{PCS}}{\sigma_{first\text{-}peak}} \qquad [8]$$

Where, $\sigma_{pcs}$ = post-crack strength, MPa, Eq. [6]

$\sigma_{first\ peak}$ = first crack strength, MPa

Obviously, if D> 1, this is a perfect strain-hardening behavior. The larger the value D, the better the ductility, and the more likely the strain-hardening response. Since $\sigma_{pcs}$ is an average postpeak residual strength up to L/m limit, ductility factor, D, resembles the residual strength factor, R, in ASTM 1018. Nevertheless, ductility factor, D, is more straightforward, more representative and less influenced by first crack measurement.

### 6.5.2 Ductility Factors for Batch #1 to Batch #16

According to the ductility factor, toughness of all batches designed were analyzed again. In this study, L/m = 300mm/60 = 5 mm was assumed as the serviceability limit.

The results of post-crack strengths for batch #1 to #16 are presented in Figure 6.9 through Figure 6.11. By using this parameter, microsteel PVA FRC (#7) showed a 17% increment of post-crack strength compared to that of PVA FRC (#2), indicating a contribution of microsteel fiber to energy absorption capacity. The post crack strength demonstrated almost all PVA fiber concrete (batch #4, #5, #6) had higher value than steel concrete (batch #3) which was not observed by JCI toughness in Figure 5.35, except that PVA concrete of batch #2 still showed similar post crack strength as steel concrete (#3).

Ductility factors for all batches are given in Figure 6.12 to Figure 6.14. The brittle matrix (#1) only obtained a ductility factor of 0.02. All the strain-hardening FRCs exhibited the ductility factor above 0.80, while the ductility factor of PVA FRC (#2)

reached 0.92, the steel FRC (#3) only showed a factor of 0.70. Therefore, this ductility factor could represent the different shapes of load-deflection curves by distinguishing strain softening behavior from strain hardening. A perfect strain hardening PVA mortar had a factor of 1.14, which was the highest value of all the batches. Freezing–thawing cycles reduced ductility factor of all PVA fiber concretes except batch #5 with methylcellulose and defoamer. However, relatively, the ductility of all the PVA and steel FRCs were not significantly affected by freeze-thaw cycling. Compared to $T_{JCI}$ in Figure 5.35 to Figure 5.37, ductility factor, D, reflected more features of strain hardening response.

## 6.6 Toughness Consideration in Design Practice

Characterization of fiber reinforced concrete with strain hardening behavior is basically established by toughness method, that is, energy absorption capacity. People do recognize and are aware of the importance of this concept. However, how to apply the toughness of fiber reinforced concrete directly into design practice is still a question and undocumented nowadays. There is limited effort in this area.

### 6.6.1 Fiber Reinforced Concrete in Current Pavement and Overlay Design

The use of fiber reinforced concrete in pavement and bridge overlays started in 1970s. Many actual applications and experimental filed studies of fiber concrete pavement overlays have been reported [Schrader 1984] [Vandenberghe et al. 1985].

However, concrete properties used in design only include compressive strength, flexural strength, and modulus of rupture. According to ACI 544 1993, typical material

properties of steel fiber reinforced concrete used in pavement and overlays are: Flexural strength = 6MPa – 8MPa, Compressive strength = 42MPa, Poisson's ratio = 0.2, and modulus of elasticity = 28GPa. There is no consideration about energy absorption capacity and toughness technique, although the potential benefit that might result from the characteristics of FRC is acknowledged by many researchers and engineers [Missouri Department of Transportation, 2001].

### 6.6.2 Available information of Toughness in Design

Little information was available on other application specifications. In 1993, the European Federation of Producers and Applicatiors of Specialist Products for Structures (EFNARC) published a "European Specification for Sprayed Concrete" [Morgan 2000]. This document is a general specification, intended primarily to shotcrete repairs. The energy absorption requirement for steel fiber reinforced shotcrete linings under special test method is specified depending on the toughness classification, as shown in table 6.1 [Vandewalle 2000].

### 6.6.3 Proposed Toughness Evaluation in Future Design

In term of the stress-strain response, the multiple cracking mechanism translates into a strain-hardening behavior (as described in Chapter 2), thus turns out to be controlled crack width, deflection and large energy absorption capacity as advantages into special application in repair, thin pavement and overlay system with such requirement.

Many of the early experimental and actual fiber reinforced concrete pavements and overlays developed full-width transverse crack within 24-36 hours after placing. It is

probably because of shrinkage and temperature changes and traffic loading. Therefore, the post-crack flexural strength is more important once cracking initiate. $\sigma_{pcs}$ could be used in the traditional overlay design to obtain a high flexural strength. Therefore, with a high post crack flexural strength, under the same cyclic loading, the thickness of the pavement or overlays could be reduced.

Ductility factor, which could differentiate the strain-softening behavior from strain-hardening behavior, might be a good indicator for load transfer efficiency and crack width control. The higher the D, the higher the load transfer efficiency. Therefore, a larger deflection for overlays would be allowed without affecting the structure in the case of strain hardening fiber reinforced concrete. In addition, ductility factor not only reflects deflection capacity, but also is a pointer of extended service life. It is because that controlled crack width prevents or reduces the aggressive environmental substance to diffuse through, leading to the corrosion or durability problem.

Moreover, the ductility factor could be related to fatigue life. That is because the flexural fatigue life of a beam is governed by a single dominated fatigue crack propagation behavior. No matter how many cracks are developed during fatigue loading, the number of fatigue cycles until failure is principally controlled by the crack bridging performance of the dominant single crack under cyclic loading [Zhang et al. 2002]. When fiber bridging stress is still sufficient to result in multiple cracking, and is able to restrict the propagation of already formed crack and delay the localization of cracking, therefore, the fatigue life of strain hardening fiber reinforced concrete could be significantly increased.

Overall, the applications of strain hardening fiber reinforced concrete are specified to the repair, thin bridge deck and pavement overlays, industrial floor etc, which requires large energy absorption capacity, controlled crack width, and longer service under cyclic, fatigue and impact loading condition.

**Table 6.1 Toughness in EFNRC recommendation**

| Toughness Classification | Energy absorption in joule for deflection until 25mm |
|---|---|
| a | 500 |
| b | 700 |
| c | 1000 |

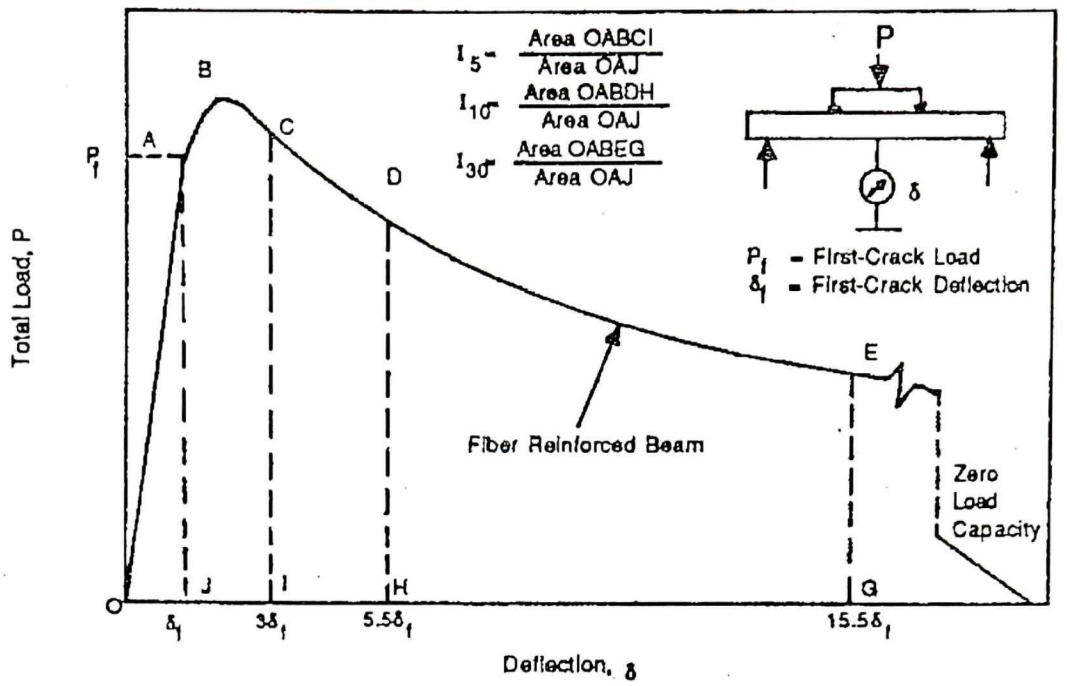


**Figure 6.1 ASTM C1018 Standard Measures of Fiber Reinforced toughness Characterization [Gopalaratnam et al. 1991]**

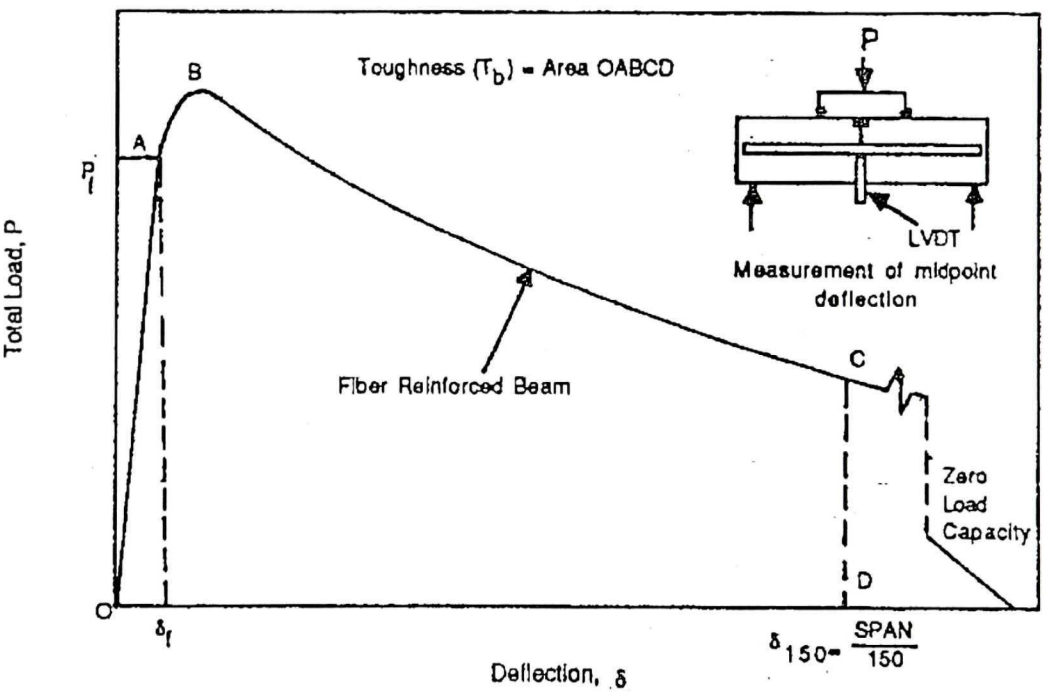


**Figure 6.2 JCI SF4 Standard Measures of Fiber Reinforced toughness Characterization[Gopalaratnam et al. 1991]**

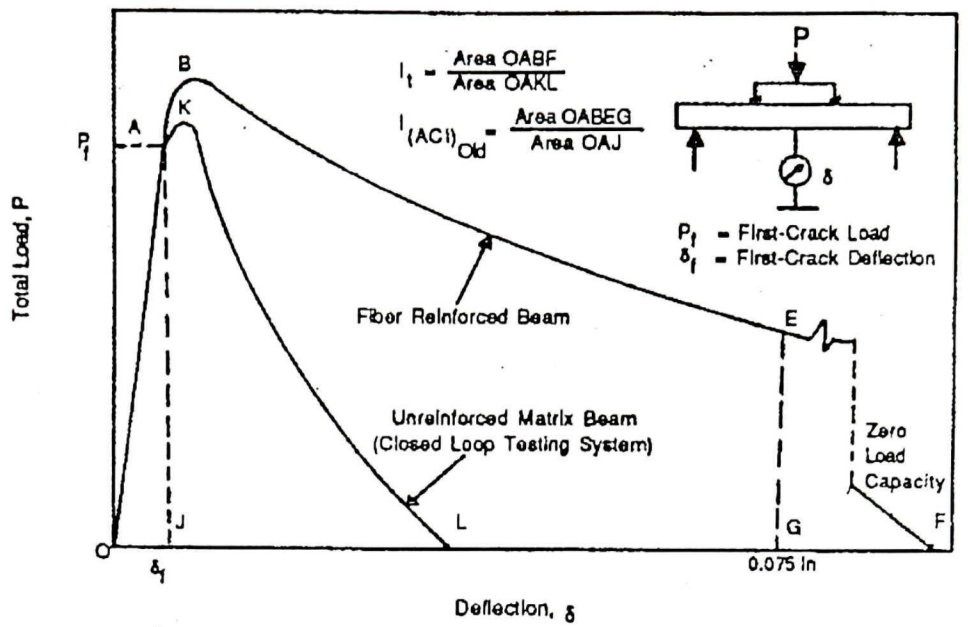


**Figure 6.3 ACI Committee 544 Measures of Fiber Reinforced toughness Characterization [Gopalaratnam et al. 1991]**

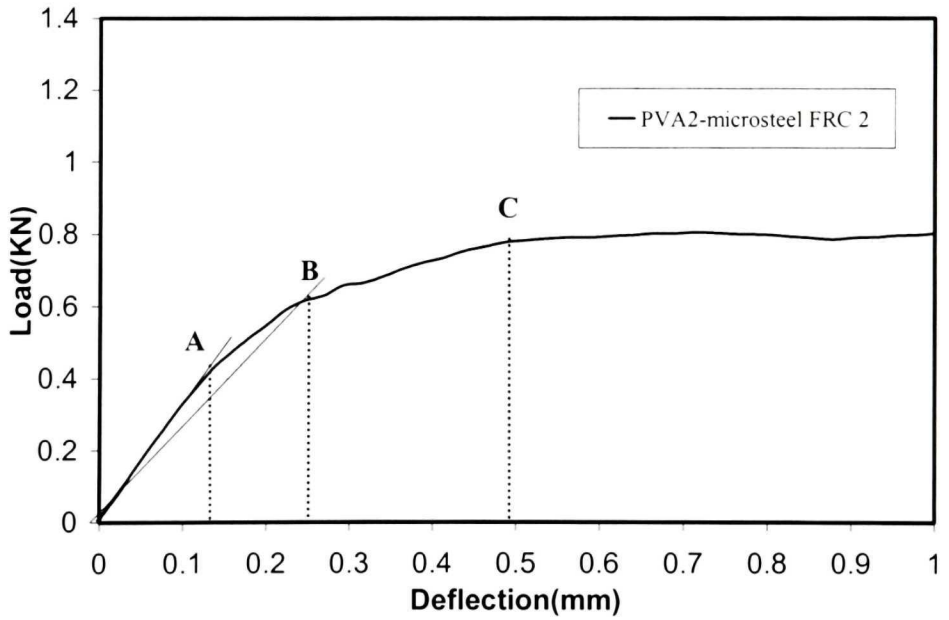


**Figure 6.4 Arbitrary values of first crack displacement on load-deflection curve (Initial ascending part of curve) of a sample.**

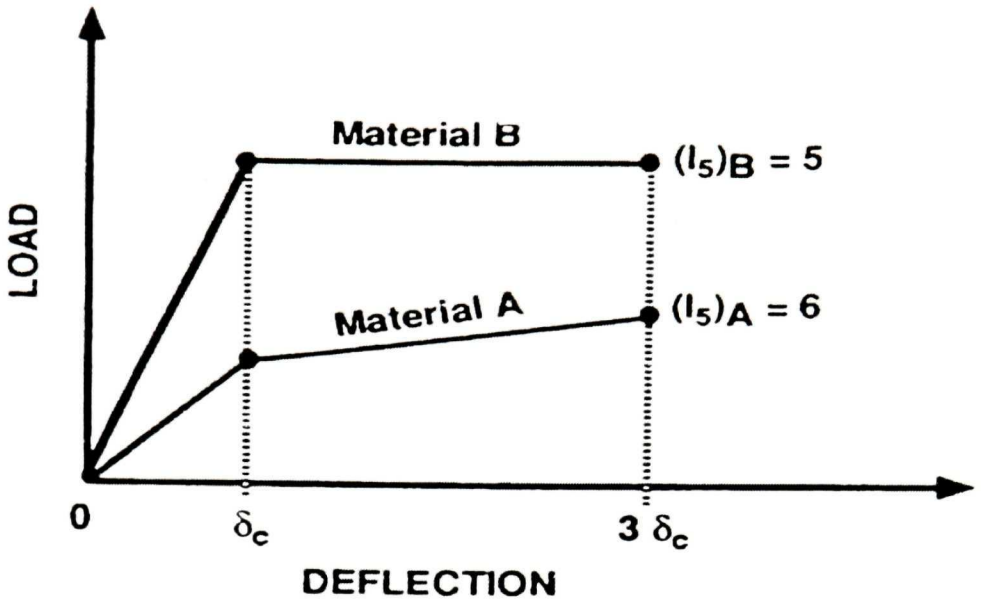


**Figure 6.5 Typical load deflection curves possible oversight in selecting composites based on toughness index [Naaman et al.1995]**

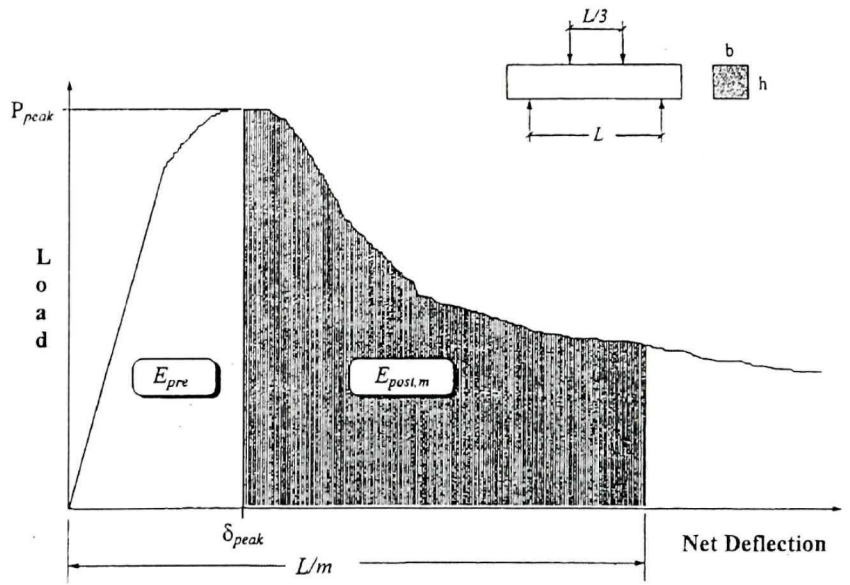


**Figure 6.6 A schematic description of the post-crack strength method of toughness characterization [Banthia et al. 1995].**

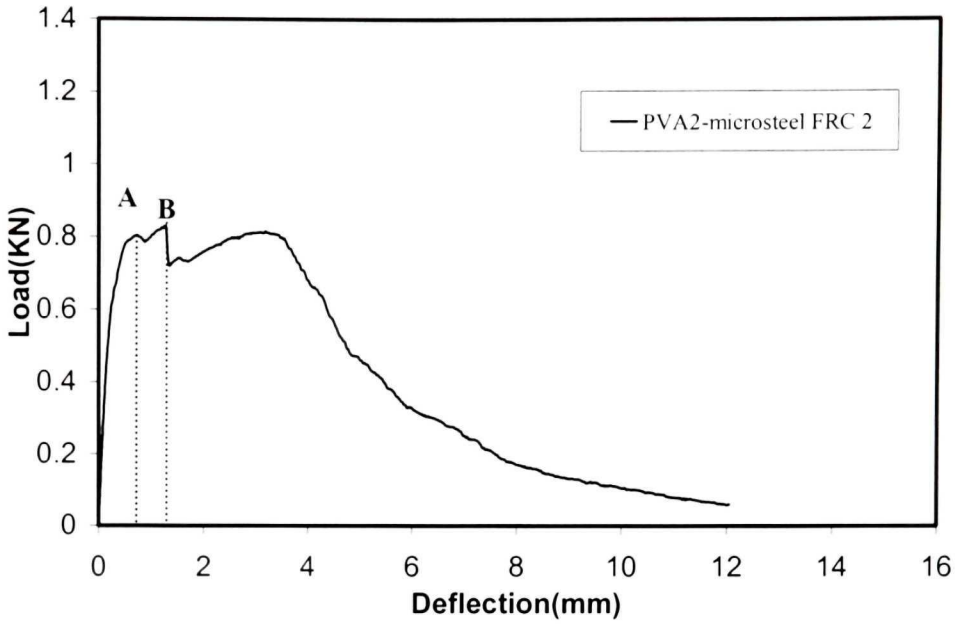


**Figure 6.7 Arbitrary values of peak value used in "Post-crack strength ($PCS_m$) method" on a sample.**

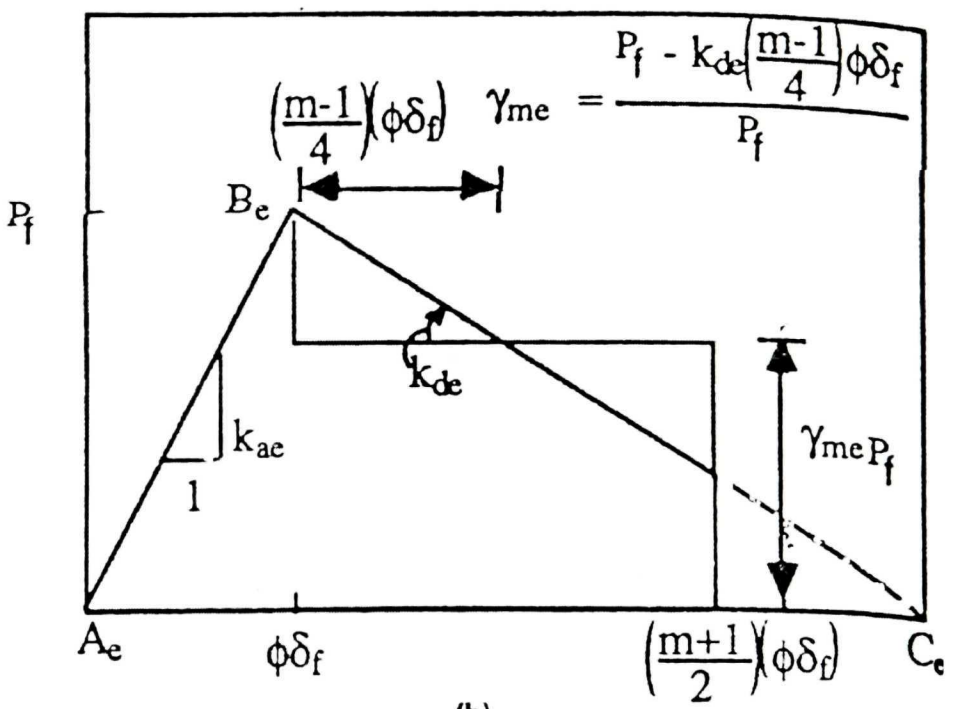


(b)

**Figure 6.8 Idealized load-deflection response of a Fiber reinforced concrete using erroneous deflection [Gopalaratnam et al. 1991].**

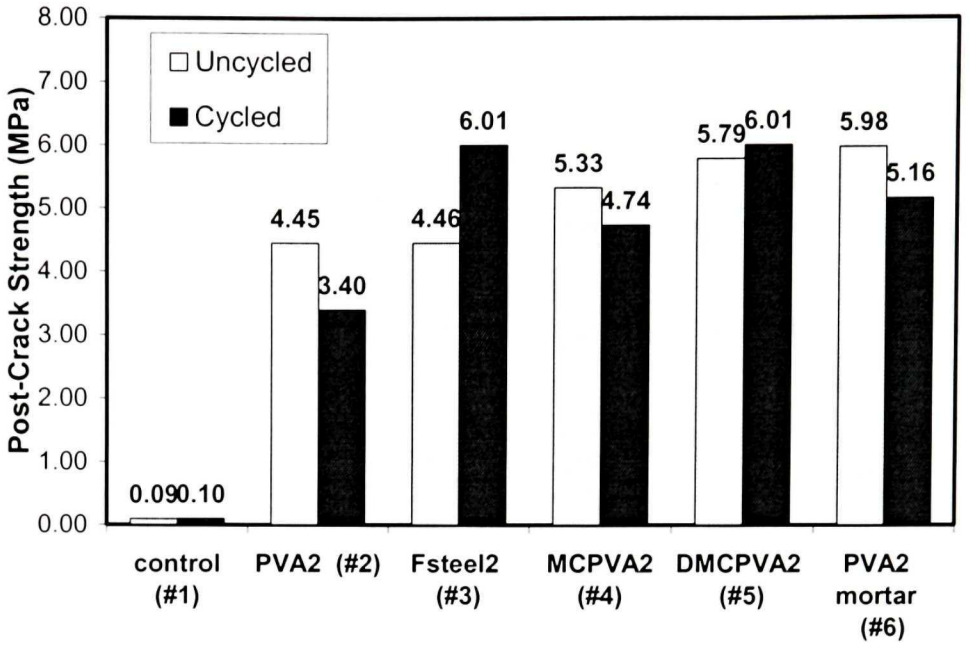


**Figure 6.9 Post-Crack Strength (Batch #1-#6)**

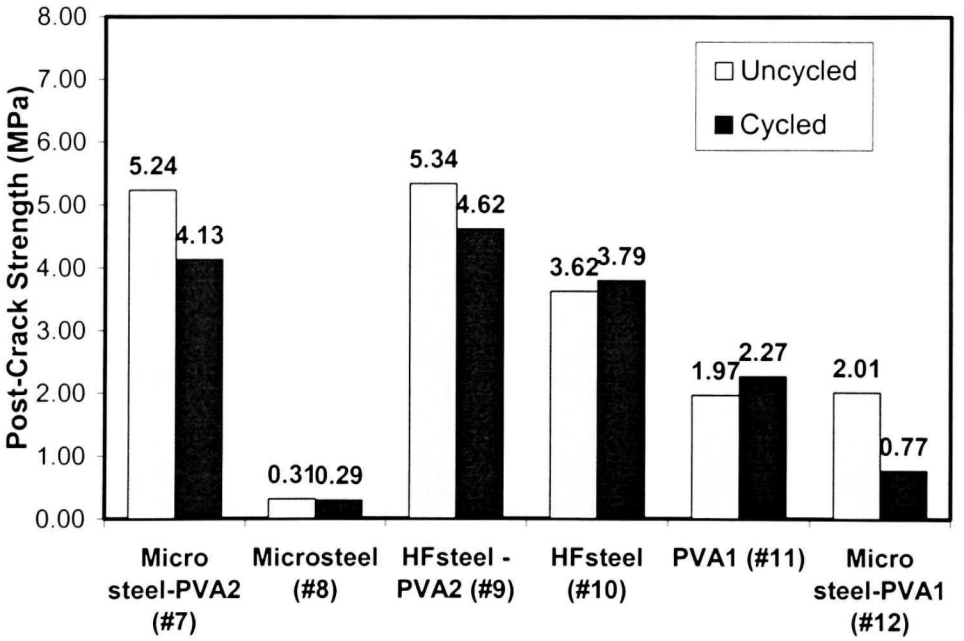


**Figure 6.10 Post-Crack Strength (Batch #7-#12)**

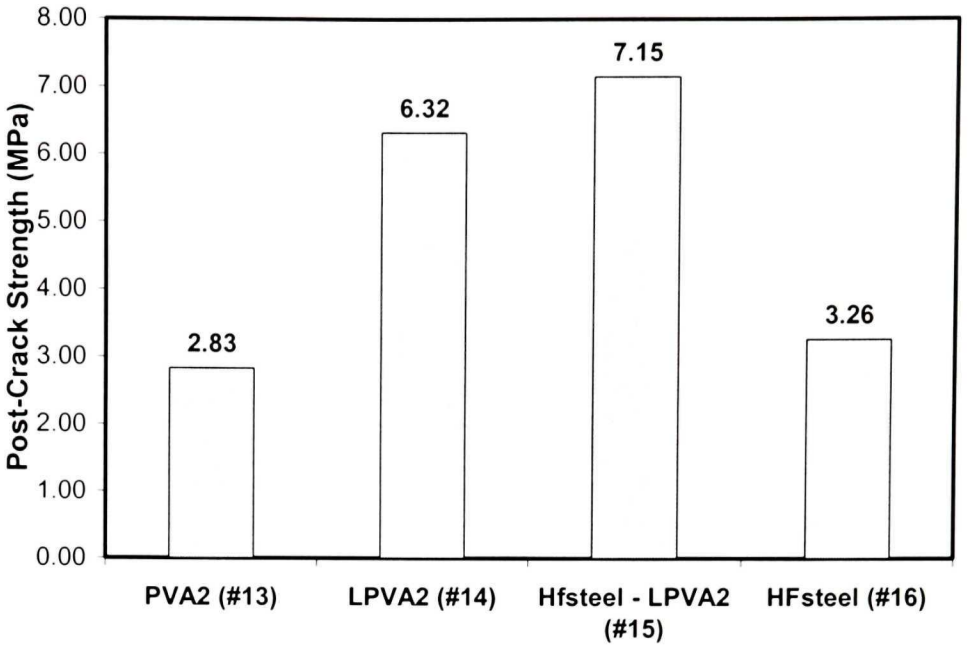


**Figure 6.11 Post-Crack Strength (Batch #13-#16)**

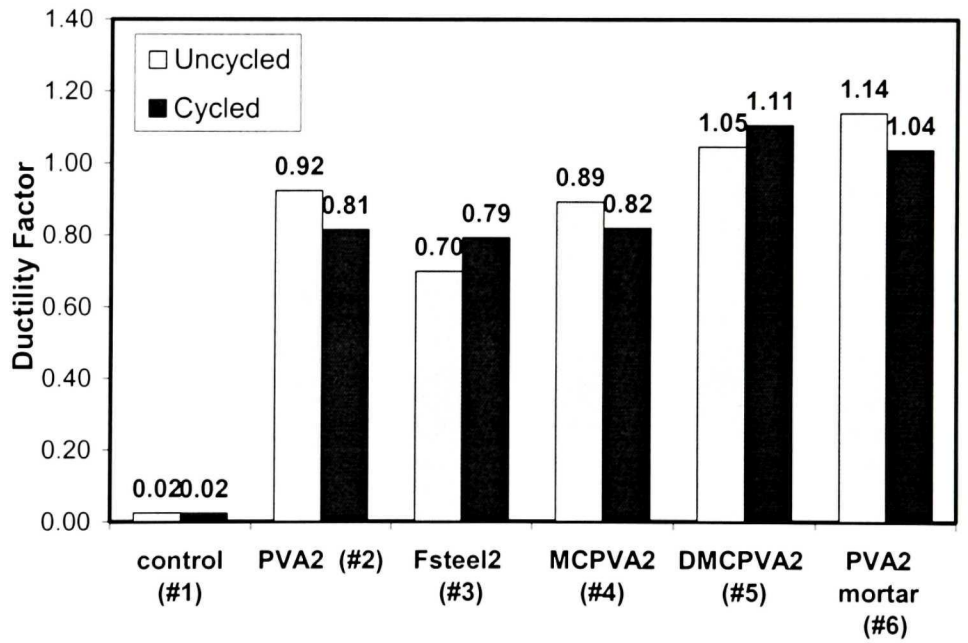


**Figure 6.12 Ductility Factor —Comparison of strain hardening level (Batch #1-#6)**

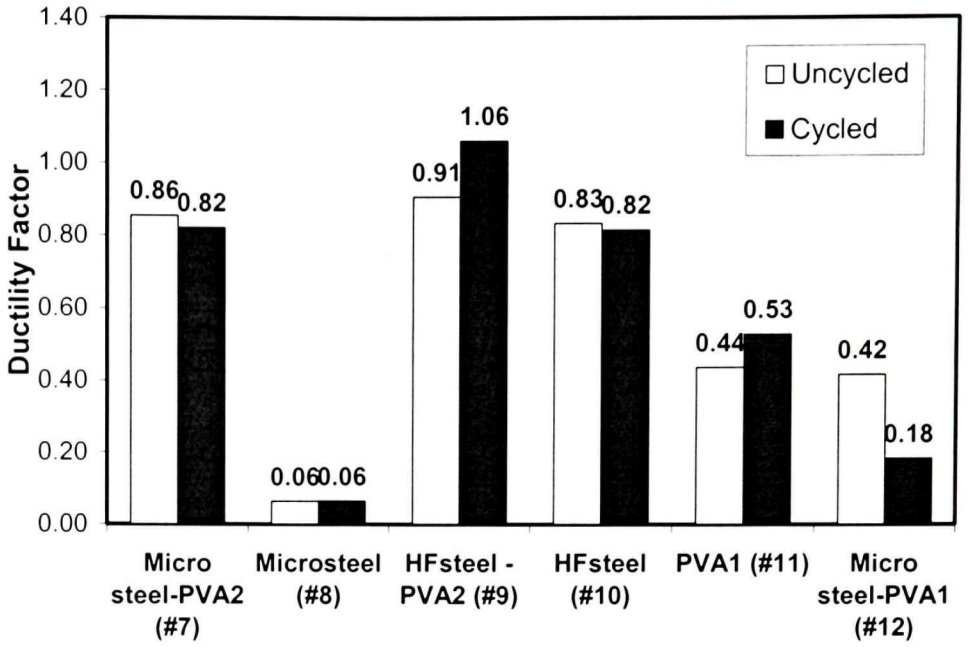


**Figure 6.13 Ductility Factor —Comparison of strain hardening level (Batch #7-#12)**

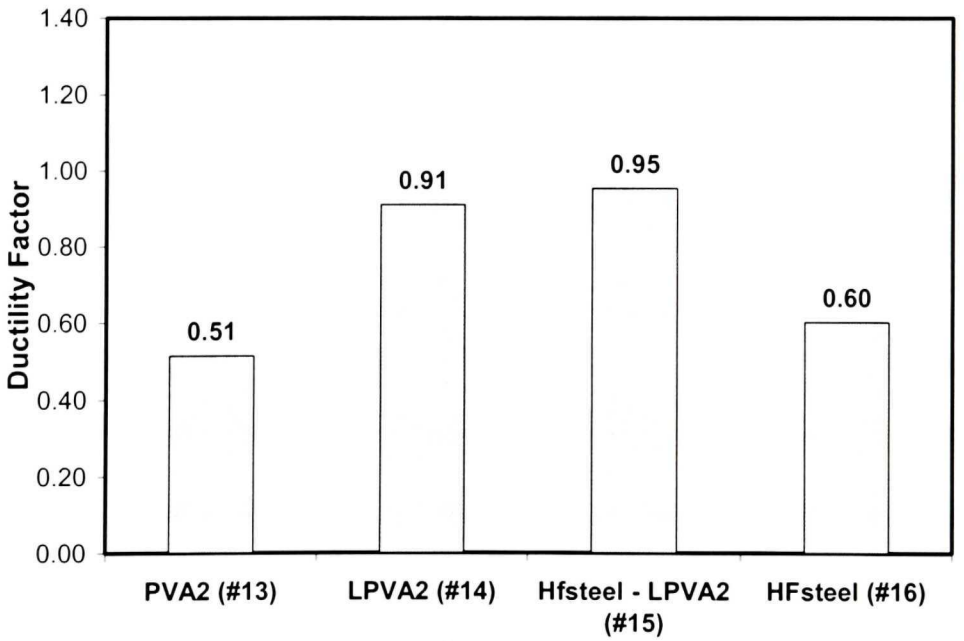


**Figure 6.14 Ductility Factor —Comparison of strain hardening level (Batch #13-#16)**

# Chapter 7 Conclusions

Fiber reinforced concrete with postpeak strain hardening behavior was studied in this thesis. Polymer modification and hybrid fiber systems were employed to enhanced the hardening response. The following conclusions are drawn:

1. PVA fiber concrete with 2% fibers by volume exhibited a quasi strain hardening behavior with multiple cracking, when certain quantity of coarse aggregates were used. However, with same amount of flat end steel fibers in the same cement mix, a strain softening behavior with single localized cracking was observed. Therefore, the type of fiber was an important parameter to determine the hardening response. Apparently, specimens with strain hardening behavior were usually accompanied with multiple cracking, and specimens with strain softening behavior always occurred with single cracking till failure.

2. The strain-hardening response of PVA FRC was reduced with a decrease in cement paste (as binder) and an increase in aggregate content and size because of the reduced binding agent.

3. Strain-hardening response of FRC was sensitive not only to the fiber types but also to the end conditions of fiber. In rich cement mix, FRC with 2% by volume of flat end steel fiber behaved strain softening under flexural load with localized single cracking, while FRC with only 0.4% by volume of hooked flat end steel fiber achieved quasi strain-hardening behavior with multiple cracking. In normal strength mix, FRC with the same amount of hooked flat end steel fiber showed strain softening behavior because of the reduced binder content.

4. The strain hardening response and multiple cracking phenomenon of PVA FRC was not observed in a concrete reinforced with 1% fibers by volume with the same PVA

fibers. Fiber volume ratio was therefore also important for strain hardening in FRC after the right fiber was chosen. In the situation of PVA fiber, volume fraction of 2% might be the optimum to achieve quasi strain hardening behavior with multiple cracking.

5. The length of PVA fiber could affect the flexural behavior of FRC. With the same amount of PVA fiber, the longer the fiber, the higher the first crack strength and the peak strength, the larger the energy absorption capacity, and the more the chance to obtain strain hardening response with multiple cracking.

6. In rich cement mix, methylcellulose as polymer addition proved to be an effective approach to achieve and improve strain hardening behavior. Methylcellulose had the ability to enhance the interfacial bond between fiber and matrix. With the help of antifoaming agent, the behavior of polymer modified PVA FRC achieved best strain-hardening behavior.

7. In rich cement mix, the steel-PVA hybrid FRC obtained better flexural strength and ductility compared to PVA or steel FRC alone. The steel fibers in hybrid FRC contributed not only to improved first crack strength and energy absorption, but also to the suppressed unloading owing to their pullout resistance. However, when only 1% PVA fiber was used in hybrid system, PVA FRC could not create strain hardening response in concrete. Furthermore, the addition of microsteel fiber had almost no effect on flexural behavior of this hybrid FRC.

8. The strain hardening response of PVA FRC and mortar would deteriorate during freeze-thaw cycling. It was possibly because of different thermal expansion coefficients between PVA fiber and concrete matrix under freeze – thaw cycling, leading to the debonding between fiber and matrix. It could also be attributed to the sensitivity of PVA

fiber to the cold temperature which might increase the fiber's brittleness and reduce its ability of stretching and load transfer.

9. With the addition of polymer, through improved interfacial bond between fiber and matrix, the PVA FRC exhibited excellent freeze-thaw resistance, that is, maintaining the good strain hardening response under severe freeze-thaw environment. However, the hybrid system with PVA and steel fiber could not stop the loss of flexural strength and energy absorption capacity caused by the bond deterioration of PVA fiber during freeze-thaw cycling. Steel fiber could not help PVA fiber to be more resistant to the frost damage.

10. All the steel FRCs would remain or gain their properties such as flexural strength, strain hardening behavior during freeze-thaw cycling. It is likely that there is no deterioration of the matrix under freeze-thaw cycling if enough air is available, and the matrix became stronger because of the ageing. Moreover, steel fiber had same thermal expansion coefficient as concrete matrix, and it was the mechanical anchor, not the adhesive bond which made no bond deterioration between steel fiber and matrix after freeze-thaw cycling. Therefore, steel FRC actually get a better behavior under frost action by gaining more strength and higher energy absorption, but still strain-softening behavior.

11. Fiber addition did not reduce significantly the free shrinkage under severe drying condition. PVA fiber concrete with methylcellulose (batch #4) had significant shrinkage compared to the other concrete batches. It was because the additional entrained air by polymer addition was provided more free spaces for water movement under severe drying condition.

12. FRCs exhibited the ability to control crack opening and reduce the crack width significantly compared to plain concrete. With large quantity of stiff and high strength steel fiber, steel FRC showed best ability of controlling crack by showing the delayed first crack and smaller crack width. PVA mortar showed early first crack, and large crack width because of the absence of coarse aggregates. Due to the addition of polymer, PVA FRC exhibited more shrinkage cracks. However, the crack width was well controlled by multiple cracking because of the enhanced bond between fiber and matrix resulted in the evenly load distribution over the concrete ring specimens.

13. To evaluate the strain hardening FRC under the flexure, all current standard and modified methods were reviewed and discussed. JCI method was used to quantify the toughness. However, it was not an effective method to represent the stain hardening response, when all the FRCs were assessed only up to 2mm deflection.

18. A ductility factor was developed and characterized based on Banthia [1995]:

**Ductility Factor:** $$D = \frac{\sigma_{pcs}}{\sigma_{first\cdot peak}}$$

Where, Post crack strength: $$\sigma_{pcs} = \frac{(E_{post,m})L}{(\frac{L}{m} - \delta_{first\cdot peak})bh^2}$$

Post crack strength was averaged post peak residual strength after cracking till certain defined deflection, which was more practical in current overlays design. Ductility factor reflected the shape of the load-deflection curve. Likely, when D was smaller than 0.8, the material would show strain softening behavior; when D was between 0.8 to 1.0, the material would be of quasi strain hardening; when D was larger than 1.0, it was excellent postpeak hardening behavior. The ductility factor analysis of all batches demonstrated

that this parameter could quantitatively distinguish the differences between strain hardening and strain softening responses.

# Appendix A

**Table A.1 Compressive strength (Batch #1~ #6)**

| Batch Number | Batch | Sample ID | Peak Load | Peak Stress | Average Stress |
|---|---|---|---|---|---|
| | | | kN | MPa | MPa |
| #1 | Control | 1 | 142.8 | 61.57 | 60.21 ± 4.05 |
| | | 2 | 128.5 | 63.40 | |
| | | 3 | 112.8 | 55.66 | |
| #2 | PVA2 | 1 | 108.0 | 53.31 | 52.12 ± 1.16 |
| | | 2 | 105.5 | 52.06 | |
| | | 3 | 103.4 | 51.00 | |
| #3 | Fsteel2 | 1 | 131.4 | 64.81 | 64.54 ± 0.64 |
| | | 2 | 131.8 | 65.01 | |
| | | 3 | 129.3 | 63.81 | |
| #4 | MCPVA2 | 1 | 84.6 | 41.75 | 43.72 ± 2.79 |
| | | 2 | 92.6 | 45.70 | |
| #5 | DMCPVA2 | 1 | 111.2 | 54.88 | 54.06 ± 1.03 |
| | | 2 | 110.3 | 54.40 | |
| | | 3 | 106.6 | 52.90 | |
| #6 | PVA2 Mortar | 1 | 128.4 | 63.33 | 64.36 ± 2.29 |
| | | 2 | 135.8 | 66.99 | |
| | | 3 | 127.2 | 62.77 | |

**Table A.2 Compressive strength (batch #7 ~ #12)**

| Batch Number | Batch | Sample ID | Peak Load | Peak Stress | Average Stress |
|---|---|---|---|---|---|
| | | | kN | MPa | Mpa |
| #7 | Microsteel-PVA2 | 1 | 115.5 | 56.98 | 51.11 ± 5.59 |
| | | 2 | 92.9 | 45.85 | |
| | | 3 | 102.4 | 50.49 | |
| #8 | Microsteel | 1 | 98.1 | 48.40 | 50.52 ± 2.07 |
| | | 2 | 106.5 | 52.54 | |
| | | 3 | 102.6 | 50.63 | |
| #9 | HFsteel-PVA2 | 1 | 90.8 | 44.80 | 43.67 ± 7.02 |
| | | 2 | 73.3 | 36.15 | |
| | | 3 | 101.5 | 50.07 | |
| #10 | HFsteel | 1 | 110.2 | 54.38 | 51.58 ± 10.29 |
| | | 2 | 122.0 | 60.18 | |
| | | 3 | 81.4 | 40.17 | |
| #11 | PVA1 | 1 | 93.4 | 46.08 | 50.10 ± 4.97 |
| | | 2 | 112.0 | 55.66 | |
| | | 3 | 98.4 | 48.55 | |
| #12 | Microsteel-PVA1 | 1 | 84.0 | 41.16 | 39.5 ± 1.79 |
| | | 2 | 80.0 | 39.75 | |
| | | 3 | 76.2 | 37.59 | |

**Table A.3 Flexural strength under four point bending test (batch #1 ~ #6)**

| Batch number | Batch | Condition | Sample I.D. | Peak Load kN | Peak Stress MPa | Average Stress MPa |
|---|---|---|---|---|---|---|
| #1 | Control | Cycled | 1* | 0.73 | 4.5 | 4.2 ± 0.25 |
| | | | 2* | 0.65 | 4.0 | |
| | | | 3* | 0.67 | 4.2 | |
| | | Uncycled | 4 | 0.55 | 3.4 | 3.8 ± 0.36 |
| | | | 5 | 0.66 | 4.1 | |
| | | | 6 | 0.64 | 3.9 | |
| #2 | PVA2 | Cycled | 1* | 0.74 | 4.6 | 4.5 ± 0.15 |
| | | | 2* | 0.70 | 4.3 | |
| | | | 3* | 0.73 | 4.5 | |
| | | Uncycled | 4 | 0.85 | 5.3 | 5.3 ± 0.35 |
| | | | 5 | 0.79 | 4.9 | |
| | | | 6 | 0.90 | 5.6 | |
| #3 | Fsteel2 | Cycled | 2* | 1.27 | 7.9 | 7.6 ± 0.93 |
| | | | 3* | 1.07 | 6.6 | |
| | | | 4* | 1.35 | 8.4 | |
| | | Uncycled | 1 | 0.94 | 5.9 | 6.4 ± 0.44 |
| | | | 5 | 1.07 | 6.6 | |
| | | | 6 | 1.08 | 6.7 | |
| #4 | MCPVA2 | Cycled | 1* | 0.95 | 5.9 | 6.2 ± 0.31 |
| | | | 2* | 1.05 | 6.5 | |
| | | | 3* | 0.98 | 6.1 | |
| | | Uncycled | 4 | 0.92 | 5.7 | 6.3 ± 0.39 |
| | | | 6 | 1.06 | 6.6 | |
| | | | 7 | 1.04 | 6.4 | |
| | | | 8 | 1.03 | 6.4 | |
| #5 | DMCPVA2 | Cycled | 4* | 1.04 | 6.4 | 6.7 ± 0.36 |
| | | | 6* | 1.07 | 6.6 | |
| | | | 7* | 1.15 | 7.1 | |
| | | Uncycled | 1 | 1.10 | 6.8 | 6.5 ± 0.24 |
| | | | 8 | 1.02 | 6.3 | |
| | | | 9 | 1.01 | 6.3 | |
| | | | 10 | 1.04 | 6.4 | |
| #6 | PVA2 Mortar | Cycled | 1 | 0.82 | 5.1 | 6.0 ± 1.27 |
| | | | 2 | 1.11 | 6.9 | |
| | | Uncycled | 5 | 1.21 | 7.5 | 7.7 ± 0.20 |
| | | | 6 | 1.28 | 7.9 | |
| | | | 7 | 1.24 | 7.7 | |

**Table A.4 Flexural strength under four point bending test (batch #7 ~ #12)**

| Batch Number | Batch | Condition | Sample I.D. | Peak Load kN | Peak Stress MPa | Average Stress MPa |
|---|---|---|---|---|---|---|
| #7 | Microsteel-PVA2 | Cycled | 1* | 0.9 | 5.56 | 5.13±0.43 |
| | | | 2* | 0.83 | 5.13 | |
| | | | 3* | 0.76 | 4.70 | |
| | | Uncycled | 4 | 1.11 | 6.86 | 6.12±0.77 |
| | | | 5 | 0.86 | 5.32 | |
| | | | 6 | 1 | 6.18 | |
| #8 | Microsteel | Cycled | 1* | 0.75 | 4.64 | 4.49±0.25 |
| | | | 2* | 0.75 | 4.64 | |
| | | | 3* | 0.68 | 4.20 | |
| | | Uncycled | 4 | 0.68 | 4.20 | 4.74±0.50 |
| | | | 5 | 0.84 | 5.19 | |
| | | | 6 | 0.78 | 4.82 | |
| #9 | HFsteel-PVA2 | Cycled | 1* | 0.99 | 6.12 | 5.21±0.84 |
| | | | 2* | 0.72 | 4.45 | |
| | | | 3* | 0.82 | 5.07 | |
| | | Uncycled | 4 | 0.79 | 4.88 | 6.22±1.86 |
| | | | 5 | 1.35 | 8.34 | |
| | | | 6 | 0.88 | 5.44 | |
| #10 | HFsteel | Cycled | 2* | 0.83 | 5.13 | 4.70±0.61 |
| | | | 3* | 0.69 | 4.26 | |
| | | Uncycled | 4 | 0.63 | 3.89 | 4.66±1.11 |
| | | | 5 | 0.67 | 4.14 | |
| | | | 6 | 0.96 | 5.93 | |
| #11 | PVA1 | Cycled | 1* | 0.67 | 4.14 | 4.33±0.55 |
| | | | 2* | 0.63 | 3.89 | |
| | | | 3* | 0.8 | 4.94 | |
| | | Uncycled | 4 | 0.67 | 4.14 | 4.53±0.34 |
| | | | 5 | 0.76 | 4.70 | |
| | | | 6 | 0.77 | 4.76 | |
| #12 | Microsteel-PVA1 | Cycled | 1* | 0.64 | 3.96 | 4.45±0.45 |
| | | | 2* | 0.78 | 4.82 | |
| | | | 3* | 0.74 | 4.57 | |
| | | Uncycled | 4 | 0.78 | 4.82 | 4.78±0.50 |
| | | | 5 | 0.69 | 4.26 | |
| | | | 6 | 0.85 | 5.25 | |

**Table A.5 Flexural strength under four point bending test (batch #13 ~ #16)**

| Batch Number | Batch Name | Sample I.D. | Peak Load kN | Peak Stress MPa | Average Stress MPa |
|---|---|---|---|---|---|
| #13 | PVA2 | 1 | 2.81 | 4.4 | 4.60 ± 0.20 |
| | | 2 | 3.08 | 4.8 | |
| | | 4 | 2.99 | 4.6 | |
| #14 | LPVA2 | 1 | 3.51 | 5.4 | 6.46 ± 0.98 |
| | | 2 | 4.11 | 6.4 | |
| | | 3 | 5.57 | 8.6 | |
| | | 4 | 4.21 | 6.5 | |
| | | 5 | 4.46 | 6.9 | |
| | | 6 | 3.67 | 5.7 | |
| | | 7 | 3.92 | 6.1 | |
| | | 8 | 3.96 | 6.1 | |
| #15 | HFsteel - LPVA2 | 7 | 5.43 | 8.4 | 7.06 ± 1.15 |
| | | 8 | 4.11 | 6.4 | |
| | | 9 | 4.16 | 6.4 | |
| #16 | HFsteel | 7 | 2.73 | 4.2 | 4.46 ± 0.25 |
| | | 8 | 3.03 | 4.7 | |
| | | 9 | 2.92 | 4.5 | |

**Table A.6 Flexural toughness under four point bending test ( Batch #1 ~ #6)**

| Batch Number | Batch | Condition | Sample | JCI | Average |
|---|---|---|---|---|---|
| | | | I.D. | mm • KN | mm • KN |
| #1 | Control | Cycled | 1* | 0.1974 | 0.2041 ± 0.015 |
| | | | 2* | 0.2222 | |
| | | | 3* | 0.1928 | |
| | | Uncycled | 4 | 0.1541 | 0.1813 ± 0.024 |
| | | | 5 | 0.1867 | |
| | | | 6 | 0.2030 | |
| #2 | PVA2 | Cycled | 1* | 1.2283 | 1.2370 ± 0.035 |
| | | | 2* | 1.2763 | |
| | | | 3* | 1.2064 | |
| | | Uncycled | 4 | 1.3963 | 1.4552 ± 0.103 |
| | | | 5 | 1.3942 | |
| | | | 6 | 1.5752 | |
| #3 | FSteel2 | Cycled | 2* | 2.1122 | 2.0058 ± 0.241 |
| | | | 3* | 1.7293 | |
| | | | 4* | 2.1758 | |
| | | Uncycled | 1 | 1.5920 | 1.6893 ± 0.098 |
| | | | 5 | 1.7893 | |
| | | | 6 | 1.6865 | |
| #4 | MCPVA2 | Cycled | 1* | 1.5598 | 1.6185± 0.064 |
| | | | 2* | 1.6873 | |
| | | | 3* | 1.6083 | |
| | | Uncycled | 4 | 1.5232 | 1.6587 ± 0.132 |
| | | | 6 | 1.8333 | |
| | | | 7 | 1.6741 | |
| | | | 8 | 1.6040 | |
| #5 | DMCPVA2 | Cycled | 4* | 1.5829 | 1.6570±0.069 |
| | | | 6* | 1.6695 | |
| | | | 7* | 1.7186 | |
| | | Uncycled | 1 | 1.7410 | 1.6318±0.085 |
| | | | 8 | 1.6489 | |
| | | | 9 | 1.5966 | |
| | | | 10 | 1.5409 | |
| #6 | PVA2 mortar | Cycled | 1 | 1.2568 | 1.4491 ± 0.271 |
| | | | 2 | 1.6414 | |
| | | Uncycled | 5 | 1.4823 | 1.6002 ± 0.120 |
| | | | 6 | 1.7234 | |
| | | | 7 | 1.5950 | |

**Table A.7 Flexural toughness under four point bending test ( Batch #7 ~ #12)**

| Batch Number | Batch | Condition | Sample | JCI | Average |
|---|---|---|---|---|---|
| | | | I.D. | mm • KN | mm • KN |
| #7 | Microsteel-PVA2 | Cycled | 1* | 1.5827 | 1.4569 ± 0.119 |
| | | | 2* | 1.4421 | |
| | | | 3* | 1.3460 | |
| | | Uncycled | 4 | 1.9948 | 1.7637 ± 0.239 |
| | | | 5 | 1.5165 | |
| | | | 6 | 1.7797 | |
| #8 | Microsteel | Cycled | 1* | 0.4254 | 0.3669 ± 0.082 |
| | | | 2* | 0.4023 | |
| | | | 3* | 0.2730 | |
| | | Uncycled | 4 | 0.2957 | 0.3938 ± 0.085 |
| | | | 5 | 0.4429 | |
| | | | 6 | 0.4428 | |
| #9 | HFsteel-PVA2 | Cycled | 1* | 1.5715 | 1.4101 ± 0.149 |
| | | | 2* | 1.2751 | |
| | | | 3* | 1.3838 | |
| | | Uncycled | 4 | 1.4159 | 1.6729 ± 0.343 |
| | | | 5 | 2.0632 | |
| | | | 6 | 1.5395 | |
| #10 | HFsteel | Cycled | 2* | 1.2274 | 1.1976 ± 0.042 |
| | | | 3* | 1.1678 | |
| | | Uncycled | 4 | 1.0333 | 1.2540 ± 0.365 |
| | | | 5 | 1.0532 | |
| | | | 6 | 1.6755 | |
| #11 | PVA1 | Cycled | 1* | 0.9480 | 0.9266 ± 0.139 |
| | | | 2* | 0.7775 | |
| | | | 3* | 1.0542 | |
| | | Uncycled | 4 | 0.9028 | 0.9113 ± 0.026 |
| | | | 5 | 0.8898 | |
| | | | 6 | 0.9414 | |
| #12 | Microsteel-PVA1 | Cycled | 1* | 0.7163 | 0.4744 ± 0.021 |
| | | | 2* | 0.3854 | |
| | | | 3* | 0.3214 | |
| | | Uncycled | 4 | 1.1372 | 1.0479 ± 0.069 |
| | | | 5 | 0.9575 | |
| | | | 6 | 1.0489 | |

**Table A.8 Flexural toughness under four point bending test (batch #13 ~ #16)**

| Batch Number | Batch | Sample I.D. | JCI mm • KN | Average mm • KN |
|---|---|---|---|---|
| #13 | PVA2 | 1 | 2.9898 | 4.1273 ± 1.017 |
| | | 2 | 4.4415 | |
| | | 4 | 4.9505 | |
| #14 | LPVA2 | 1 | 4.8783 | 5.8560 ± 1.126 |
| | | 2 | 6.1582 | |
| | | 3 | 8.1625 | |
| | | 4 | 6.3343 | |
| | | 5 | 6.0335 | |
| | | 6 | 4.8190 | |
| | | 7 | 4.7851 | |
| | | 8 | 5.6767 | |
| #15 | HFsteel -LPVA2 | 7 | 8.7542 | 7.5455 ± 1.060 |
| | | 8 | 6.7684 | |
| | | 9 | 7.1138 | |
| #16 | HFsteel | 7 | 2.1194 | 3.4084 ± 1.150 |
| | | 8 | 3.7755 | |
| | | 9 | 4.3302 | |

**Table A.9 Post-Crack Strength ( Batch #1 ~ #6)**

| Batch Number | Batch | Condition | Sample I.D. | $\sigma_{pcs}$ mm • KN | Average mm • KN |
|---|---|---|---|---|---|
| #1 | Control | Cycled | 1* | 0.0947 | 0.0998±0.013 |
| | | | 2* | 0.1145 | |
| | | | 3* | 0.0902 | |
| | | Uncycled | 4 | 0.0668 | 0.0943±0.027 |
| | | | 5 | 0.0945 | |
| | | | 6 | 0.1214 | |
| #2 | PVA2 | Cycled | 1* | 4.1390 | 3.3994±0.642 |
| | | | 2* | 3.0667 | |
| | | | 3* | 2.9926 | |
| | | Uncycled | 4 | 4.9784 | 4.4528±0.506 |
| | | | 5 | 4.4108 | |
| | | | 6 | 3.9691 | |
| #3 | FSteel2 | Cycled | 2* | 6.2439 | 6.0114±0.480 |
| | | | 3* | 5.4593 | |
| | | | 4* | 6.3309 | |
| | | Uncycled | 1 | 4.2051 | 4.4607±0.242 |
| | | | 5 | 4.4906 | |
| | | | 6 | 4.6862 | |
| #4 | MCPVA2 | Cycled | 1* | 4.7844 | 4.7419±1.083 |
| | | | 2* | 5.8031 | |
| | | | 3* | 3.6383 | |
| | | Uncycled | 4 | 5.1113 | 5.3341±1.045 |
| | | | 6 | 6.2572 | |
| | | | 7 | 6.0159 | |
| | | | 8 | 3.9518 | |
| #5 | DMCPVA2 | Cycled | 4* | 5.6660 | 6.0108±0.338 |
| | | | 6* | 6.0250 | |
| | | | 7* | 6.3412 | |
| | | Uncycled | 1 | 6.2968 | 5.7944±0.346 |
| | | | 8 | 5.5041 | |
| | | | 9 | 5.6726 | |
| | | | 10 | 5.7039 | |
| #6 | PVA2 mortar | Cycled | 1 | 4.4559 | 5.1641±1.002 |
| | | | 2 | 5.8724 | |
| | | Uncycled | 5 | 5.4430 | 5.9764±0.489 |
| | | | 6 | 6.4303 | |
| | | | 7 | 6.0558 | |

**Table A.10 Post-Crack Strength ( Batch #7 ~ #12)**

| Batch Number | Batch | Condition | Sample I.D. | $\sigma_{apcs}$ MPa | Average MPa |
|---|---|---|---|---|---|
| #7 | Microsteel-PVA2 | Cycled | 1* | 4.9048 | 4.1321±1.033 |
| | | | 2* | 4.5324 | |
| | | | 3* | 2.9590 | |
| | | Uncycled | 4 | 6.5266 | 5.2356±1.137 |
| | | | 5 | 4.7960 | |
| | | | 6 | 4.3842 | |
| #8 | Microsteel | Cycled | 1* | 0.3062 | 0.2914±0.044 |
| | | | 2* | 0.3263 | |
| | | | 3* | 0.2418 | |
| | | Uncycled | 4 | 0.2337 | 0.3092±0.068 |
| | | | 5 | 0.3663 | |
| | | | 6 | 0.3277 | |
| #9 | HFsteel-PVA2 | Cycled | 1* | 5.4699 | 4.6169±0.740 |
| | | | 2* | 4.1451 | |
| | | | 3* | 4.2357 | |
| | | Uncycled | 4 | 3.4764 | 5.3392±2.423 |
| | | | 5 | 8.0786 | |
| | | | 6 | 4.4626 | |
| #10 | HFsteel | Cycled | 2* | 4.0184 | 3.7945±0.317 |
| | | | 3* | 3.5706 | |
| | | Uncycled | 4 | 3.2812 | 3.6208±1.328 |
| | | | 5 | 2.4955 | |
| | | | 6 | 5.0857 | |
| #11 | PVA1 | Cycled | 1* | 2.4832 | 2.2673±0.354 |
| | | | 2* | 1.8593 | |
| | | | 3* | 2.4594 | |
| | | Uncycled | 4 | 1.9742 | 1.9703±0.005 |
| | | | 5 | 1.9721 | |
| | | | 6 | 1.9644 | |
| #12 | Microsteel-PVA1 | Cycled | 1* | 1.4937 | 0.7702±0.628 |
| | | | 2* | 0.4527 | |
| | | | 3* | 0.3641 | |
| | | Uncycled | 4 | 2.4523 | 2.0097±0.445 |
| | | | 5 | 1.5629 | |
| | | | 6 | 2.0139 | |

**Table A.11 Post-Crack Strength (batch #13 ~ #16)**

| Batch Number | Batch | Sample I.D. | $\sigma_{apcs}$ mm • KN | Average mm • KN |
|---|---|---|---|---|
| #13 | PVA2 | 1 | 1.7556 | 2.8347±0.936 |
| | | 2 | 3.3289 | |
| | | 4 | 3.4197 | |
| #14 | LPVA2 | 1 | 5.3991 | 6.3197±1.180 |
| | | 2 | 6.2758 | |
| | | 3 | 8.6782 | |
| | | 4 | 6.6138 | |
| | | 5 | 7.1525 | |
| | | 6 | 4.9680 | |
| | | 7 | 5.5952 | |
| | | 8 | 5.8750 | |
| #15 | HFsteel -LPVA2 | 7 | 7.8072 | 7.1536 ±0.609 |
| | | 8 | 6.6010 | |
| | | 9 | 7.0527 | |
| #16 | HFsteel | 7 | 1.9080 | 3.2633 ±1.227 |
| | | 8 | 3.5841 | |
| | | 9 | 4.2979 | |

**Table A.12 Ductility factor (strain hardening level) ( Batch #1 ~ #6)**

| Batch Number | Batch | Condition | Sample I.D. | $P_{first\ peak}$ | $E_{post}$ | D | Average |
|---|---|---|---|---|---|---|---|
| #1 | Control | Cycled | 1* | 0.7295 | 0.0722 | 0.0209 | 0.0237±0.004 |
| | | | 2* | 0.6494 | 0.0866 | 0.0284 | |
| | | | 3* | 0.6714 | 0.0687 | 0.0217 | |
| | | Uncycled | 4 | 0.5514 | 0.0508 | 0.0195 | 0.0245±0.006 |
| | | | 5 | 0.6554 | 0.0722 | 0.0233 | |
| | | | 6 | 0.6368 | 0.0928 | 0.0308 | |
| #2 | PVA2 | Cycled | 1* | 0.632 | 3.0516 | 1.0563 | 0.8149±0.221 |
| | | | 2* | 0.683 | 2.3398 | 0.7242 | |
| | | | 3* | 0.7267 | 2.2702 | 0.6642 | |
| | | Uncycled | 4 | 0.7348 | 3.6766 | 1.0928 | 0.9235±0.165 |
| | | | 5 | 0.7784 | 3.2612 | 0.9140 | |
| | | | 6 | 0.8383 | 3.0373 | 0.7637 | |
| #3 | FSteel2 | Cycled | 2* | 1.2662 | 3.5606 | 0.7954 | 0.7925±0.035 |
| | | | 3* | 1.0659 | 3.5282 | 0.8261 | |
| | | | 4* | 1.3507 | 3.5402 | 0.7560 | |
| | | Uncycled | 1 | 0.9445 | 2.8541 | 0.7181 | 0.6990±0.018 |
| | | | 5 | 1.0632 | 3.1148 | 0.6812 | |
| | | | 6 | 1.0834 | 3.3669 | 0.6977 | |
| #4 | MCPVA2 | Cycled | 1* | 0.9488 | 3.4853 | 0.8133 | 0.8242±0.133 |
| | | | 2* | 0.9725 | 4.2537 | 0.9624 | |
| | | | 3* | 0.9831 | 2.6885 | 0.6969 | |
| | | Uncycled | 4 | 0.9053 | 3.7203 | 0.9106 | 0.8934±0.193 |
| | | | 6 | 1.0106 | 4.6651 | 0.9986 | |
| | | | 7 | 0.9263 | 4.3463 | 1.0475 | |
| | | | 8 | 1.0335 | 2.9201 | 0.6167 | |
| #5 | DMCPVA2 | Cycled | 4* | 0.8444 | 4.2893 | 1.0823 | 1.1062±0.068 |
| | | | 6* | 0.9225 | 4.5085 | 1.0534 | |
| | | | 7* | 0.8647 | 4.8178 | 1.1828 | |
| | | Uncycled | 1 | 0.9037 | 4.6376 | 1.1238 | 1.0457±0.059 |
| | | | 8 | 0.9027 | 4.0858 | 0.9835 | |
| | | | 9 | 0.8713 | 4.2539 | 1.0501 | |
| | | | 10 | 0.897 | 4.2341 | 1.0256 | |
| #6 | PVA2 mortar | Cycled | 1 | 0.6976 | 3.1777 | 1.0302 | 1.0371±0.010 |
| | | | 2 | 0.9073 | 3.8753 | 1.0439 | |
| | | Uncycled | 5 | 0.8322 | 3.2021 | 1.0549 | 1.1395±0.082 |
| | | | 6 | 0.9058 | 4.5281 | 1.1450 | |
| | | | 7 | 0.8016 | 3.8000 | 1.2185 | |

**Table A.13 Ductility factor (strain hardening level) ( Batch #7 ~ #12)**

| Batch Number | Batch | Condition | Sample I.D. | $P_{first\ peak}$ KN | $E_{post}$ KN • mm | D | Average |
|---|---|---|---|---|---|---|---|
| #7 | Microsteel -PVA2 | Cycled | 1* | 0.8539 | 3.4576 | 0.9265 | 0.8217±0.167 |
| | | | 2* | 0.8037 | 3.1315 | 0.9096 | |
| | | | 3* | 0.7586 | 2.1641 | 0.6291 | |
| | | Uncycled | 4 | 1.1047 | 4.5099 | 0.9529 | 0.8552±0.127 |
| | | | 5 | 0.8587 | 3.3484 | 0.9008 | |
| | | | 6 | 0.9934 | 3.1522 | 0.7118 | |
| #8 | Microsteel | Cycled | 1* | 0.7496 | 0.2283 | 0.0659 | 0.0646±0.006 |
| | | | 2* | 0.7489 | 0.2476 | 0.0703 | |
| | | | 3* | 0.677 | 0.1837 | 0.0576 | |
| | | Uncycled | 4 | 0.6829 | 0.178 | 0.0552 | 0.0640±0.008 |
| | | | 5 | 0.8583 | 0.2773 | 0.0688 | |
| | | | 6 | 0.7776 | 0.245 | 0.0680 | |
| #9 | HFsteel-PVA2 | Cycled | 1* | 0.7438 | 4.0133 | 1.1861 | 1.0621±0.110 |
| | | | 2* | 0.6519 | 3.0497 | 1.0256 | |
| | | | 3* | 0.7009 | 3.1450 | 0.9747 | |
| | | Uncycled | 4 | 0.7917 | 2.5963 | 0.7082 | 0.9078±0.224 |
| | | | 5 | 1.1335 | 5.3424 | 1.1495 | |
| | | | 6 | 0.8315 | 3.1575 | 0.8656 | |
| #10 | HFsteel | Cycled | 2* | 0.8336 | 2.9497 | 0.7775 | 0.8163±0.055 |
| | | | 3* | 0.6735 | 2.7224 | 0.8551 | |
| | | Uncycled | 4 | 0.6231 | 2.4803 | 0.8493 | 0.8343±0.137 |
| | | | 5 | 0.5832 | 1.8639 | 0.6902 | |
| | | | 6 | 0.8515 | 3.7868 | 0.9633 | |
| #11 | PVA1 | Cycled | 1* | 0.6613 | 1.8912 | 0.6056 | 0.5282±0.069 |
| | | | 2* | 0.6342 | 1.4297 | 0.4729 | |
| | | | 3* | 0.7836 | 1.9033 | 0.5062 | |
| | | Uncycled | 4 | 0.6687 | 1.4874 | 0.4762 | 0.4363±0.035 |
| | | | 5 | 0.7544 | 1.4963 | 0.4216 | |
| | | | 6 | 0.7716 | 1.4852 | 0.4106 | |
| #12 | Microsteel -PVA1 | Cycled | 1* | 0.6384 | 1.1462 | 0.3774 | 0.1832±0.168 |
| | | | 2* | 0.7879 | 0.3606 | 0.0927 | |
| | | | 3* | 0.7395 | 0.2902 | 0.0794 | |
| | | Uncycled | 4 | 0.7837 | 1.8053 | 0.5047 | 0.4164±0.077 |
| | | | 5 | 0.6924 | 1.1731 | 0.3641 | |
| | | | 6 | 0.8539 | 1.4970 | 0.3804 | |

**Table A.14 Ductility factor (strain hardening level) (batch #13 ~ #16)**

| Batch Number | Batch | Sample I.D. | $P_{first\ peak}$ KN | $E_{post}$ KN • mm | D | Average |
|---|---|---|---|---|---|---|
| #13 | PVA2 | 1 | 2.8115 | 4.4242 | 0.3345 | 0.5142±0.156 |
| | | 2 | 3.0785 | 8.3890 | 0.5896 | |
| | | 4 | 2.9879 | 8.6177 | 0.6184 | |
| #14 | LPVA2 | 1 | 3.3229 | 13.6060 | 0.8845 | 0.9106±0.137 |
| | | 2 | 4.1141 | 15.8152 | 0.8368 | |
| | | 3 | 4.3824 | 21.8695 | 1.1260 | |
| | | 4 | 4.0208 | 16.6671 | 0.9103 | |
| | | 5 | 3.5533 | 18.0246 | 1.1040 | |
| | | 6 | 3.6669 | 12.5194 | 0.7462 | |
| | | 7 | 3.9197 | 14.1001 | 0.7939 | |
| | | 8 | 3.8 | 14.8051 | 0.8830 | |
| #15 | HFsteel - LPVA2 | 7 | 5.0312 | 19.6743 | 0.8690 | 0.9533±0.131 |
| | | 8 | 4.11 | 16.6348 | 0.8873 | |
| | | 9 | 4.0384 | 17.7732 | 1.1037 | |
| #16 | HFsteel | 7 | 2.9221 | 4.8082 | 0.3501 | 0.6024±0.237 |
| | | 8 | 3.0346 | 9.0320 | 0.6364 | |
| | | 9 | 2.7272 | 10.8310 | 0.8207 | |

# Appendix B

## Load-deflection curves under four point bending test

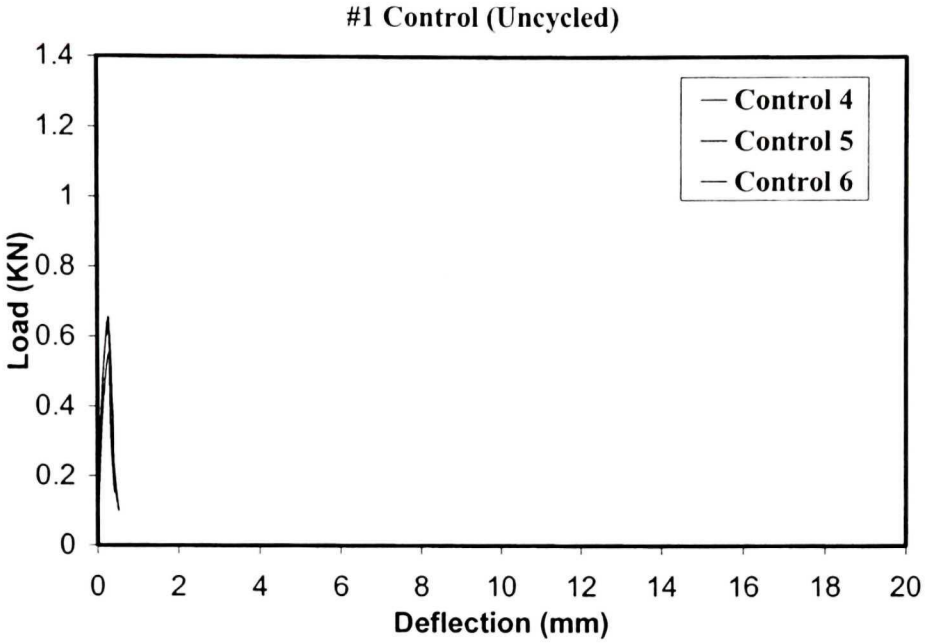


Figure B.1 Load–deflection curves before freeze-thaw cycles ( #1 )

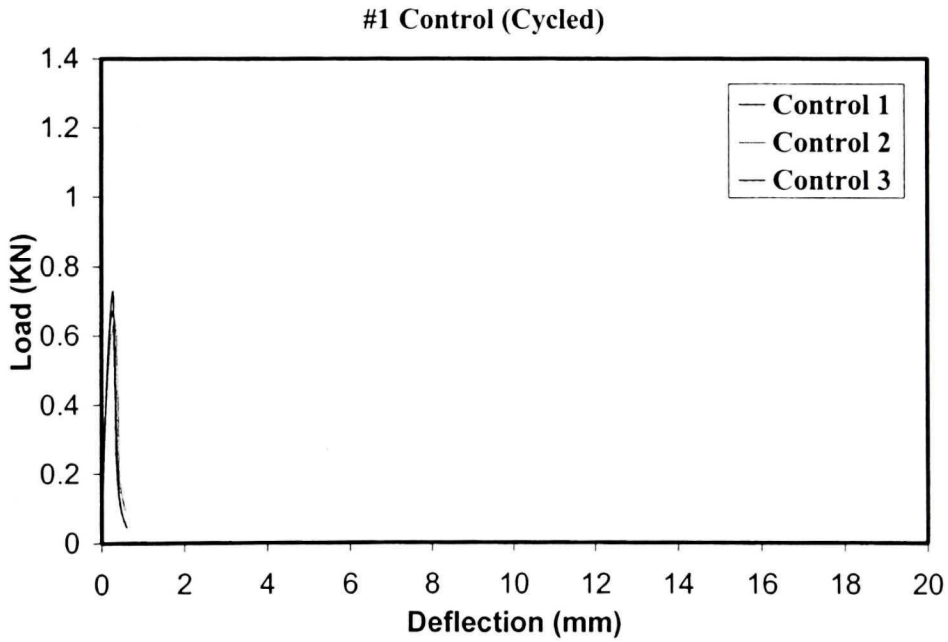


Figure B.2 Load–deflection curves after freeze-thaw cycles ( #1 )

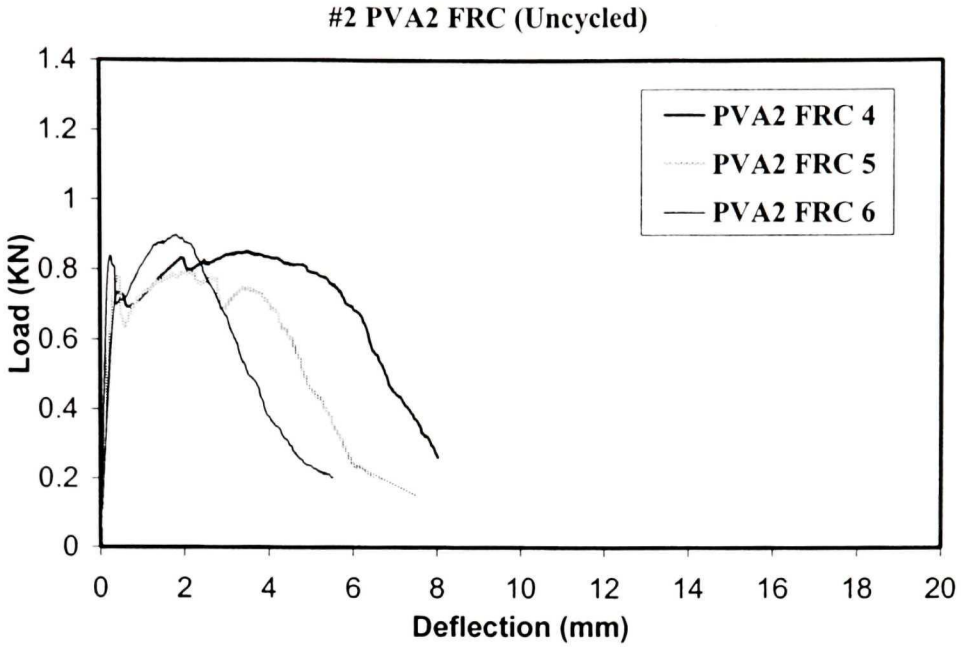


Figure B.3 Load–deflection curves before freeze-thaw cycles ( #2 )

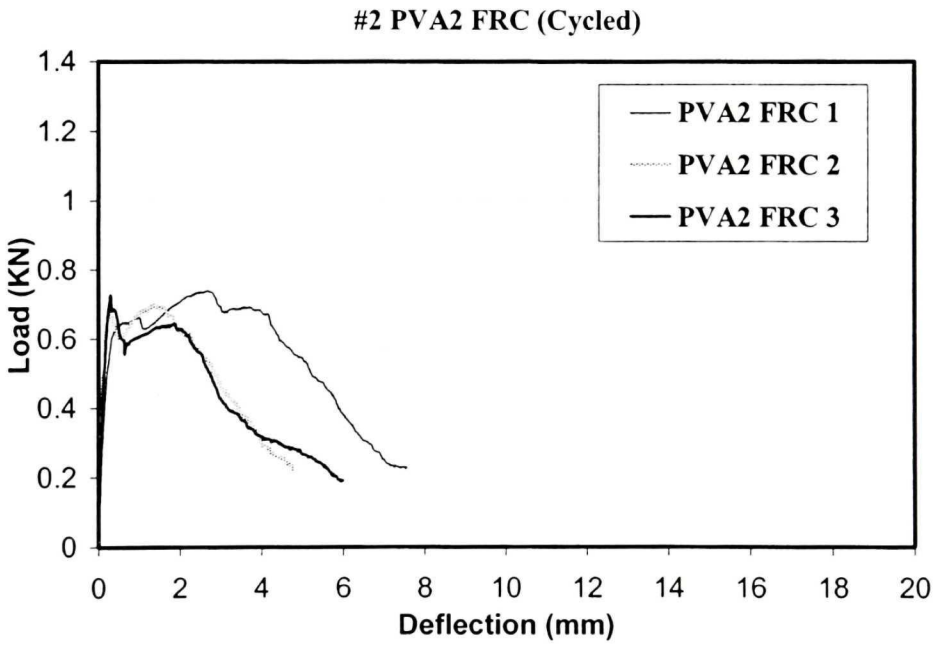


Figure B.4 Load–deflection curves after freeze-thaw cycles ( #2 )

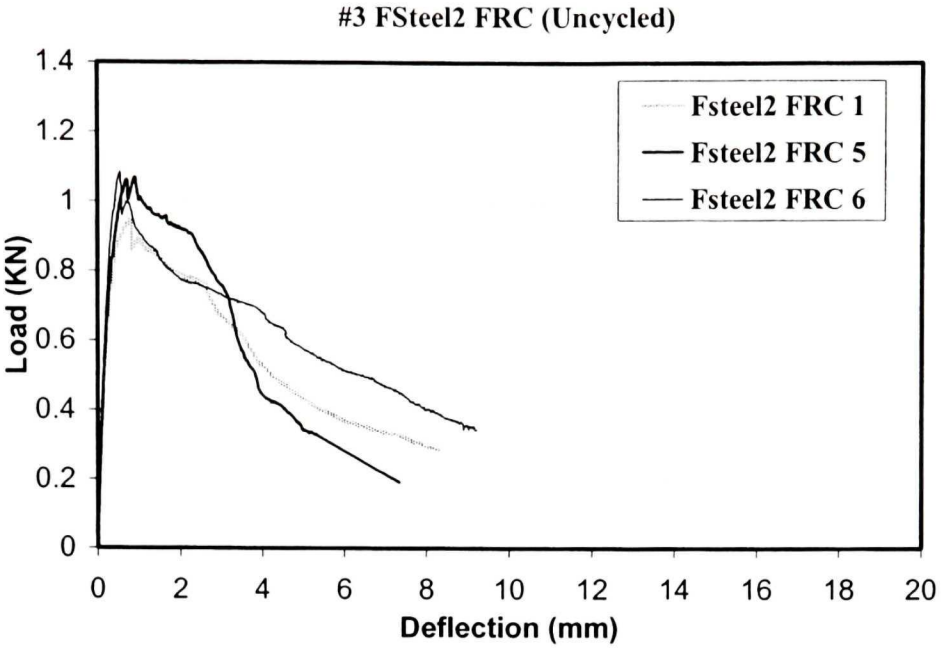


Figure B.5 Load–deflection curves before freeze-thaw cycles ( #3)

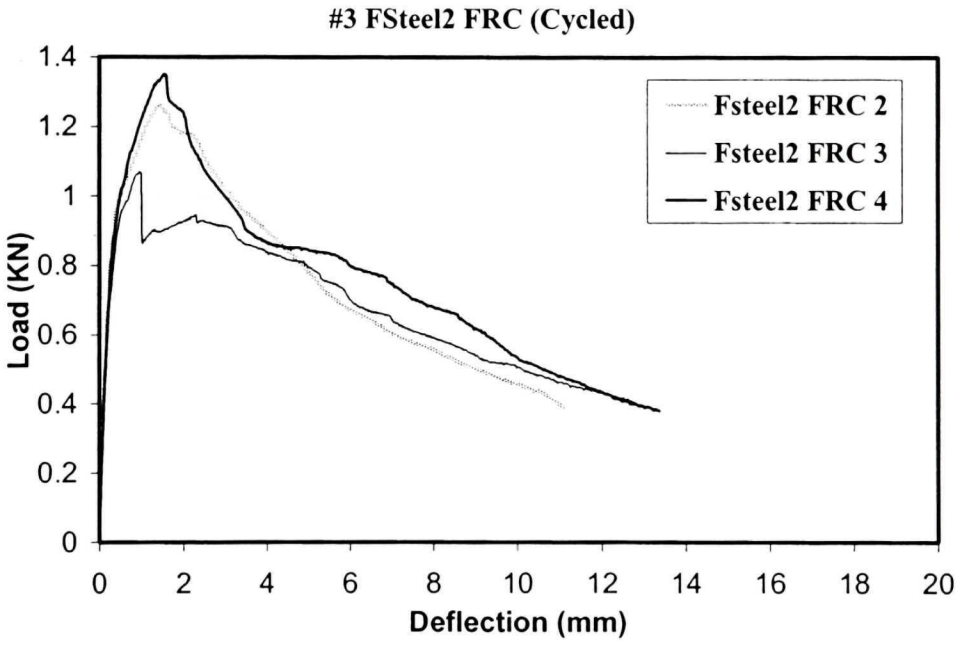


Figure B.6 Load–deflection curves after freeze-thaw cycles ( #3)

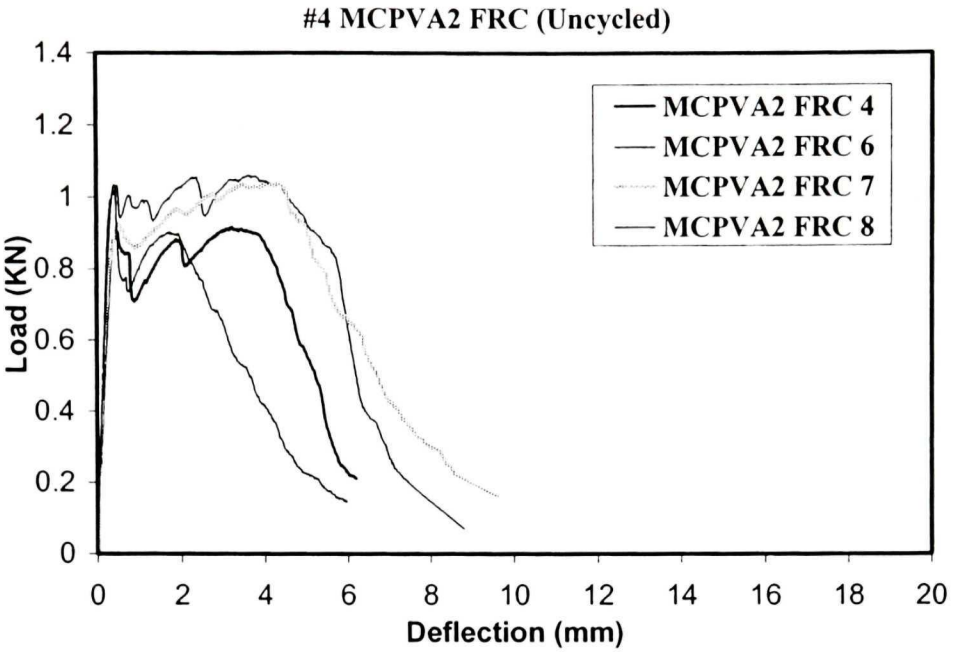


Figure B.7 Load–deflection curves before freeze-thaw cycles ( #4 )

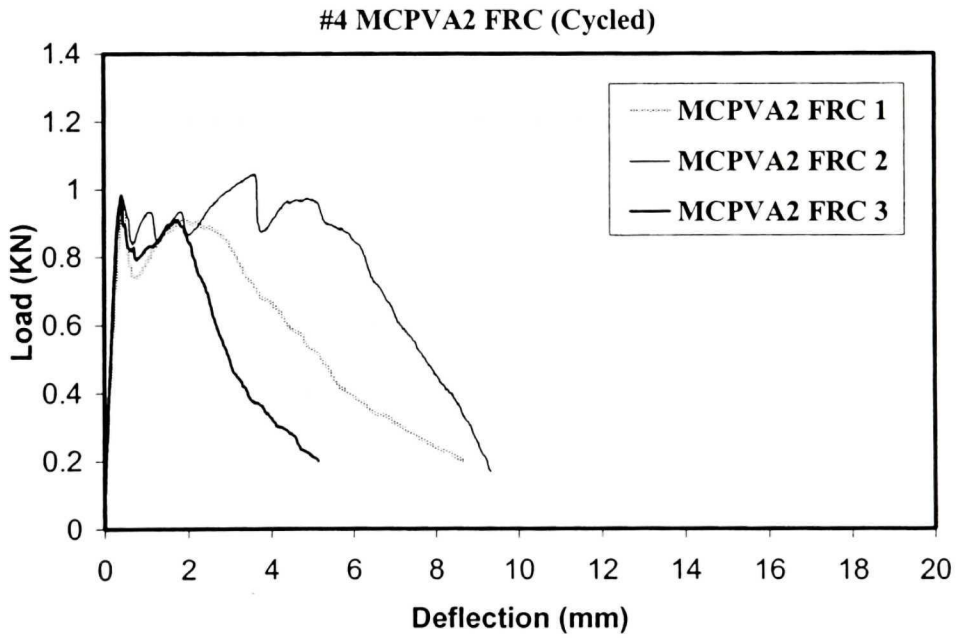


Figure B.8 Load–deflection curves after freeze-thaw cycles ( # 4 )

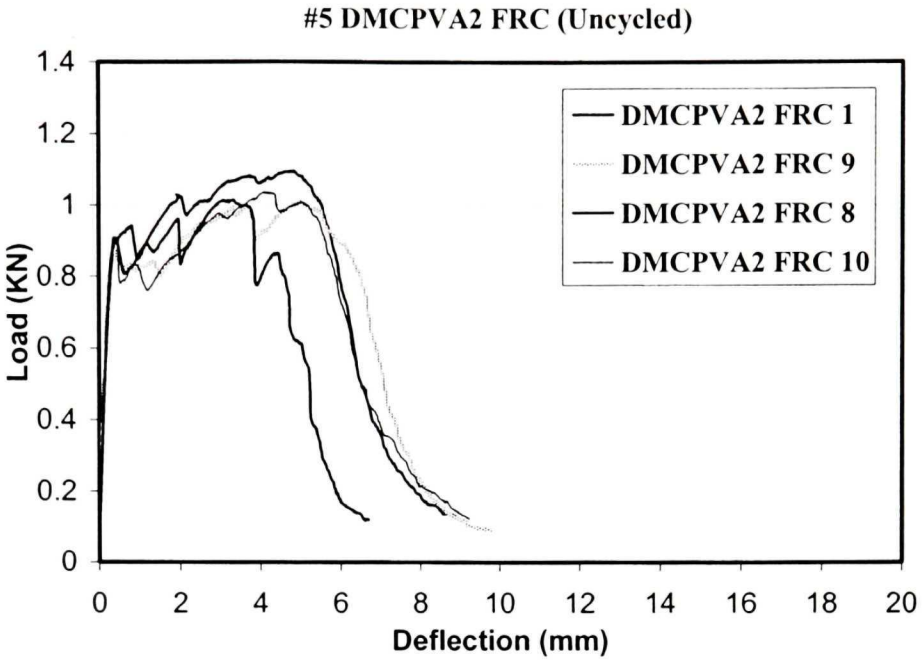


Figure B.9 Load–deflection curves before freeze-thaw cycles ( #5 )

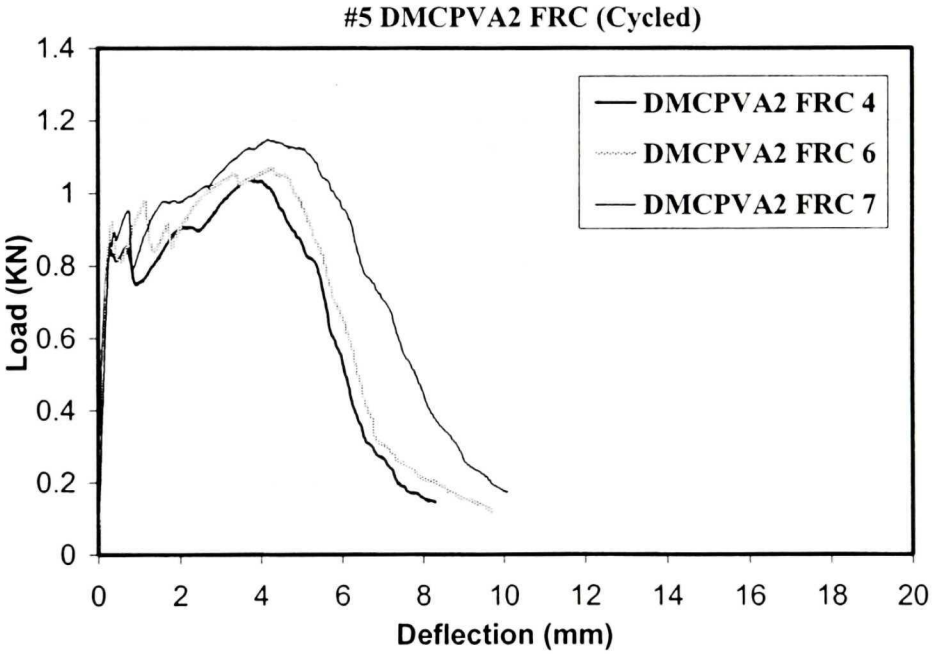


Figure B.10 Load–deflection curves after freeze-thaw cycles ( #5 )

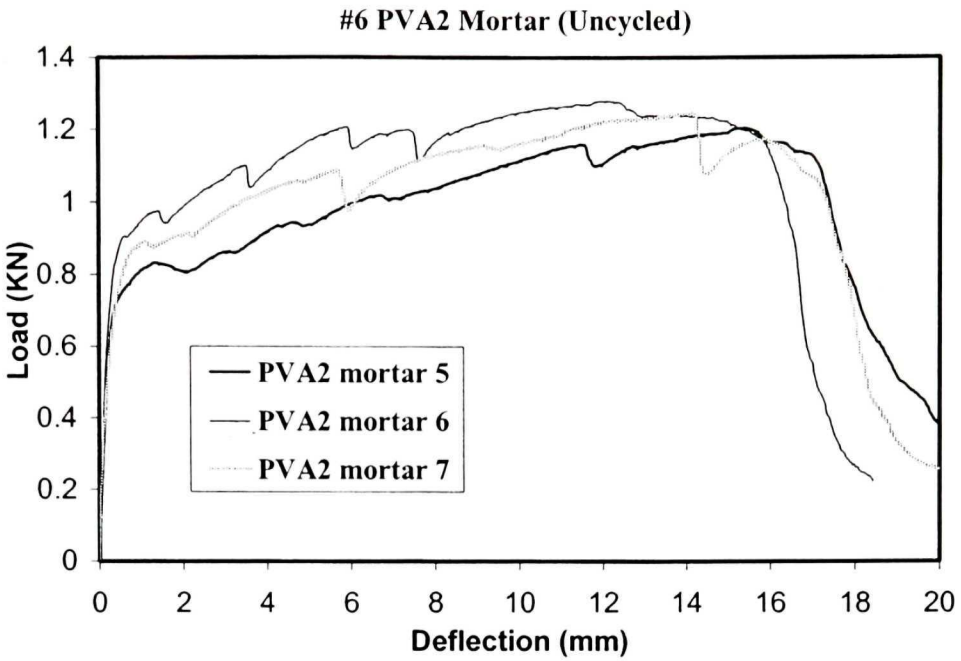


Figure B.11 Load–deflection curves before freeze-thaw cycles ( #6 )

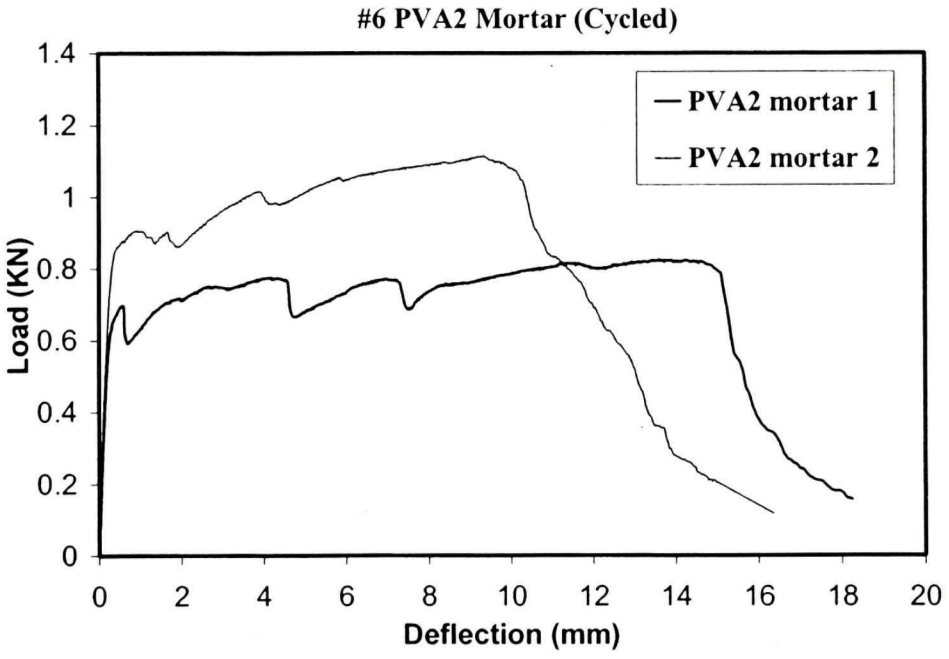


Figure B.12 Load–deflection curves after freeze-thaw cycles ( #6 )

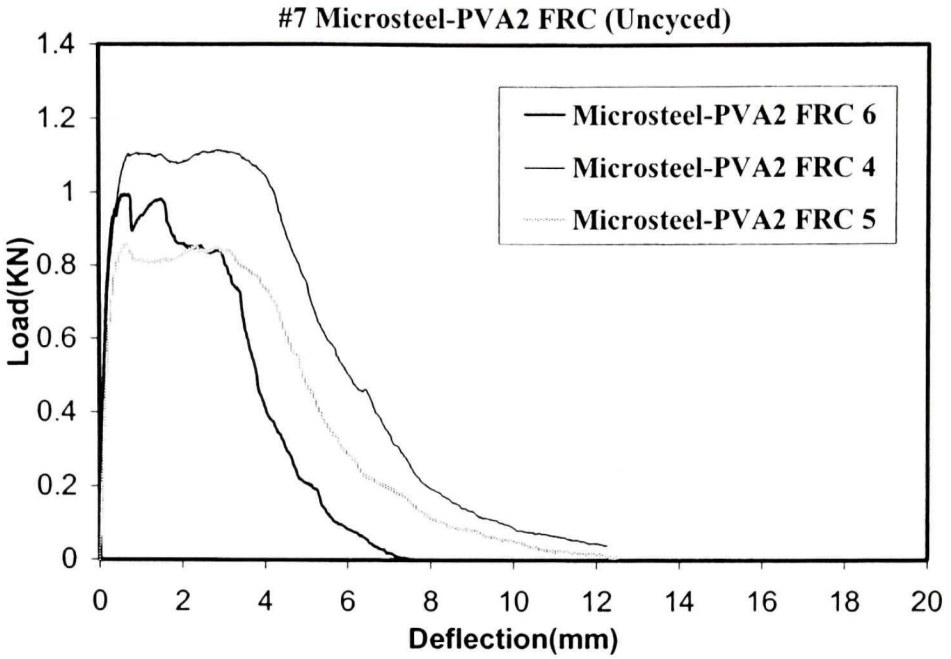


Figure B.13 Load–deflection curves before freeze-thaw cycles ( #7 )

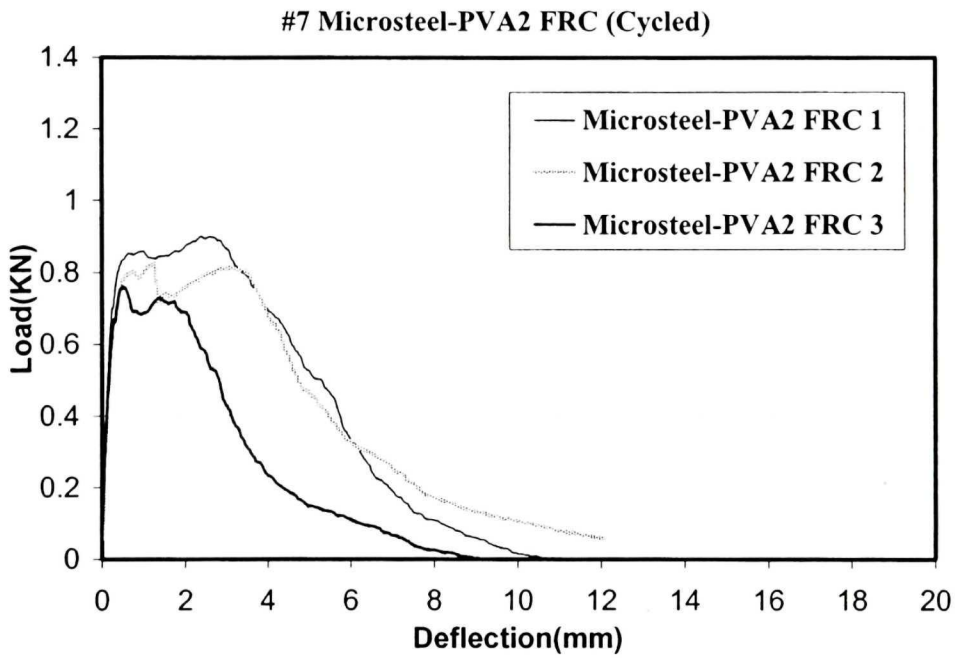


Figure B.14 Load–deflection curves after freeze-thaw cycles ( #7 )

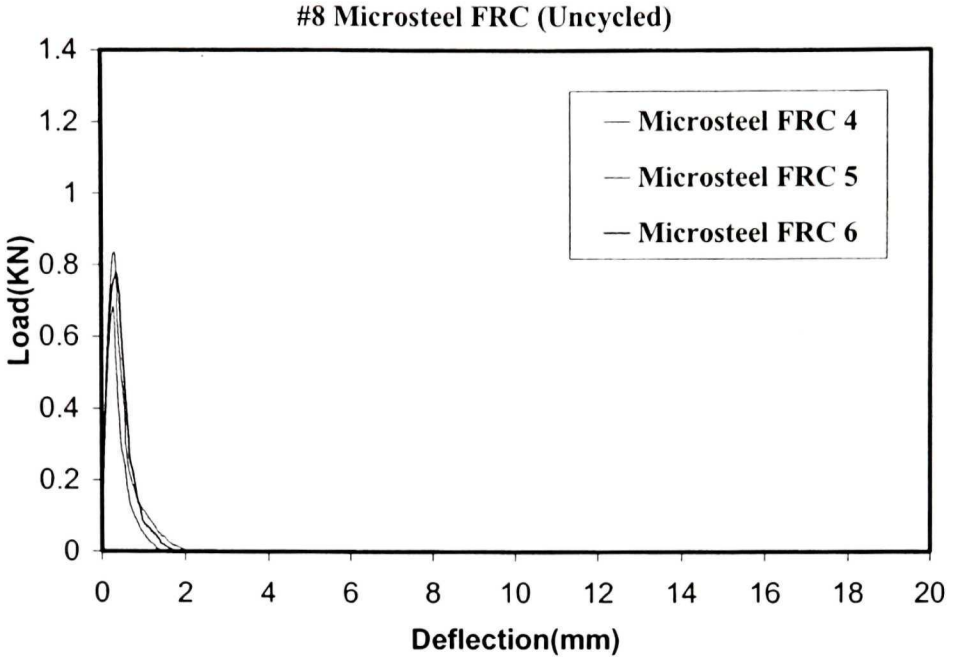


Figure B.15 Load–deflection curves before freeze-thaw cycles ( #8 )

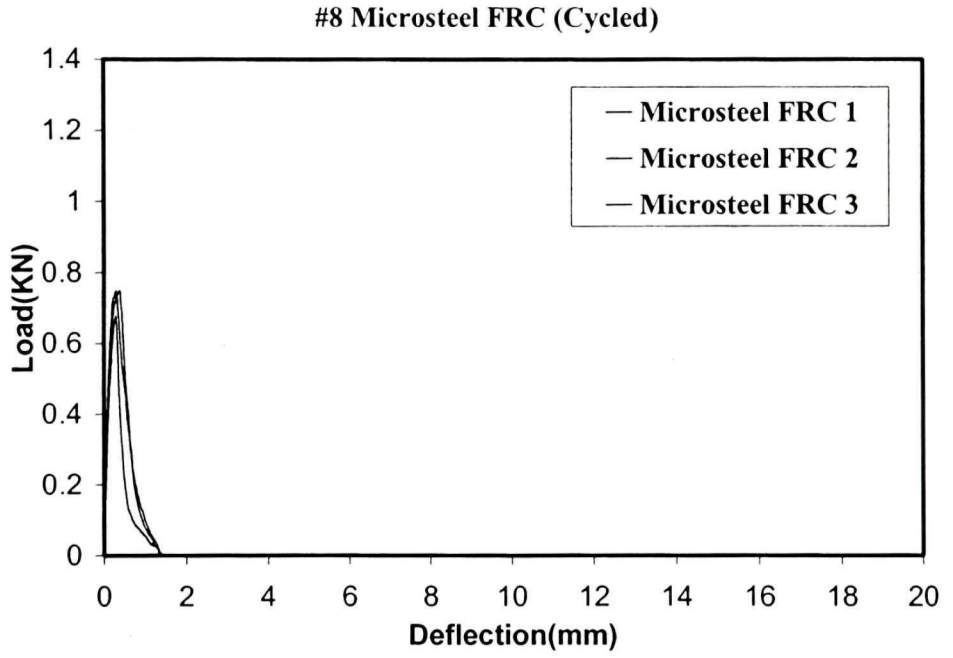


Figure B.16 Load–deflection curves after freeze-thaw cycles ( #8 )

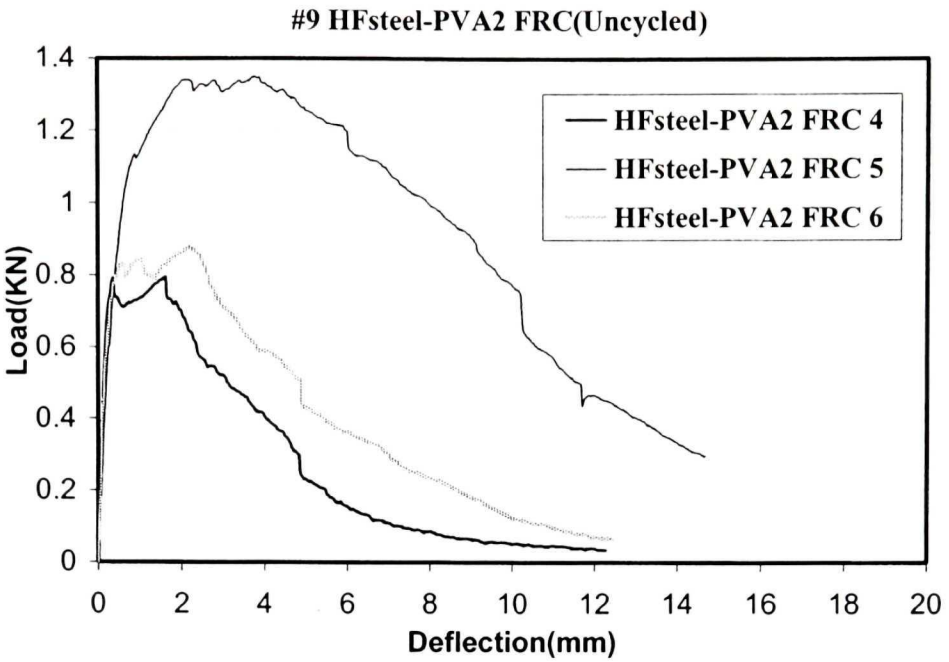


Figure B.17 Load–deflection curves before freeze-thaw cycles ( #9 )

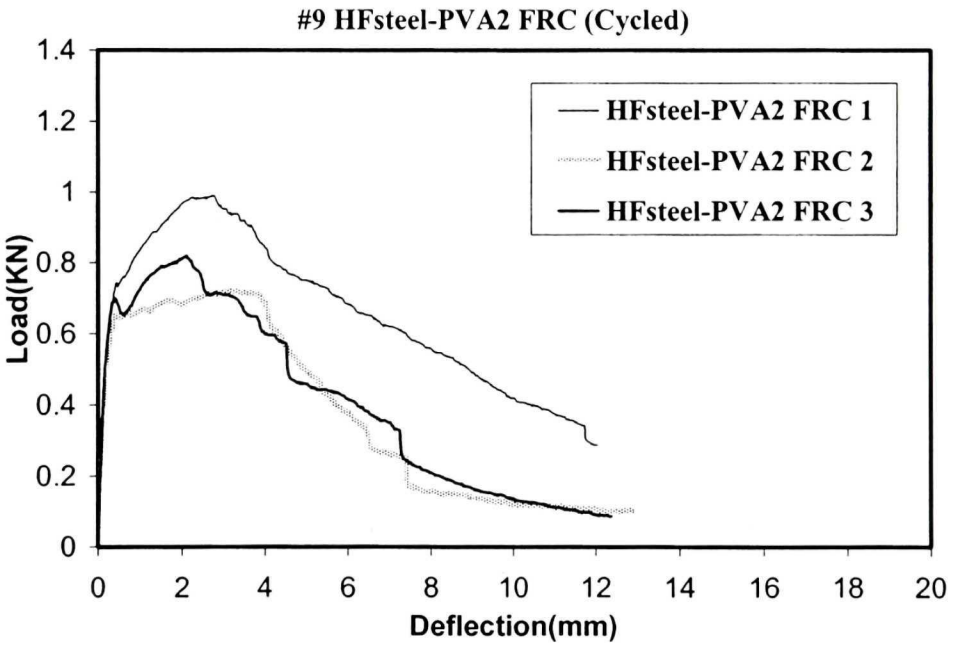


Figure B.18 Load–deflection curves after freeze-thaw cycles ( #9 )

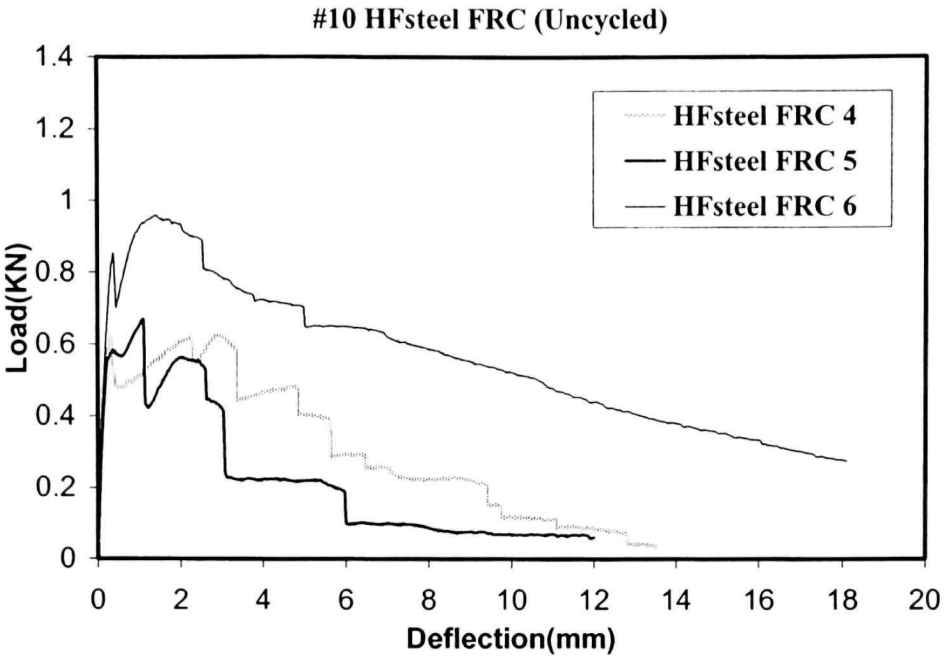


Figure B.19 Load–deflection curves before freeze-thaw cycles ( #10 )

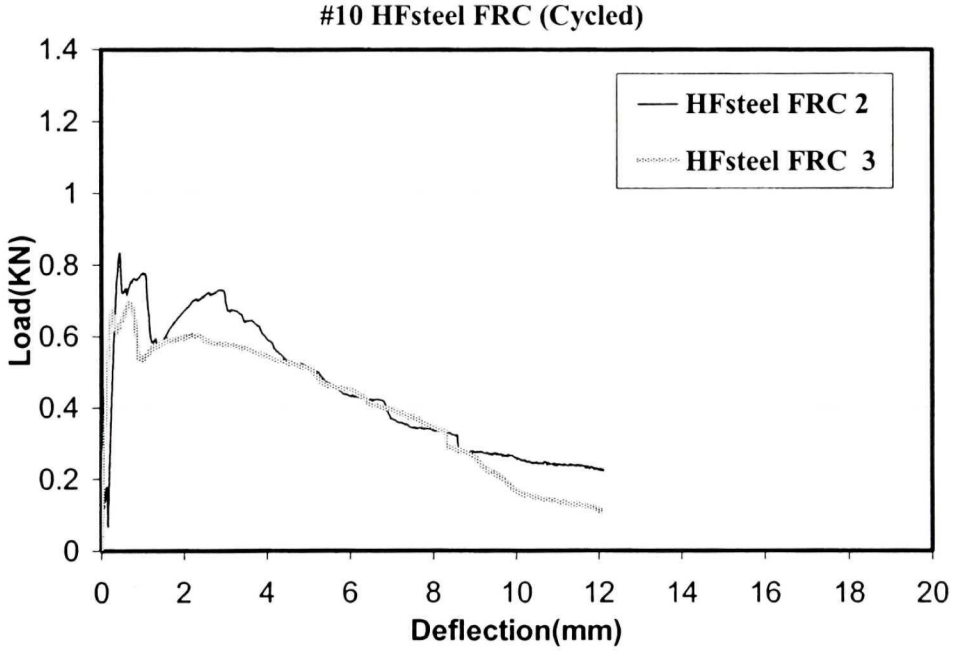


Figure B.20 Load–deflection curves after freeze-thaw cycles ( #10 )

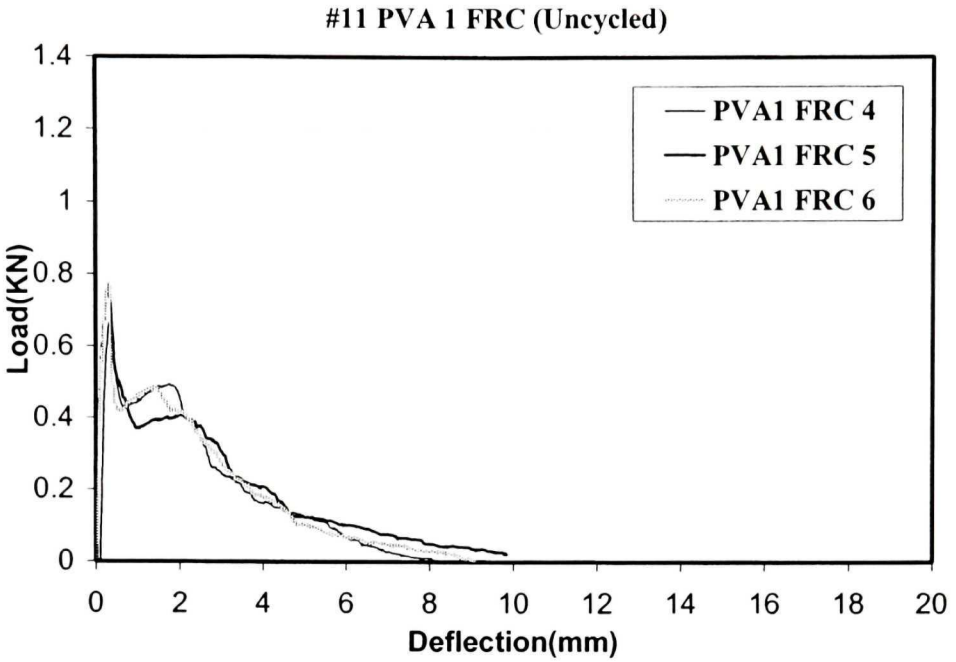


Figure B.21 Load–deflection curves before freeze-thaw cycles ( #11 )

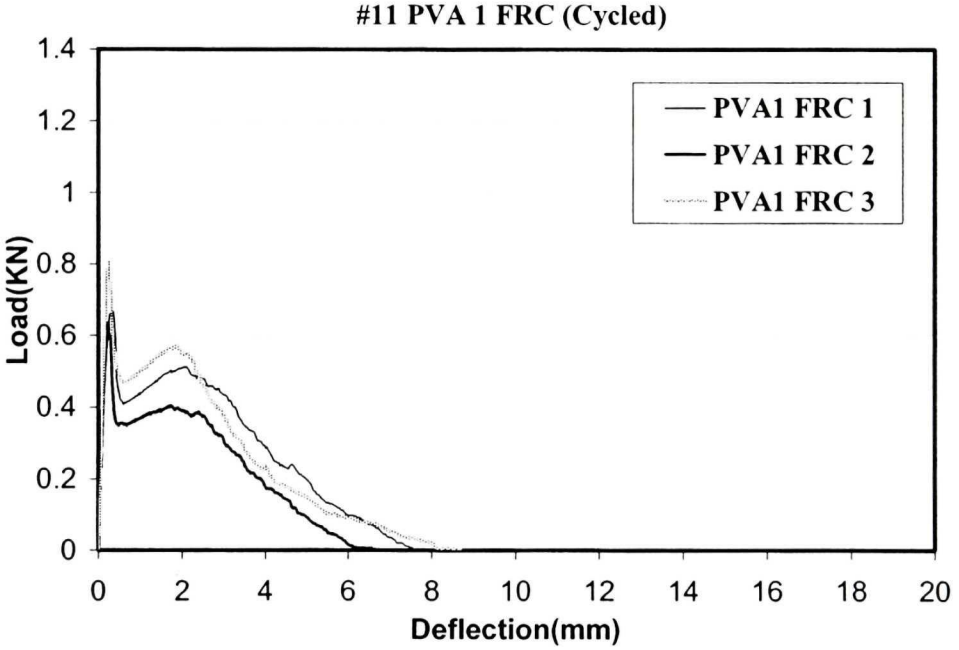


Figure B.22 Load–deflection curves after freeze-thaw cycles ( #11 )

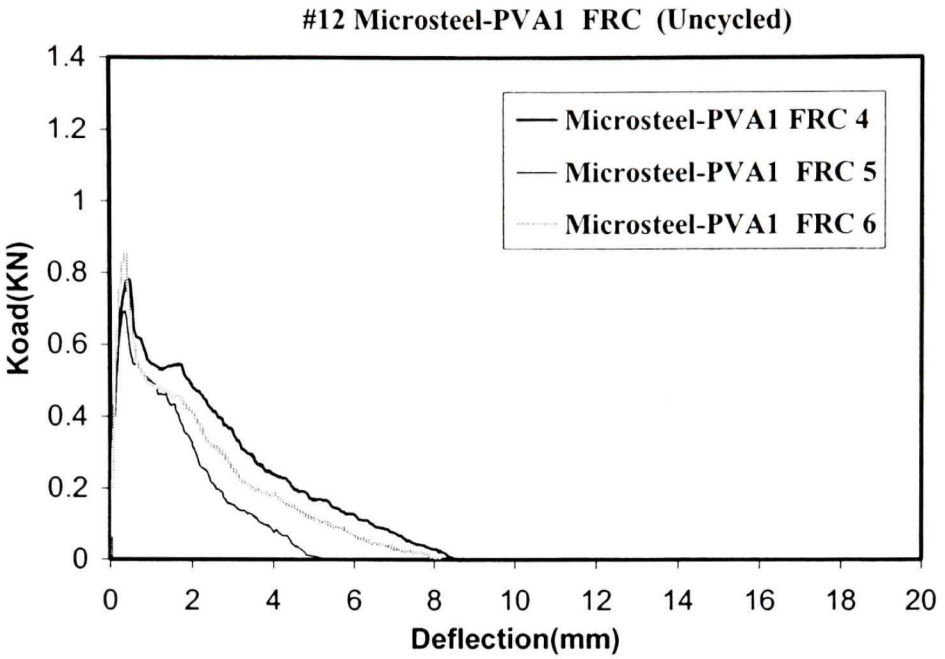


Figure B.23 Load–deflection curves before freeze-thaw cycles ( #12 )

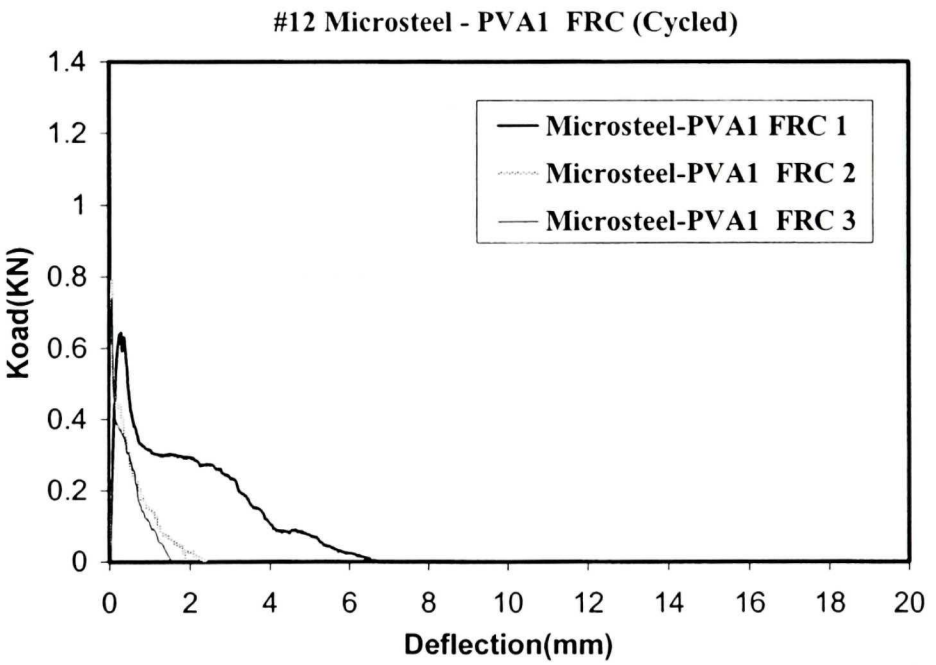


Figure B.24 Load–deflection curves after freeze-thaw cycles ( #12 )

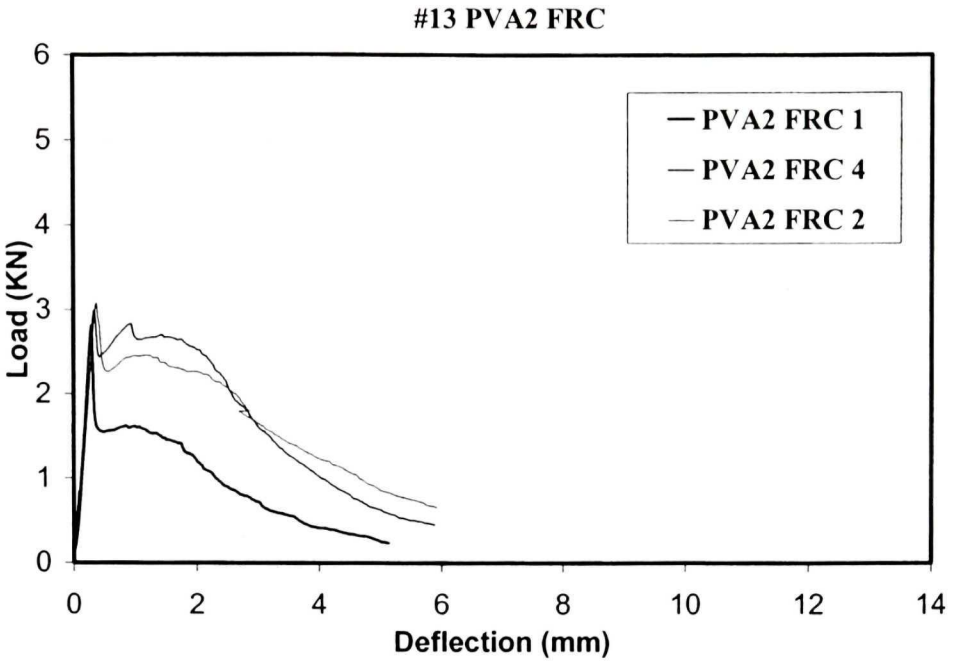


Figure B.25 Load–deflection curves under flexure ( #13 )

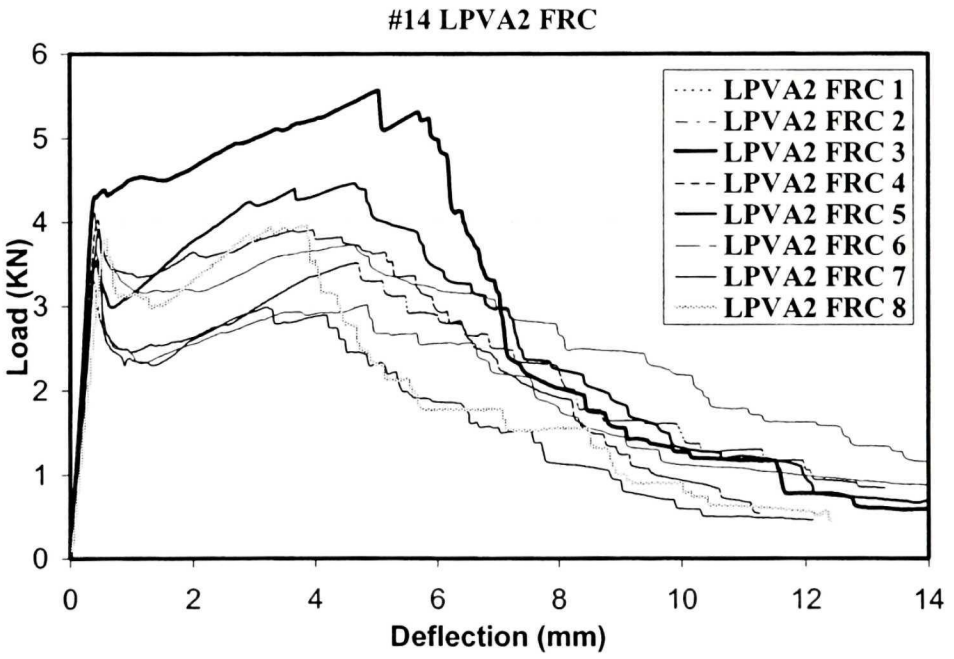


Figure B.26 Load–deflection curves under flexure ( #14 )

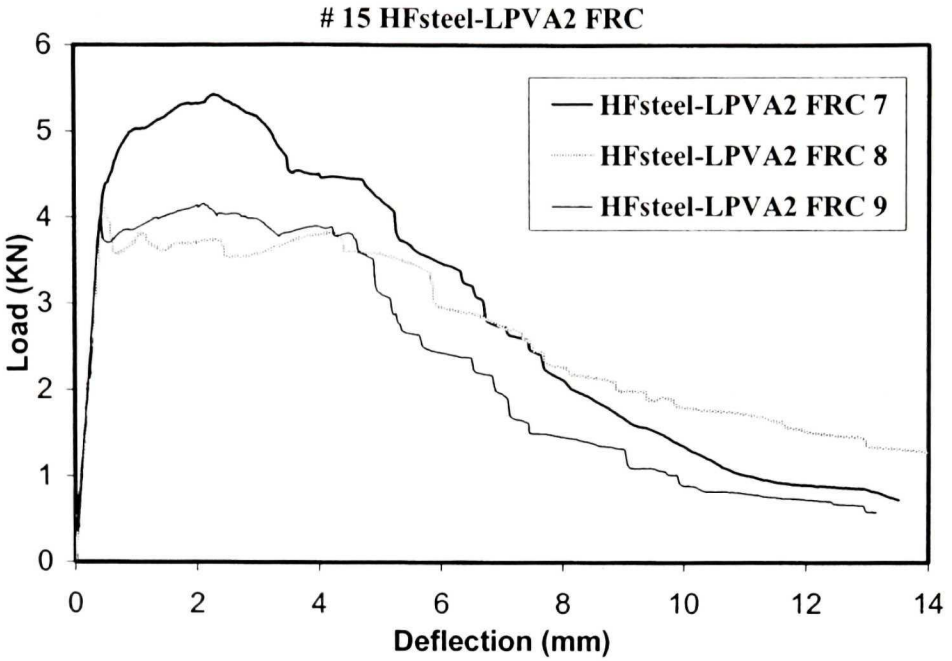


Figure B.27 Load–deflection curves under flexure ( #15 )

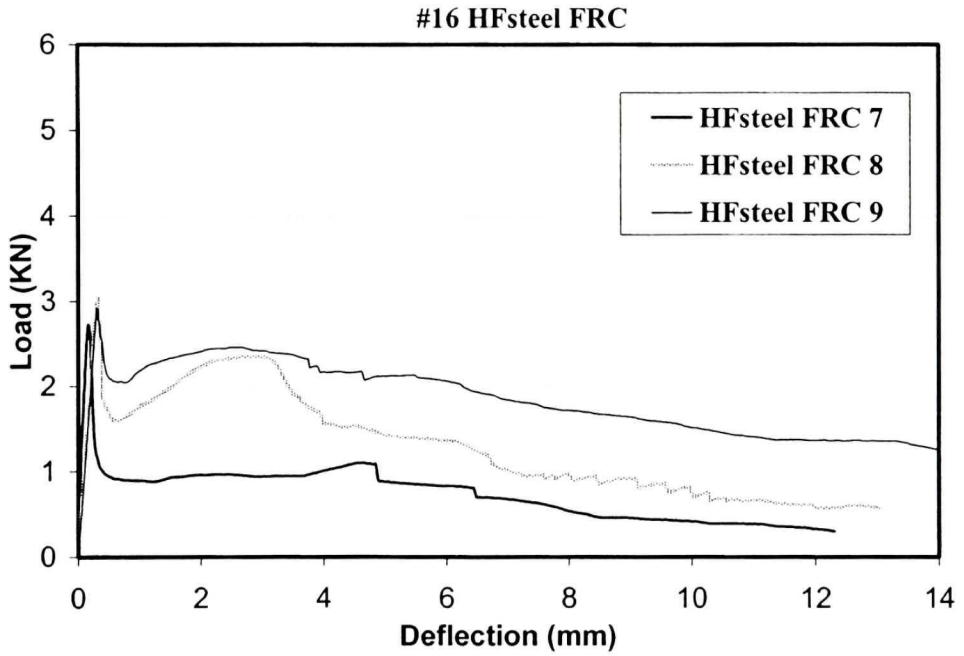


Figure B.28 Load–deflection curves under flexure ( #16 )

# References


ACI Committee 544, (1988), "Measurement of Properties of Fiber Reinforced concrete," ACI Materials Journal, V.85, No. 6, Nov, 1988, pp 583-593.

ACI Committee 544, (1993), "Guide for Specifying, Proportioning, Mixing, Placing, and Finishing Steel Fiber Reinforced Concrete'. ACI Materials Journal, Jan-Feb, Vol. 90, No. 1, pp 94-101.

ASTM (1997): "Standard Test Method for Flexural Toughness and First-Crack Strength of Fiber-Reinforced Concrete (Using Beam with Third Point Loading), ASTM C1018-97.

ASTM (1998) : " Test Method for Obtaining Average Residual-Strength of Fiber-Reinforced Concrete", ASTM C1399-98.

Bantahia, N. and Dubey, A., (1999), " Measurement of Flexural Toughness of Fiber Reinforced Concrete Using a Novel Technique — Part 1: Assessment and Calibration", ACI Materials Journal, November 1999, pp 651-655.

Bantahia, N. and Dubey, A., (2000), " Measurement of Flexural Toughness of Fiber Reinforced Concrete Using a Novel Technique — Part 2: Performance of Various Composites ", ACI Materials Journal, January 2000, pp 3-11.

Banthia, N. and Trottier, J., (1995), "Test Methods for Flexural Toughness Characterization of Fiber Reinforced Concrete: Some Concerns and A Proposition" , ACI Materials Journal , January 1995, pp 48-57.

Bayasi, Z. and Zeng, J., (1993), " Properties of Polypropylene Fiber Reinforced Concrete", ACI Materials Journal, November, 1993, pp 605-610.

Bentur, A., Diamond, S., (1985), "The Microstructure of the Steel Fiber-Cement interface", Journal of materials Science Vol. 20, 1985, pp 3610-3620.

Chen, P and Chung, D.D.L., (1996), "A Comparative Study of Concretes Reinforced with Carbon, Polyethylene and Steel Fiber and Their improvement by latex modification", ACI Materials Journal, March-April 1996, pp129-133.

Dogan, E. and Hill, H., et. al., (2000), "Suggested Design Guidelines for Seismic Retrofit with SIMCON and SIFCON", High-Performance Fiber-Reinforced Concrete in Infrastructural Repair and Retrofit. ACI, SP-185, 2000, pp 207-248.

Fu, X and Chung, D.D.L., (1998), "Improving the Bond Strength of Concrete to Reinforcement by Adding Methylcellulose to Concrete", ACI Materials Journal, V.95, No.5, September-October 1998, pp 601-607.

Garcia, S. and Antoine E., (1997), "Experimental investigation on the potential use of poly (vinyl alcohol) short fibers in fiber-reinforced cement-based composite", Materials and Structures, Vol.30, January-February 1997, pp 43-52.

Gopalaratnam, V. S. and Shah, S.P., et al., (1991), "Fracture Toughness of Fiber Reinforced Concrete". ACI Materials Journal, July 1991, pp 339-353.

Hughes, B.P., (1977), "Load-Deflection Curves for Fiber-Reinforced Concrete Beam in Flexural", Magazine of Concrete Research, Vol 29 (101), December, 1977, pp 199-206.

JCI: " Method of Test for Flexural Strength and Flexural Toughness of Fiber Reinforced Concrete, (Standard SF 4), JCI Standards for Test Methods of Fiber Reinforced Concrete, Japan, Concrete Institute.

Khayat, K. H., (1995), "Effects of Antiwashout Admixtures on Fresh Concrete Properties", ACI Structural Journal, Vol 92, No. 2, March-April 1995, pp 164-171.

Krstulovic-Opara, N., Haghayeghi, A. R., Haidar, M., and Krauss, P.D., (1995), "Use of Conventional and High-Performance Steel-Fiber Reinforced concrete for Bridge Deck Overlays", ACI Materials Journal, V.92, No.6, November-December 1995, pp 669-677.

Krstulovic-opara, N., LaFave, J. M. et. al, (2000) "Seismic Retrofit with Discontinuous Slurry Infiltrated Mat Concrete (SIMCON) Jackets". High-Performance Fiber-Reinforced Concrete in Infrastructural Repair and Retrofit. ACI, SP-185, 2000, pp 141-185.

Lankard, D.R., (1983), "Use of SIFCON for Concrete Pavement Overlays", Lankard Materials Laboratory, Inc., Columbus, Ohio, Dec. 1983

Lankard, D.R., (1985), " Preparation, Properties, and Applications of Cement-Based Composites Containing 5 to 20 Percent Steel Fibers", Steel Fiber Concrete, U.S.-Sweden Joint Seminar, (NSF-STU) June, 1985

Li, V. C., Wang, S., Wu, C., (2001), "Tensile Strain-Hardening Behavior of polyvinyl Alcohol Engineer Cementitious Composite (PVA-ECC), ACI materials Journal, November-December 2001, pp 483-493.

Li, V. C., Wu, H. C., (1996), " Tensile Behavior of Cement-Based Composites with Random Discontinuous Steel Fibers", J. Am. Ceram Soc. Vol 79. No.1,1996, pp 74-78.

Li, V. C., Chan, Y.W and Wu, H. C., (1994), "Interface Strengthening Mechanisms in Polymeric Fiber Reinforced Cementitious Composites", Proc. Int. Symp. "Brittle Matrix composites 4", September 13-15,1994, pp 7-16.

Li, V. C., and Wu. H.C, (1991), " Conditions for Pseudo Strain-Hardening in Fiber Reinforced Brittle Matrix Composites". Applied Mechanics Reviews, V.45 No.8, 1992, pp 390-398.

Li, Z., (1991), "Characterization of interfacial Properties in Fiber-Reinforced Cementitious Composites", J. Am. Ceram. Soc., Vol 74, No.9, 1991, pp 2156-2164.

Maalej, M and Li, V. C., (1995), "Introduction of Strain-Hardening Engineered Cementitious Composites in Design of Reinforced Concrete Flexural Members for Improved Durability", ACI Structural Journal, March-April, 1995, pp 167-176.

Missouri Department of Transportation, (2001) "Fiber–Reinforced PCC Unbonded Overlay, Research Development and Technology" Division,. January, 2001.

Morgan, D.R., (2000), "Shotcrete Guides and Specifications", Shotcrete Magazine, Fall 2000, pp 8-11.

Naaman, A.E., (2000), "HPFRCCS: Properties and Applications in Repair and Rehabilitation", High-Performance Fiber-Reinforced Concrete in Infrastructural Repair and Retrofit. ACI, SP-185, 2000, pp 2-3.

Naaman, A.E., and Reinhardt, H. W., (1995), "High Performance Fiber Reinforced Cement Composites -Volume 2)", Pre-Proceeding: 2nd International Workshop, June 11-14, 1995.

Robinson, C., Angelo, C., And Boyd, G., (1991), " Steel Fibers Reinforce Auto Assembly Plant Floor". Concrete International, April, 1991, pp 30-35.

Scott, H., (1998), " Investigation and Accelerated Performance Testing of Ultra-Thin Fiber Reinforced Concrete Overlay on Asphalt and Concrete", First Annual, Synthetic Fiber Reinforced Concrete Symposium, January, 1998, pp 35-61.

Schrader, E. K., (1984), "Design Methods for Pavements With Special Concretes. Fiber Reinforced Concrete". American Concrete Institute, Detroit, MI, pp. 197-212. (ACI SP-81)

Shah, S.P., Ludirdja, D., Daniel, J.I., and Mobasher, B., (1988), "Toughness-Durability of Glass Fiber Reinforced Concrete Systems", ACI Materials Journal, September 1988, pp 352-357.

Shao, Y., Srinivasan, R., and Shah, S.P., (2000), "Parameters affecting High-Performance Response in Fiber-Reinforced Concrete". High-Performance Fiber-Reinforced Concrete in Infrastructural Repair and Retrofit. ACI, SP-185-2, 2000, pp 17-24.

Shao, Y. and Shah, S.P., (1997), "Mechanical Properties of PVA Fiber Reinforced Cement Composites Fabricated by Extrusion Processing", ACI Materials Journal, Vol. 94, No. 6, November-December, 1997, pp 555-564.

Soroushian, P. and Bayasi, Z., (1991), "Fiber-Type Effects on the Performance of Steel Fiber Reinforced Concrete", ACI Materials Journal, March 1991, pp 129-133.

Tjiptobroto, P., and Hansen, W., (1993), "Tensile Strain Hardening and multiple Cracking in High-Performance Cement-Based Composites Containing Discontinuous Fibers", ACI Materials Journal, January –February, 1993, pp 16-25.

Vandenberghe, M. P. and Nemegeer, D. E., (1985), 'Industrial Flooring With Steel Fiber Reinforced Concrete". Concrete International, Mar. 1985, Vol. 7, No. 3, pp 54-57.

Vandewalle, M. A., (2000), "Design of Steel Fiber Reinforced Concrete and Shotcrete for Tunnel Linings", Tunnelling Asia 2000, New Delhi, September 2000.

Zhang, J. and Li, V. C., (2002), "Monotonic and Fatigue Performance in Bending of Fiber-Reinforced Engineered Cementitious Composite in Overlay System", Cement and Concrete Research , Vol.32, 2002, pp 415-423.

Zeng, J., Klingenberg, P., and Bayasi, Z., (2000), "Slurry Infiltrated Mat Concrete (SIMCON) for Rehabilitation of Bridge and Pavement", High-Performance Fiber-Reinforced Concrete in Infrastructural Repair and Retrofit. ACI, SP-185, 2000, pp 55-68.

Zia, P., Ahmad, S. and Leming, M., (1989-1994), "High-Performance Concretes", A State-of-Art Report U.S. Department of Transportation Federal Highway Administration, http://www.tfhrc.gov////structur/hpc/hpc2/contnt.htm.